THE HIGHLY PREORGANIZED LIGAND 2,9-BIS(HYDROXYMETHYL)-1,10-PHENANTHROLINE, AND ITS COMPLEXATION PROPERTIES WITH METAL IONS

Raymond Thomas Gephart, III

A Thesis Submitted to the
University of North Carolina Wilmington in Partial Fulfillment
Of the Requirements for the Degree of
Master of Science

Department of Chemistry

University of North Carolina Wilmington

2006

Approved by

Advisory Committee

_____ _____

_____
Chair

Accepted by

_____
Dean, Graduate School

TABLE OF CONTENTS

ABSTRACT

Preorganization has been shown to be an important concept in inorganic chemistry. Preorganization increases the thermodynamic stability of complexes and metal ion selectivity of ligands. A ligand is more highly preorganized the more nearly it is constrained as the free ligand to be in the conformation required to complex the metal ion. The ligand 2,9-bis(hydroxymethyl)-1,10-phenanthroline (PDALC) was used to study the effects of preorganization and effects of addition of neutral oxygen donor atoms on the thermodynamic complex stability. The rigid extended aromatic backbone of PDALC should lead to unprecedented levels of preorganization for a non-macrocyclic ligand. PDALC was synthesized and characterized using NMR and IR analysis. UV/Vis spectrophotometry was used in titrations to determine protonation constants of the free ligand and its formation constants with metal ions. These were obtained by plotting absorbance, corrected for dilution caused by addition of acid or base during the titration, against pH. Log K_1 values for PDALC were obtained for Ba(II), Bi(III), Ca(II), Cd(II), Co(II), Cu(II), Gd(III), In(III), La(III), Mg(II), Ni(II), Pb(II), Sr(II), Zn(II), and Zr(IV) in 0.1 *M* $NaClO_4$ at 25 ^oC. A titration with Zr(IV) was used to determine the charge of the complex at biological pH for potential use in positron emission tomography (PET). The crystal structures of the PDALC complexes $[Bi(PDALC)(H_2O)_2](ClO_4)_3 \cdot H_2O$, $[Pb(PDALC)(ClO_4)_2] \cdot H_2O$, and $[Ca(PDALC)_2](ClO_4)_2 \cdot H_2O$ are reported. The stability constants along with crystal structures are discussed in relation to the high level of preorganization of the PDALC ligand, and the effects of the neutral O-donors of the hydroxymethyl groups of PDALC on its complexes.

ACKNOWLEDGEMENTS

I would like to thank my advisor, Dr. Robert Hancock for giving me the opportunity to work in his research group. I have learned more than I ever could have expected under his guidance over the past couple years. My committee members, Dr. John Tyrell and Dr. S. Bart Jones, have been very helpful when asked for input in the areas of their expertise.

I would like to give a special thank you to my parents, Raymond and Dorothy Gephart, who have always loved and supported me in everything I set out to accomplish. I also wish to thank my sister and brother-in-law who have helped me grow into the man I am today.

I would also like to thank the faculty and my friends at UNCW, especially Darren Melton, F. Crisp McDonald and the rest of the Inorganic lab group who paved the way in this project and shared their experience whenever I needed some. To the triathlon club, you have given me an opportunity to do what I love, race, and with that came some great friendships. Finally, Martha Marie Roth, you have made my time here in Wilmington very enjoyable, and I will always cherish the time spent here with you.

DEDICATION

I would like to dedicate this thesis to my parents, of whom I am very proud. My life has taken many twists and turns, but you have always stood by my side and supported everything I chose to do.

LIST OF TABLES

LIST OF FIGURES

INTRODUCTION

Inorganic chemistry is an important area of medicinal chemistry, with many uses ranging from essential elements used for mineral supplements to therapeutic agents. Pharmaceutical industries have been dominated by organic chemistry. The success of cisplatin, a popular anti-cancer drug, initially brought inorganic chemistry into the pharmaceutical industry. The success of other metallic complexes has increased the interest in inorganic chemistry for pharmaceutical chemistry.

There are several examples of recent discoveries in medicinal inorganic chemistry. The complex of titanocene dichloride is now being injected into patients for anti-metastatic activity in anti-cancer treatment.[1] Complexes with Ru^{III} have also shown promise for anti-metastatic activity.[1] Magnetic resonance imaging (MRI) contrast agents like Gd^{III} can safely be injected into humans with ligands that can control their toxicity.[1] When used with ligands, metals are used in radiodiagnostics and radiotherapeutic isotopes such as ^{99m}Tc and ^{186}Re.[1] Gold has been used for antiarthritis drugs and bismuth has been used for antiulcer drugs.[1] There is also potential for several other uses such as manganese superoxide dismutase mimics, vanadium insulin mimics, ruthenium nitric oxide scavengers, lanthanide-based photosensitizers, and metal-targeted organic agents.[1]

Bond strength and speed of formation

Ligands are compounds that bind to metal ions. There are six basic factors that affect the thermodynamic stability of complexes. These include the hard and soft acids and bases theory (HSAB),[2,3] chelate ring size,[4] number of neutral oxygen donors,[5,6] number of negative oxygen donors,[7] preorganization[8,9] and coordination number.[10]

The concept of HSAB[2,3,11] states that there is an increase in stability of an acid-base pair if both the acid and base are hard or both the acid and base are soft. Figure 1 provides a chart of Pearson's classification of Lewis acids (essentially metal ions) and bases for the HSAB concept[11]. Pearson also defined the terms soft base, hard base, soft acid, and hard acid. A soft base is a donor atom that has high polarizability, low electronegativity, and is easily oxidized. A hard base is a donor atom that has low polarizability, high electronegativity, and is not easily oxidized. A soft acid is an acceptor atom that has a low positive charge, large size and outer electrons that are easily excited. A hard acid is an acceptor atom that has a large positive charge, small size, and lacks easily excited outer electrons. The simplest hard acid is the proton and the simplest soft acid is the methylmercury cation. It is important to note that the terms hard and soft are not the same as strong and weak. These are two separate properties that describe both acids and bases alike.[2]

The explanation for the HSAB[2,3,11] concept includes various degrees of ionic and covalent σ-bonding, π-bonding, electron correlation phenomena, and solvation effects. The ionic-covalent theory states that acids of high positive charge and small size and bases of large negative charge and small size will favor ionic bonding. For soft acids and bases, the repulsion portion of the potential energy curve is lower, allowing for better overlap of wave functions used in covalent bonding. For the π-bonding theory, hard acids have tightly held outer electrons and empty orbitals that are not too high in energy and harder basic atoms could form π-bonds by donating electrons from the ligand into the empty orbital of the metal. Soft acids have loosely held outer d-orbital electrons which can form π-bonds by donating electrons to ligands that have empty d-orbitals. These

Classification of Lewis Acids

Class (a)/Hard	Class (b)/Soft
H^+, Li^+, Na^+, K^+	Cu^+, Ag^+, Au^+, Tl^+, Hg^+, Cs^+
Be^{2+}, Mg^{2+}, Ca^{2+}, Sr^{2+}, Sn^{2+}	Pd^{2+}, Cd^{2+}, Pt^{2+}, Hg^{2+}
Al^{3+}, Se^{3+}, Ga^{3+}, In^{3+}, La^{3+}	CH_3Hg^+
Cr^{3+}, Co^{3+}, Fe^{3+}, As^{3+}, Ir^{3+}	Tl^{3+}, $Tl(CH_3)_3$, RH_3
Si^{4+}, Ti^{4+}, Zr^{4+}, Th^{4+}, Pu^{4+}, VO^{2+}	RS^+, RSe^+, RTe^+
UO_2^{2+}, $(CH_3)_2Sn^{2+}$	I^+, Br^+, HO^+, RO^+
$BeMe_2$, BF_3, BCl_3, $B(OR)_3$	I_2, Br_2, INC, etc.
$Al(CH_3)_3$, $Ga(CH_3)_3$, $In(CH_3)_3$	Trinitrobenzene, etc.
RPO_2^+, $ROPO_2^+$	Chloranil, quinones, etc.
RSO_2^+, $ROSO_2^+$, SO_3	Tetracyanoethylene, etc.
I^{7+}, I^{5+}, Cl^{7+}	O, Cl, Br, I, R_3C
R_3C^+, RCO^+, CO_2, NC^+	M^0 (metal atoms)
	Bulk metals
HX (hydrogen-bonding molecules)	
Borderline	
Fe^{2+}, Co^{2+}, Ni^{2+}, Cu^{2+}, Zn^{2+}, Pb^{2+}	
$B(CH_3)_3$, SO_2, NO^+	

Classification of Lewis Bases

Hard	Soft
H_2O, OH^-, F^-	R_2S, RSH, RS^-
CH_3CO_2, PO_4^{3-}, SO_4^{2-}	I^-, SCN^-, $S_2O_3^{2-}$
Cl^-, CO_3^{2-}, ClO_4, NO_3^-	R_3P, R_3As, $(RO)_3P$
ROH, RO^-, R_2O	CN^-, RNC, CO
NH_3, RNH_2, N_2H_4	C_2H_4, C_6H_6
	H^-, R^-
Borderline	
$C_6H_5NH_2$, C_5H_5N, N_3^-, Br^-, NO_2^-, SO_3^{2-}, N_2	

Figure 1: Chart of Pearson's HSAB classification system.[11]

types of ligands are soft bases. The electron correlation effect suggests that van der Waals forces between atoms or groups in the same molecule may lead to stabilization of the molecule. Stability due to these van der Waals forces will be present when a complex forms between a polarizable acid and a polarizable base (a soft acid and a soft base). Finally, solvation theory explains how solvents can reduce the basicity of small anions and in doing so, causes large anions to appear stronger. Solvation generally destroys hardness and strengthens softness. This does not explain why some acids prefer hard bases and why some prefer soft bases, but the three previous concepts explain the HSAB principle sufficiently.[3]

Metal ion size is a factor that determines ligand selectivity based on the size of the chelate ring that is formed[12]. Larger metal ions prefer to form complexes with a chelate ring size of five while smaller metal ions prefer to form complexes with a chelate ring size of six. In organic chemistry, the six-membered ring, cyclohexane, is the ideal ring size for carbon atoms. In this ring, the carbon atoms are equidistant from each other with the hydrogen atoms being staggered. In organic chemistry, all of the atoms are similar in size to the carbon atom, not including the hydrogen atom which is not a member of the ring.

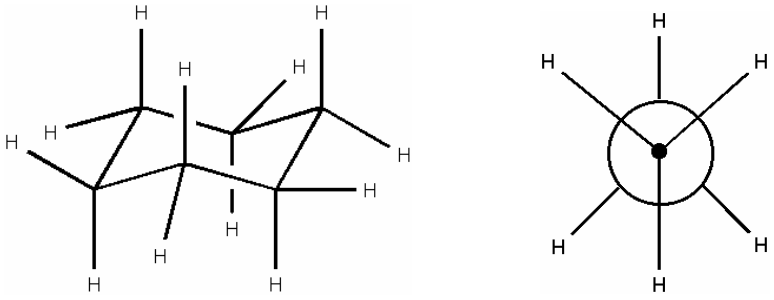

In inorganic chemistry, metal ions vary in ionic radius[13] from 0.27 Å of Be^{2+} to 1.19 Å of Pb^{2+}. The figure below shows the preference of chelate ring sizes of five and six.

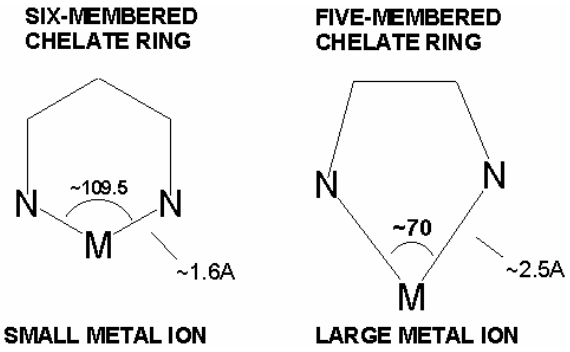

The large metal ions form more stable complexes with five-membered rings and less stable complexes with six-membered rings. The five-membered carbon ring, cyclopentane, is not very stable because the axial hydrogens eclipse each other. When complexed with a large metal ion, however, the hydrogen atoms become staggered because of the change in the bond angles. The reason that the six-membered ring complex with large metal ions becomes less stable is because the hydrogen atoms change from being staggered to being eclipsed. This makes the complex sterically strained. Smaller metal ions, however, are more similar to the carbon atom and when the complex is formed, the ring remains in the stable geometry. A small metal ion in a five-membered ring does not promote any conformational change and it remains unfavorable.[4]

The neutral oxygen donor is a very important donor atom among ligands because of its role in solubility in the most important solvent, water. The neutral oxygen donor is found in important ligands such as crown ethers and cryptands, and naturally occurring ligands monensin and nonactin.[5] Neutral oxygen donor atoms in a ligand favor the binding of large metal ions. This selectivity appears to be due to steric effects in the chelate ring. The neutral oxygen prefers to be close to a triganol planar geometry which is found in five-membered chelate ring systems.[5] As discussed above, the five-membered chelate ring is selective for larger metal ions.[5, 12] Size selectivity can be obtained from macrocycles, due to the size of the cavity produced and rigidity of the cavity. The neutral oxygen donor, however, can provide a greater selectivity for larger

metal ions over smaller metal ions. This is important because it is much easier synthetically to add a neutral oxygen to a ligand than it is to produce a macrocycle of the appropriate size.[6]

A negatively charged oxygen donor atom increases the affinity for highly charged metal ions such as iron (III) and aluminum (III). A negative oxygen can be found as a donor group in ligands of interest such as catecholates, phenolates, hydroxymates, and phosphonates. These ligands are important for uses that include the removal of Fe(III) to treat Cooley's anemia,[14-18] complexing Al(III) to treat aluminum intoxication,[7] complexing with In(III) and Gd(III) as imaging agents,[19] and complexing actinide elements.[20] The strength of the complexes formed with varying metal ions correlates with metal ion affinity for the hydroxide ion.[7]

Ligands that are flexible can adopt many conformations in aqueous solution. Restricting the conformation of such a ligand to that required to form a complex with a metal ion is an energetically unfavorable contribution to complex-formation. Such a ligand is said to have a low level of preorganization. When a ligand is rigid, and is constrained as the free ligand to the conformation required to complex the target metal ion, it is said to be "preorganized" for that metal ion.

Preorganization is the concept that the ligand is in the correct geometrical shape necessary to bind to a particular metal ion. The less rigid a ligand is, the more it will be able to adopt a variety of conformations, and therefore the less likely all of the donor atoms will be in the conformation necessary to bind to the metal ion.[8] The more flexible a ligand is, the greater the number of metal ions that are able to complex with it and the less selective it will be. Thus preorganization becomes an important tool in the development of ligands that are extremely selective by not allowing them to rearrange into a conformation that suits metal ions of a different size.[9]

Coordination number refers to the number of binding sites on a particular metal which determine how many donor atoms are needed to complex with that metal. When a ligand has more than one donor atom, it is referred to as a chelate. The effect of a chelate is that it provides an increase in the logarithm of formation constant, log K_1, of the complex over that of the analogous monodentate ligands. As the number of chelate rings in a chelating ligand increases, referred to as denticity, the formation constant increases. This can be seen in the chart below that shows the formation constants of increasing polyamines complexes with Ni(II).[21]

Polyamine	EN	DIEN	TRIEN	TETREN	PENTEN
denticity, n	2	3	4	5	6
log β_n (NH_3)	5.08	6.85	8.12	8.93	9.08
log K_1 (polyamine)	7.47	10.7	14.4	17.4	19.1

Ionic Strength =	0.5 M
EN	$NH_2CH_2CH_2NH_2$
DIEN	$NH_2(CH_2CH_2NH)_2H$
TRIEN	$NH_2(CH_2CH_2NH)_3H$
TETREN	$NH_2(CH_2CH_2NH)_4H$
PENTEN	$NH_2(CH_2CH_2NH)_5H$
Log $\beta_n(NH_3)$ =	log($K_1 \times K_2$ ----- $\times K_n$)

Note that the chelate effect increases with denticity increase.

There are many examples of preorganized ligands that have increased stability with metals of the correct size. One type of ligand that is less able to rearrange to allow for a larger or smaller cavity for the metal to bind is the macrocycles. Macrocycles have rings of various sizes that have several donor atoms bonded together to form a ring. The ring structure of a macrocycle does not allow for donor atoms to move around as easily as their open-chain counterparts because they are constrained by the ring structure. This creates selectivity for a particular sized metal to be better able to complex in the cavity. An increased selectivity due to preorganization

can be gained by making substitutions on the ring that further reduce the flexibility of the ligand.[9] These substitutions can also be used to increase the water solubility of the complex.[22] By changing which substituents are added to the ligand, the solubility can be altered as desired. Of course, by making the structure more rigid and increasing the binding strength, a decrease in kinetics of metal ion complexation will also tend to be found.[23]

Zirconium use for PET

The use of positron emission tomography (PET) has potential for use in diagnosing and treating cancer.[24-26] This method has three major advantages over the whole-body scintigraphy.[24] One advantage is better spatial and temporal resolution, resulting in detection of smaller lesions. A second advantage is more accuracy in localization which can give three-dimensional information. The third advantage is the ability to accurately quantify the uptake which will give better estimates for radiation dosages.[24] Other current methods for detection of tumors such as CT and MRI have difficulty detecting tumors that are smaller than 1 cm. It is believed that replacing these methods with PET will improve tumor detection because of its higher resolution and quantitative imaging.[25]

There are several requirements for a positron emitter to be appropriate for use in immuno-PET.[24-26] The first requirement is the emitter half-life needs to be compatible with the pharmacokinetics of the radiolabeled monoclonal antibodies (monoclonal antibodies = moAbs).[24-26] The positron emitting isotopes should also have no γ-photons with an energy near 511 keV so the quantitative accuracy is optimized. The β^+-energy should also be as small as possible to improve the resolution. A final requirement is that of stable coupling between the positron emitter and the moAbs.[25]

Commonly used positron emitters such as ^{11}C, ^{13}N, ^{15}O and ^{18}F do not satisfy the first requirement because they have very short half-lives.[24] For this use, ^{64}Cu and ^{86}Y also have half-lives that are too short (12.7 and 14.7 hours respectively).[24] This would not allow for enough time to use the complex before too much decay has occurred. Positron emitters such as ^{89}Zr and ^{124}I are much better suited with half-lives of 78 and 100 hours respectively.[24-27] Zirconium was chosen to be studied with PDALC to determine whether or not it would form a strong, neutral complex at biological pH. If possible, PDALC could be complexed with Zr to cross the blood-brain barrier and used to detect brain tumors. In order to cross the blood brain barrier a complex should be small and neutral. If the hydroxymethyl groups of PDALC were deprotonated by Zr(IV) in its bis-PDALC complex, $[Zr(PDALCH_{-2})_2]$, this might be able to cross the blood-brain barrier.

The ligand PDALC studied here presents the possibility of a non-macrocyclic ligand with a very high level of preorganization. The 1,10-phenanthroline backbone of PDALC is very rigid, and should make PDALC much more highly preorganized than its analog EDDE.

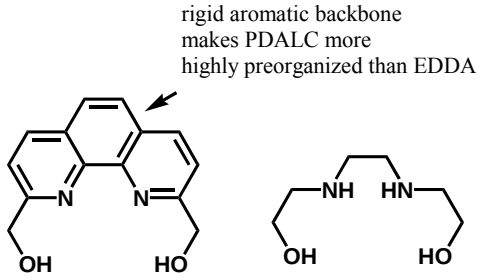

PDALC EDDE

In addition, the neutral oxygen donors of the hydroxymethyl groups of PDALC, as noted above, should increase the selectivity of PDALC for large metal ions. The design of PDALC is such that it should show strong selectivity for large metal ions, which is the subject of this research.

METHODS

All chemicals and reagents used were of analytical grade, and were purchased commercially. Aqueous solutions of metal ions and ligands were prepared using deionized (DI, see a list of abbreviations in appendix) water.

The ligand and metal-ligand complexes were characterized by using ^{1}H-NMR and FT-IR analysis. A Bruker 400 MHz NMR spectrometer was used to obtain ^{1}H-NMR spectra for analysis of all organic synthesis products. All samples for ^{1}H-NMR analysis were prepared and referenced using DMSO-d_6. A Polaris IR-10410 FT-IR instrument (Mattson, Inc.) with WinFIRST software was used to obtain infrared absorption spectra of all organic products synthesized, and for all crystallized metal-ligand complexes collected. Samples were prepared for FT-IR analysis as KBr Pellets.

Aqueous metal-ligand titration experiments were carried out using a double beam Cary 1E UV/Vis spectrophotometer (Varian, Inc.) with WinUV Version 2.00(25) software. For the UV/Vis absorption spectra, a 1.0 cm quartz flow cell, fitted with a peristaltic pump, was used to mix the aqueous metal-ligand solution after each titrant addition was made to the solution. A diagram of the flow cell apparatus is shown in Figure 2. An equilibration time of at least seven minutes was used for all titrant additions that were made. Longer equilibration times did not result in any drifting in the spectra, but an effort was made to keep these additions as close to seven minutes apart as possible. The absorbance scan range used was from 190 to 350 nm at a rate of 600.00 nm/min for all samples. All absorbance spectra were referenced by placing a 1.0 cm quartz cell filled with DI water in the reference beam path.

All pH values for the titration experiments were recorded using a SympHony SR60IC pH meter (VWR Scientific, Inc.), which was calibrated prior to each titration experiment using pH

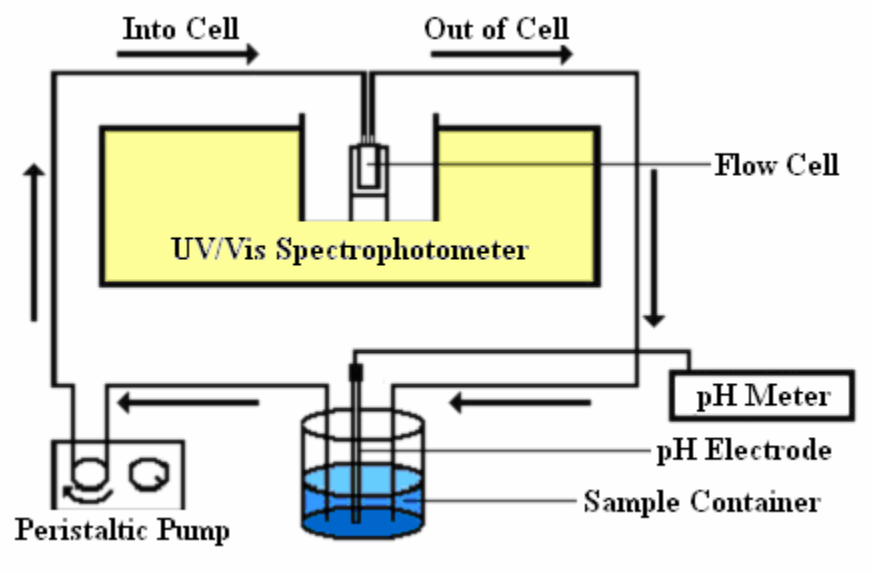

Figure 2: Scheme of the flow cell apparatus used in the titration experiments.

4.01, 7.00, and 10.01 buffer solutions. Aqueous metal-ligand samples used in the titration experiments were of 0.10 *M* $NaClO_4$ for ionic strength and maintained at a constant temperature of 25.0 ± 0.1 °C throughout the experiment.

Synthesis of PDALC

The synthesis of PDALC (2,9-bis(hydroxymethyl)-1,10-phenanthroline) followed the basic method described in the literature[28] with a few modifications. In Figure 3, a scheme is given that outlines the synthesis. The products were characterized using both ^{1}H-NMR and FT-IR analysis.

A mixture of 2.9836g of 2,9-dimethyl-1,10-phenanthroline monohydrate (14.396 mmol, Alfa Aesar, 99%) and 7.5155 g of selenium dioxide (67.732 mmol, Alfa Aesar, 99+%) was placed in 200 mL of 5% DI H_2O/p-dioxane (Alfa Aesar, 99+%) in a 500 mL round bottom flask. The mixture was heated to 101 ºC while stirring in a wax bath and held under reflux for 3 hours. The hot solution was filtered through filter paper (Whatman) and refrigerated overnight. A yellow-orange precipitate formed from the cold filtrate which was separated by vacuum filtration and allowed to dry. The synthesis yielded 0.9625g of unpurified 1,10-phenanthroline-2,9-dicarboxaldehyde (4.075mmol, 28.30%) which was not taken through any purification steps.

The non-purified 1,10-phenanthroline-2,9-dicarboxaldehyde was reduced to form 2,9-bis(hydroxymethyl)-1,10-phenanthroline. A solution of 0.9625 g of unpurified 1,10-phenanthroline-2,9-dicarboxaldehyde (4.075 mmol) and 0.2145 g of $NaBH_4$ (6.158 mmol, Sigma-Aldrich, 98+%) in 100 mL of pure ethanol was placed in a 250 mL round bottom flask. The mixture was stirred and heated to 78 ºC for 2 hours. The hot solution was filtered through filter paper to remove any excess SeO_2 from the previous step in the synthesis. A white

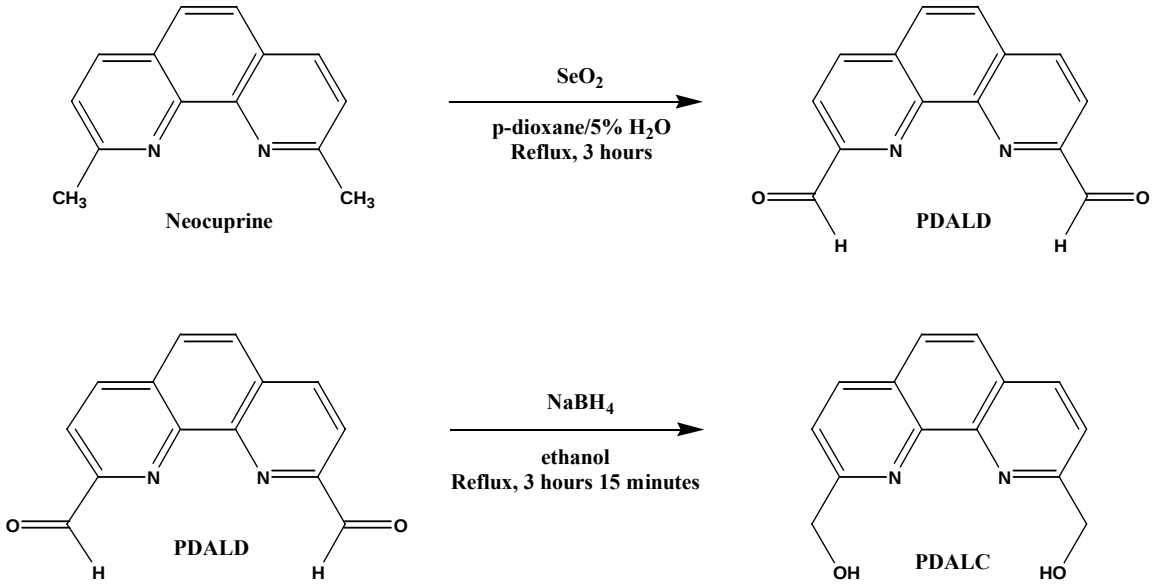

Figure 3: Scheme showing of the synthesis of PDALC as reported by Chandler *et. al.*[28]

precipitate formed from the cold filtrate which was concentrated by evaporation of the ethanol on a rotary evaporator. To purify the product, the precipitate was recrystallized from DI water and 0.4415 g of 2,9-bis(hydroxymethyl)-1,10-phenanthroline (1.838mmol, 45.10%) was recovered. The product was collected as white needles. The 0.4415 g of pure product obtained represented 12.76% overall yield for both synthetic steps and recrystallization of the product.

UV-Vis spectrophotometry titrations involving PDALC

Acid-base titrations of aqueous metal-PDALC solutions were monitored using UV-Vis spectrophotometry. For most metals, only one titration was necessary. Those experiments involved the metal with PDALC. Some metal ions formed a very strong complex with PDALC and required a second titration. This second titration used a competing ligand, EGTA (ethylenebis(oxyethylenenitrilo) tetra-ethylene glycol bis(2-aminoethyl ether)-N,N,N'N'-tetraacetic acid), with the metal and PDALC. Stock solutions of 4.096×10^{-4} *M* PDALC (0.0246 g into 250 mL of DI H_2O), 1.002 *M* $NaClO_4$ (12.2649 g, 0.1002 mol, Alfa Aesar, 98.0-102.0%, into 100 mL of DI H_2O), 1.020 *M* $NaClO_4$ (12.4911 g, 0.1020 mol, into 100 mL of DI H_2O), 1.000 *M* $NaClO_4$ (12.2440 g, 0.1000 mol, into 100 mL of DI H_2O), and 0.00100 *M* EGTA (0.0952 g, 0.2503 mmol, Acros Organics, 99%, into 250 mL of DI H_2O) were used in the titration experiments. Various metal stock solutions were used and the preparation of these is described below. Titrant solutions of 0.100 *M* $HClO_4$ (4.25 mL of 11.7 *M* $HClO_4$, 70% Alfa Aesar, 99.9985% (metals basis) in 500 mL of DI H_2O) and 0.100 *M* NaOH (2.50 mL of 10.00 ± 0.05 *M* NaOH, VWR, into 250 mL of DI H_2O) were used to adjust the pH of the sample solutions. The ionic strength of each titration solution was held at a constant 0.1.

Solution for titration of PDALC

To determine the protonation constant for PDALC, 250 mL of 2×10^{-5} *M* PDALC (12.20 mL of 4.096×10^{-4} *M*) in 0.1 *M* $NaClO_4$ (3.061 g) was prepared. A 50.00 ± 0.05 mL aliquot of this solution was placed in the flow cell apparatus described above and titrated with 0.1 *M* $HClO_4$. The absorbance values were collected from 204 nm, 228 nm, 237 nm, 260 nm, 271 nm, 279 nm, 293 nm, and 315 nm from each spectrum, and pH values were recorded for each titrant addition.

Solution for titration of PDALC with barium (II)

A stock solution of 0.9999 *M* $Ba(ClO_4)_2$ was prepared (16.8096 g, Aldrich 97%, $Ba(ClO_4)_2$ in 50 mL of DI H_2O) for use in the titration experiment. A 50 mL solution of 2×10^{-5} *M* PDALC and 0.0333 *M* Ba(II) was prepared. This solution contained 2.440 mL of the 4.096×10^{-4} *M* PDALC stock solution and 1.665 mL of the 0.9999 *M* $Ba(ClO_4)_2$ stock solution. The 50.00 ± 0.05 mL solution was placed in the flow cell apparatus described above and titrated with 0.1 *M* $HClO_4$.

Solution for titration of PDALC with bismuth (III)

A stock solution of 0.01312 *M* $Bi(NO_3)_3$ in 0.1 *M* $HClO_4$ was prepared (0.6361 g $Bi(NO_3)_3\cdot5H_2O$ (Aldrich, 99.999%), 8.62 mL of 11.6 *M* $HClO_4$ in 100 mL of DI H_2O) for use in both titration experiments. For the first experiment, a 50 mL solution of 2×10^{-5} *M* PDALC, 2×10^{-5} *M* Bi(III), and 0.1 *M* $NaClO_4$ was prepared. This solution contained 2.440 mL of the 4.096×10^{-4} *M* PDALC stock solution, 76 µL of the 0.01312 *M* $Bi(NO_3)_3$ stock solution, 4.90 mL of the 1.020 *M* $NaClO_4$ stock solution, and 2 mL of the 0.1 *M* $HClO_4$ stock solution was added to

lower the initial pH. The 50.00 ± 0.05 mL solution was placed in the flow cell apparatus described above and titrated with 0.1 *M* NaOH. The second experiment involved a competing ligand, EGTA. A 50 mL solution of 2×10^{-5} *M* PDALC, 2×10^{-5} *M* Bi(III), 2×10^{-5} *M* EGTA, and 0.1 *M* $NaClO_4$ was prepared. This solution contained 2.440 mL of the 4.096×10^{-4} *M* PDALC stock solution, 76 μL of the 0.01312 *M* $Bi(NO_3)_3$ stock solution, 1.000 mL of the 0.00100 *M* EGTA stock solution, and 4.90 mL of the 1.020 *M* $NaClO_4$ stock solution with 200 μL of 0.1 *M* NaOH added to raise the initial pH. The 50.00 ± 0.05 mL solution was placed in the flow cell apparatus described above and titrated with 0.1 *M* $HClO_4$. Before titrating with 0.1 *M* $HClO_4$, 1.00 mL of 0.1 *M* NaOH was added to raise the initial pH to be closer to 11. A 50 mL solution of 4×10^{-5} *M* PDALC, 4×10^{-5} *M* Bi(III), and 0.1 *M* $NaClO_4$ was prepared. This solution contained 4.880 mL of the 4.096×10^{-4} *M* PDALC stock solution, 152 μL of the 0.01312 *M* $Bi(NO_3)_3$ stock solution, and 4.90 mL of the 1.020 *M* $NaClO_4$ stock solution with 1.50 mL of 0.1 *M* $HClO_4$ added to lower the initial pH. The 50.00 ± 0.05 mL solution was placed in the flow cell apparatus described above and titrated with 0.1 *M* NaOH.

Solutions for titration of PDALC with cadmium (II)

A stock solution of 0.003366 *M* $Cd(ClO_4)_2$ was prepared (0.0554 g, Aldrich, in 50 mL of DI H_2O) for use in both titration experiments. For the first experiment, a 100 mL solution of 2×10^{-5} *M* PDALC, 2×10^{-5} *M* Cd(II), and 0.1 *M* $NaClO_4$ was prepared. This solution contained 4.882 mL of the 4.096×10^{-4} *M* PDALC stock solution, 594 μL of the 0.003366 *M* $Cd(ClO_4)_2$ stock solution and 1.224 g of $NaClO_4$. A 50.00 ± 0.05 mL portion of this solution was placed in the flow cell apparatus described above and titrated with 0.1 *M* $HClO_4$. A second titration was conducted starting with an acidic solution and titrating with 0.1 *M* NaOH (prepared by diluting 5

mL of 10.00 *M* NaOH to 500 mL). For the second experiment, a 50 mL solution of 2×10^{-5} *M* PDALC, 2×10^{-5} *M* Cd(II), 0.033 *M* $HClO_4$, and 0.067 *M* $NaClO_4$ was prepared. This solution contained 2.440 mL of the 4.096×10^{-4} *M* PDALC stock solution, 297 µL of the 0.003366 *M* $Cd(ClO_4)_2$ stock solution, 16.5 mL of the 0.1 *M* $HClO_4$ stock solution, and 3.343 mL of the 1.002 *M* $NaClO_4$ stock solution. This 50.00 ± 0.05 mL solution was placed in the flow cell apparatus described above and titrated with 0.1 *M* NaOH.

Solution for titration of PDALC with calcium (II)

A 50 mL solution of 2×10^{-5} *M* PDALC, 0.0333 *M* $Ca(ClO_4)_2$ was prepared. This solution contained 2.440 mL of the 4.096×10^{-4} *M* PDALC stock solution and 0.5279 g of $Ca(ClO_4)_2\cdot4H_2O$ (Aldrich, 99%). The 50.00 ± 0.05 mL solution was placed in the flow cell apparatus described above and titrated with 0.1 *M* $HClO_4$.

Solution for titration of PDALC with cobalt (II)

A stock solution of 0.03329 *M* $CoCl_2$ was prepared (0.2161 g, Fisher Scientific, 99.9%, in 50 mL of DI H_2O) for use in the titration experiment. A 50 mL solution of 2×10^{-5} *M* PDALC, 2×10^{-5} *M* Co(II), and 0.1 *M* $NaClO_4$ was prepared. This solution contained 2.440 mL of the 4.096×10^{-4} *M* PDALC stock solution, 30 µL of the 0.03329 *M* $Cu(ClO_4)_2$ stock solution and 4.99 mL of the 1.002 *M* $NaClO_4$ stock solutions. The 50.00 ± 0.05 mL solution was placed in the flow cell apparatus described above and titrated with 0.1 *M* $HClO_4$.

Solutions for titration of PDALC with copper (II)

A stock solution of 0.03320 *M* $Cu(ClO_4)_2$ was prepared (0.6151g, Aldrich 98%, in 50 mL DI H_2O) for use in the titration experiments. For the first experiment, a 50 mL solution of 2×10^{-5} *M* PDALC, 2×10^{-5} *M* Cu(II), and 0.1 *M* $NaClO_4$ was prepared. This solution contained 2.440 mL of the 4.096×10^{-4} *M* PDALC stock solution, 30 µL of the 0.03320 *M* $Cu(ClO_4)_2$ stock solution and 4.99 mL of the 1.002 *M* $NaClO_4$ stock solution. The 50.00 ± 0.05 mL solution was placed in the flow cell apparatus described above and titrated with 0.1 *M* $HClO_4$. The second experiment involved a competing ligand, EGTA. A 50 mL solution of 2×10^{-5} *M* PDALC, 2×10^{-5} *M* Cu(II), 2×10^{-5} *M* EGTA, and 0.1 *M* $NaClO_4$ was prepared. This solution contained 2.440 mL of the 4.096×10^{-4} *M* PDALC stock solution, 30 µL of the 0.03320 *M* $Cu(ClO_4)_2$ stock solution, 1.000 mL of the 0.00100 *M* EGTA stock solution, and 4.90 mL of the 1.020 *M* $NaClO_4$ stock solution with 100 µL of 0.1 *M* NaOH added to raise the initial pH. The 50.00 ± 0.05 mL solution was placed in the flow cell apparatus described above and titrated with 0.1 *M* $HClO_4$. A third experiment was run with lowered concentrations of PDALC and Cu(II). For the this experiment, a 50 mL solution of 1×10^{-5} *M* PDALC, 1×10^{-5} *M* Cu(II), and 0.1 *M* $NaClO_4$ was prepared. This solution contained 1.220 mL of the 4.096×10^{-4} *M* PDALC stock solution, 15 µL of the 0.03320 *M* $Cu(ClO_4)_2$ stock solution and 4.90 mL of the 1.020 *M* $NaClO_4$ stock solution. The 50.00 ± 0.05 mL solution was placed in the flow cell apparatus described above and titrated with 0.1 *M* $HClO_4$. The fourth experiment involved a competing ligand, EGTA. A 50 mL solution of 1.5×10^{-5} *M* PDALC, 1.5×10^{-5} *M* Cu(II), and 0.1 *M* $NaClO_4$ was prepared. This solution contained 1.83 mL of the 4.096×10^{-4} *M* PDALC stock solution, 23 µL of the 0.03320 *M* $Cu(ClO_4)_2$ stock solution, and 4.90 mL of the 1.020 *M* $NaClO_4$ stock solution. The 50.00 ± 0.05 mL solution was placed in the flow cell apparatus described above and titrated with 0.1 *M*

$HClO_4$. A fifth experiment was run with higher concentrations of PDALC and Cu(II) and starting with an acidic solution. For the this experiment, a 50 mL solution of 4×10^{-5} *M* PDALC, 4×10^{-5} *M* Cu(II), 0.033 *M* $HClO_4$, and 0.067 *M* $NaClO_4$ was prepared. This solution contained 4.880 mL of the 4.096×10^{-4} *M* PDALC stock solution, 60 µL of the 0.03320 *M* $Cu(ClO_4)_2$ stock solution, 16.5 mL of the 0.1 *M* $HClO_4$ stock solution and 3.28 mL of the 1.020 *M* $NaClO_4$ stock solution. The 50.00 ± 0.05 mL solution was placed in the flow cell apparatus described above and titrated with 0.1 *M* NaOH. A sixth experiment was run with lower concentrations of PDALC and Cu(II) and starting with an acidic solution. For the this experiment, a 50 mL solution of 2×10^{-5} *M* PDALC, 2×10^{-5} *M* Cu(II), 0.033 *M* $HClO_4$, and 0.067 *M* $NaClO_4$ was prepared. This solution contained 2.440 mL of the 4.096×10^{-4} *M* PDALC stock solution, 30 µL of the 0.03320 *M* $Cu(ClO_4)_2$ stock solution, 16.5 mL of the 0.1 *M* $HClO_4$ stock solution and 3.35 mL of the 1.000 *M* $NaClO_4$ stock solution. The 50.00 ± 0.05 mL solution was placed in the flow cell apparatus described above and titrated with 0.1 *M* NaOH.

Solution for titration of PDALC with gadolinium (III)

A stock solution of 0.02783 *M* $Gd(NO_3)_3$ was prepared (0.6280 g, Aldrich 99.9%, in 50 mL DI H_2O). A 50 mL solution of 2×10^{-5} *M* PDALC, 2×10^{-5} *M* Gd(III), and 0.1 *M* $NaClO_4$ was prepared. This solution contained 2.440 mL of the 4.096×10^{-4} *M* PDALC stock solution, 36 µL of the 0.02783 *M* $Gd(NO_3)_3$ stock solution and 4.99 mL of the 1.002 *M* $NaClO_4$ stock solution. The 50.00 ± 0.05 mL solution was placed in the flow cell apparatus described above and titrated with 0.1 *M* $HClO_4$.

Solution for titration of PDALC with indium (III)

A stock solution of 0.01479 *M* $In(NO_3)_3$ was prepared (.2225g, Aldrich 99%, in 50 mL DI H_2O) for use in the titration experiment. A 50 mL solution of 2×10^{-5} *M* PDALC, 2×10^{-5} *M* In(III), and 0.1 *M* $NaClO_4$ was prepared. This solution contained 2.440 mL of the 4.096×10^{-4} *M* PDALC stock solution, 68 μL of the 0.01479 *M* $In(NO_3)_3$ stock solution and 4.99 mL of the 1.002 *M* $NaClO_4$ stock solution. The 50.00 ± 0.05 mL solution was placed in the flow cell apparatus described above and titrated with 0.1 *M* $HClO_4$.

Solution for titration of PDALC with lanthanum (III)

A stock solution of 0.001671 *M* $La(ClO_4)_3$ in 0.01 *M* HCl was prepared (0.0456 g, Strem Chemicals, 5 mL of 0.1 *M* HCl, in 50 mL DI H_2O) for use in the titration experiment. A 50 mL solution of 2×10^{-5} *M* PDALC, 2×10^{-5} *M* La(III), and 0.1 *M* $NaClO_4$ was prepared. This solution contained 2.440 mL of the 4.096×10^{-4} *M* PDALC stock solution, 598 μL of the 0.001671 *M* $La(ClO_4)_3$ in 0.01 *M* HCl stock solution, 4.99 mL of the 1.002 *M* $NaClO_4$ stock solution, and 30 μL of the 0.1 *M* NaOH stock solution. The 50.00 ± 0.05 mL solution was placed in the flow cell apparatus described above and titrated with 0.1 *M* $HClO_4$. Before titrating with $HClO_4$, 65 μL of 0.1 *M* NaOH was added to raise the starting pH.

Solutions for titration of PDALC with lead (II)

Stock solutions of 0.003315 *M* $Pb(ClO_4)_2$ (0.0763 g, Aldrich, 97% min, in 50 mL DI H_2O) and 0.03316 *M* $Pb(ClO_4)_2\cdot3H_2O$ (0.7629 g, in 50 mL DI H_2O) were prepared for use in both titration experiments. For the first experiment, a 50 mL solution of 2×10^{-5} *M* PDALC, 2×10^{-5} *M* Pb(II), and 0.1 *M* $NaClO_4$ was prepared. This solution contained 2.440 mL of the

4.096×10^{-4} *M* PDALC stock solution, 30 µL of the 0.03316 *M* $Pb(ClO_4)_2$ stock solution and 4.99 mL of the 1.002 *M* $NaClO_4$ stock solution. The 50.00 ± 0.05 mL solution was placed in the flow cell apparatus described above and titrated with 0.1 *M* $HClO_4$. The second experiment involved a competing ligand, EGTA (ethylenebis(oxyethylenenitrilo) tetra-ethylene glycol bis(2-aminoethyl ether)-N,N,N'N'-tetraacetic acid). A 50 mL solution of 2×10^{-5} *M* PDALC, 2×10^{-5} *M* Pb(II), 2×10^{-5} *M* EGTA, and 0.1 *M* $NaClO_4$ was prepared. This solution contained 2.440 mL of the 4.096×10^{-4} *M* PDALC stock solution, 302 µL of the 0.003315 *M* $Pb(ClO_4)_2$ stock solution, 1.000 mL of the 0.00100 *M* EGTA stock solution, and 4.90 mL of the 1.020 *M* $NaClO_4$ stock solution with 100 µL of the 0.1 *M* NaOH stock solution added to raise the initial pH. The 50.00 ± 0.05 mL solution was placed in the flow cell apparatus described above and titrated with 0.1 *M* $HClO_4$. A third experiment was run with lowered concentrations of PDALC and Pb(II). In this experiment, a 50 mL solution of 2×10^{-6} *M* PDALC, 2×10^{-6} *M* Pb(II), and 0.1 *M* $NaClO_4$ was prepared. This solution contained 0.244 mL of the 4.096×10^{-4} *M* PDALC stock solution, 30 µL of the 0.003315 *M* $Pb(ClO_4)_2$ stock solution and 4.90 mL of the 1.020 *M* $NaClO_4$ stock solution. The 50.00 ± 0.05 mL solution was placed in the flow cell apparatus described above and titrated with 0.1 *M* $HClO_4$. A fourth experiment was run with different concentrations of PDALC and Pb(II). In this experiment, a 50 mL solution of 1×10^{-5} *M* PDALC, 1×10^{-5} *M* Pb(II), and 0.1 *M* $NaClO_4$ was prepared. This solution contained 1.220 mL of the 4.096×10^{-4} *M* PDALC stock solution, 15 µL of the 0.03316 *M* $Pb(ClO_4)_2$ stock solution and 4.90 mL of the 1.020 *M* $NaClO_4$ stock solution. The 50.00 ± 0.05 mL solution was placed in the flow cell apparatus described above and titrated with 0.1 *M* $HClO_4$. A fifth experiment was run with different concentrations of PDALC and Pb(II). In this experiment, a 50 mL solution of 1.5×10^{-5} *M* PDALC, 1.5×10^{-5} *M* Pb(II), and 0.1 *M* $NaClO_4$ was prepared. This solution contained 1.830 mL of the 4.096×10^{-4} *M*

PDALC stock solution, 23 μL of the 0.03316 *M* $Pb(ClO_4)_2$ stock solution and 4.90 mL of the 1.020 *M* $NaClO_4$ stock solution. The 50.00 ± 0.05 mL solution was placed in the flow cell apparatus described above and titrated with 0.1 *M* $HClO_4$. A sixth experiment was run with different concentrations of PDALC and Pb(II) and starting with an acidic solution. In this experiment, 50 mL of a 4×10^{-5} *M* PDALC, 4×10^{-5} *M* Pb(II), 0.033 *M* $HClO_4$ and 0.066 *M* $NaClO_4$ solution was prepared. This solution contained 4.880 mL of the 4.096×10^{-4} *M* PDALC stock solution, 60 μL of the 0.03316 *M* $Pb(ClO_4)_2$ stock solution, 16.5 mL of the 0.1 *M* $HClO_4$ stock solution and 3.28 mL of the 1.020 *M* $NaClO_4$ stock solution. The 50.00 ± 0.05 mL solution was placed in the flow cell apparatus described above and titrated with 0.1 *M* NaOH. A seventh experiment was run with different concentrations of PDALC and Pb(II) and starting with an acidic solution. In this experiment, a 50 mL solution of 2×10^{-5} *M* PDALC, 2×10^{-5} *M* Pb(II), 0.033 *M* $HClO_4$ and 0.066 *M* $NaClO_4$ was prepared. This solution contained 2.440 mL of the 4.096×10^{-4} *M* PDALC stock solution, 30 μL of the 0.03316 *M* $Pb(ClO_4)_2$ stock solution, 16.5 mL of the 0.1 *M* $HClO_4$ stock solution and 3.28 mL of the 1.020 *M* $NaClO_4$ stock solution. The 50.00 ± 0.05 mL solution was placed in the flow cell apparatus described above and titrated with 0.1 *M* NaOH.

Solution for titration of PDALC with magnesium (II)

A stock solution of 0.9993 *M* $Mg(ClO_4)_2$ was prepared (16.5549 g, Alfa Aesar, 99% (metals basis), in 50 mL DI H_2O) for use in the titration experiment. A 50 mL solution of 2×10^{-5} *M* PDALC, 0.0333 *M* $Mg(ClO_4)_2$ was prepared. This solution contained 2.440 mL of the 4.096×10^{-4} *M* PDALC stock solution and 1.666 mL of the 0.9993 *M* $Mg(ClO_4)_2$ stock solution.

The 50.00 ± 0.05 mL solution was placed in the flow cell apparatus described above and titrated with 0.1 *M* $HClO_4$.

Solution for titration of PDALC with nickel (II)

A stock solution of 0.09969 *M* $NiCl_2$ was prepared (1.1848 g, Fisher Scientific, 99.8%, in 50 mL DI H_2O) for use in the titration experiment. A 50 mL solution of 2×10^{-5} *M* PDALC, 2×10^{-5} *M* Ni(II), and 0.1 *M* $NaClO_4$ was prepared. This solution contained 2.440 mL of the 4.096×10^{-4} *M* PDALC stock solution, 10 µL of the 0.09969 *M* $NiCl_2$ stock solution and 4.99 mL of the 1.002 *M* $NaClO_4$ stock solution. The 50.00 ± 0.05 mL solution was placed in the flow cell apparatus described above and titrated with 0.1 *M* $HClO_4$.

Solution for titration of PDALC with strontium (II)

A stock solution of 0.5000 *M* $Sr(ClO_4)_2$ was prepared (7.163 g, Aldrich, in 50 mL DI H_2O) for use in the titration experiment. A 50 mL solution of 2×10^{-5} *M* PDALC and 0.0333 *M* Sr(II) was prepared. This solution contained 2.440 mL of the 4.096×10^{-4} *M* PDALC stock solution and 3.330 mL of the 0.5000 *M* $Sr(ClO_4)_2$ stock solution. The 50.00 ± 0.05 mL solution was placed in the flow cell apparatus described above and titrated with 0.1 *M* $HClO_4$.

Solution for titration of PDALC with zinc (II)

A stock solution of 0.09989 *M* $Zn(ClO_4)_2$ was prepared (1.8599 g, Aldrich, in 50 mL DI H_2O) for use in the titration experiment. A 50 mL solution of 2×10^{-5} *M* PDALC, 2×10^{-5} *M* Zn(II), and 0.1 *M* $NaClO_4$ was prepared. This solution contained 2.440 mL of the 4.096×10^{-4} *M*

PDALC stock solution, 10 µL of the 0.09989 *M* $Zn(ClO_4)_2$ stock solution and 0.6143 g of $NaClO_4$. The 50.00 ± 0.05 mL solution was placed in the flow cell apparatus described above and titrated with 0.1 *M* $HClO_4$.

Solution for titration of PDALC with zirconium (IV)

A stock solution of 0.01192 *M* $ZrCl_4$ was prepared (0.1389 g, Alfa Aesar, 99.5+% (metals basis), in 50 mL DI H_2O) for use in the titration experiment. For the first experiment, a 50 mL solution of 2×10^{-5} *M* PDALC, 2×10^{-5} *M* Zr(IV), 0.033 *M* $HClO_4$ and 0.067 *M* $NaClO_4$ was prepared. This solution contained 2.440 mL of the 4.096×10^{-4} *M* PDALC stock solution, 84 µL of the 0.01192 *M* $ZrCl_4$ stock solution, 16.5 mL of the 0.1 *M* $HClO_4$ stock solution and 3.284 mL of the 1.020 *M* $NaClO_4$ stock solution. The 50.00 ± 0.05 mL solution was placed in the flow cell apparatus described above and titrated with 0.1 *M* $HClO_4$. For the second experiment, a 2:1 PDALC:Zr(IV) was prepared. A 50 mL solution of a 2×10^{-5} *M* PDALC, 1×10^{-5} *M* Zr(IV), 0.033 *M* $HClO_4$ and 0.067 *M* $NaClO_4$ was prepared. This solution contained 2.440 mL of the 4.096×10^{-4} *M* PDALC stock solution, 42 µL of the 0.01192 *M* $ZrCl_4$ stock solution, 16.5 mL of the 0.1 *M* $HClO_4$ stock solution and 3.284 mL of the 1.020 *M* $NaClO_4$ stock solution. The 50.00 ± 0.05 mL solution was placed in the flow cell apparatus described above and titrated with 0.1 *M* $HClO_4$.

Potentiometric titrations involving EDDE

Acid-base titrations of aqueous metal-EDDE (N,N'-Bis(2-hydroxyethyl)-ethylenediamine) solutions were monitored using a glass electrode measuring changes in millivolts (mV) with additions of acid or base. For these experiments, the following solutions

were prepared. A solution of 0.01 *M* HNO_3 in 0.09 *M* $NaNO_3$ was prepared by adding 5.00 mL of 1.000 ± 0.005 *M* HNO_3 (VWR) and 3.8258 g $NaNO_3$ (purified grade, Aldrich) into a 500 mL volumetric flask and filling with DI H_2O. A solution of 0.01 *M* NaOH in 0.09 *M* $NaNO_3$ was prepared first by adding 0.250 mL of 10.00 ± 0.05 *M* NaOH (VWR) and 1.9105 g $NaNO_3$ into a 250 mL volumetric flask and filling with DI H_2O and a second time by adding 0.500 mL of 10.00 *M* NaOH and 3.8262 g $NaNO_3$ into a 500 mL volumetric flask and filling with DI H_2O. A solution of 0.01 *M* EDDE in 0.1 *M* $NaNO_3$ was prepared by adding 0.7410 g EDDE and 4.2558 g of $NaNO_3$ into a 500 mL volumetric flask and filling with DI H_2O. A solution of 0.01 *M* EDDE was prepared by adding 0.1490 g EDDE into a 100 mL volumetric flask and filling with DI H_2O. The NaOH and HNO_3 solutions were used to calibrate the electrode immediately before the titration took place.

Acid- base titrations of aqueous metal-EDDE solutions were monitored using a glass electrode to measure the potential. The potential was measured with a Fisher Scientific AB15 accumet pH meter a sympHony glass electrode from VWR. The potential readings were measured to the nearest ±1 mV (±0.01 pH unit) and kept at a constant temperature of 25.0°C ± 0.05°C using a constant temperature bath to circulate water through a jacketed cell. The ionic strength of each titration solution was held at a constant 0.1. Before each titration was performed, the pH meter was calibrated by titrating the standard 0.01 *M* NaOH in 0.09 $NaNO_3$ solution with 0.01 *M* HNO_3 in 0.09 $NaNO_3$. The potential was recorded for each addition and a Nernstian slope was fitted to the plot of these potentials *vs.* the calculated pH.

Solution for titration of EDDE

A 30.00 ± 0.05 mL aliquot of 0.01 *M* EDDE in 0.1 *M* $NaNO_3$ was placed into a triple-necked tapered jacketed cell along with 30 μL of 10.00 *M* NaOH and titrated with 0.01 *M* HNO_3 in 0.09 *M* $NaNO_3$. The potential was recorded for each addition.

Solution for titration of EDDE with Ca (II)

A solution of 0.01 *M* EDDE, and 0.0333 *M* $Ca(NO_3)_2$ was prepared by dissolving 0.2359 g of $Ca(NO_3)_2 \cdot 4H_2O$ in 30 mL of stock EDDE solution in the triple-necked tapered jacketed cell. The solution was titrated with 0.01 *M* HNO_3 in 0.09 *M* $NaNO_3$ and the potential was recorded for each addition.

Solution for titration of EDDE with La (III)

A solution of 0.01 *M* EDDE, 0.1 *M* $NaNO_3$, and 0.01 *M* $La(NO_3)_3$ was prepared by dissolving 0.1300 g of $La(NO_3)_3 \cdot 6H_2O$ in 30 mL of the 0.01 *M* EDDE in 0.1 *M* $NaNO_3$ stock solution in the three-neck tapered jacketed cell. A 50 μL addition of 10.00 *M* NaOH was made to increase the initial pH of this solution. The solution was titrated with 0.01 *M* HNO_3 in 0.09 *M* $NaNO_3$ and the potential was recorded for each addition.

Solution for titration of EDDE with Mg (II)

A solution of 0.01 *M* EDDE and 0.0333 *M* $Mg(NO_3)_2$ was prepared by dissolving 0.2552 g of $Mg(NO_3)_2 \cdot 6H_2O$ in 30 mL of the 0.01 *M* EDDE in 0.1 *M* $NaNO_3$ stock solution in the three-neck tapered jacketed cell. A 10 μL addition of 10.00 *M* NaOH was made to increase the initial

pH of this solution. The solution was titrated with 0.01 *M* HNO_3 in 0.09 *M* $NaNO_3$ and the potential was recorded for each addition.

Preparation of Crystals Submitted for X-ray Crystallography

$[Bi(PDALC)(H_2O)_2](NO_3)_3 \cdot H_2O$ crystal preparation

The synthesis of $[Bi(PDALC)(H_2O)_2](NO_3)_3 \cdot H_2O$ crystals was carried out by first dissolving 0.0222 g of PDALC (0.09240 mmol) in *n*-butanol in a 50 mL beaker. Then 7.043 mL of 0.01312 *M* $Bi(NO_3)_3$ was added along with enough DI H_2O to make the two layers approximately equal in volume. The beaker was covered with parafilm with just the lip of the beaker uncovered. This allowed for PDALC to diffuse into the aqueous layer and complex with Bi very slowly, as each are only soluble in their respective layers. As the layers evaporated, the complex slowly crystallized out of solution. The crystals of $[Bi(PDALC)(H_2O)_2](NO_3)_3 \cdot H_2O$ were separated and dried under vacuum. IR analysis and X-ray crystallography were performed on the $[Bi(PDALC)(H_2O)_2](NO_3)_3 \cdot H_2O$ crystals.

$[Ca(PDALC)_2] \cdot H_2O$ crystal preparation

The synthesis of $[Ca(PDALC)_2] \cdot H_2O$ crystals was carried out by first dissolving 0.0161 g of PDALC (0.06701 mmol) in *n*-butanol in a 50 mL beaker. Then 2.009 mL of 0.03335 *M* $Ca(ClO_4)_2 \cdot 4H_2O$ (1.0373 g, Aldrich 99%, in 100 mL DI H_2O) was added along with enough DI H_2O to make the two layers approximately equal in volume. The beaker was covered with parafilm with just the lip of the beaker uncovered. This approach allowed for PDALC to diffuse into the aqueous layer and complex with Ca very slowly, as each are soluble only in their respective layers. As the layers evaporated, the complex slowly crystallized out of solution. The

crystals of $[Ca(PDALC)_2]\cdot H_2O$ were separated and dried under vacuum. IR analysis and X-ray crystallography were carried out on the $[Ca(PDALC)_2]\cdot H_2O$ crystals.

$[Cd(PDALC)](NO_3)_2$ crystal preparation

The synthesis of $[Cd(PDALC)](NO_3)_2$ crystals was carried out by first dissolving 0.0204 g of PDALC (0.08491 mmol) in *n*-butanol in a 50 mL beaker. Then 835 µL of 0.1016 *M* $Cd(NO_3)_2$ was added along with enough DI H_2O to make the two layers approximately equal in volume. The beaker was covered with parafilm with just the lip of the beaker uncovered. This allowed for PDALC to diffuse into the aqueous layer and complex with Cd very slowly, as each are only soluble in their respective layers. As the layers evaporated, the complex slowly crystallized out of solution. The crystals of $[Cd(PDALC)](NO_3)_2$ were separated and dried under vacuum. IR analysis and X-ray crystallography were performed on the $[Cd(PDALC)](NO_3)_2$ crystals.

$[Co(PDALC)](ClO_4)_2$ crystal preparation

The synthesis of $[Co(PDALC)](ClO_4)_2$ crystals was carried out by first dissolving 0.0197 g of PDALC (0.0820 mmol) in *n*-butanol in a 50 mL beaker. Then 82 µL of 0.999 *M* $Co(ClO_4)_2$ was added along with enough DI H_2O to make the two layers approximately equal in volume. The beaker was covered with parafilm with just the lip of the beaker uncovered. This allowed for PDALC to diffuse into the aqueous layer and complex with Co very slowly, as each are soluble only in their respective layers. As the layers evaporated, the complex slowly crystallized out of solution. The crystals of $[Co(PDALC)](ClO_4)_2$ were separated and dried under vacuum. IR analysis and X-ray crystallography were performed on the $[Co(PDALC)](ClO_4)_2$ crystals.

[Cu(PDALC)]$(ClO_4)_2$ crystal preparation

The synthesis of [Cu(PDALC)]$(ClO_4)_2$ crystals was carried out by first dissolving 0.0218 g of PDALC (0.09073 mmol) in *n*-butanol in a 50 mL beaker. Then 2.733 mL of 0.03320 *M* $Cu(ClO_4)_2$ was added along with enough DI H_2O to make the two layers approximately equal in volume. The beaker was covered with parafilm with just the lip of the beaker uncovered. This allowed for PDALC to diffuse into the aqueous layer and complex with Cu very slowly, as each are soluble only in their respective layers. As the layers evaporated, the complex slowly crystallized out of solution. The crystals of [Cu(PDALC)]$(ClO_4)_2$ were separated and dried under vacuum. IR analysis and X-ray crystallography were performed on the [Cu(PDALC)]$(ClO_4)_2$ crystals.

[Gd(PDALC)]$(NO_3)_2$ crystal preparation

The synthesis of [Gd(PDALC)]$(NO_3)_2$ crystals was carried out by first dissolving 0.0257 g of PDALC (0.1070 mmol) in *n*-butanol in a 50 mL beaker. Then 3.84 mL of 0.02783 *M* $Gd(NO_3)_3$ was added along with enough DI H_2O to make the two layers approximately equal in volume. The beaker was covered with parafilm with just the lip of the beaker uncovered. This allowed for PDALC to diffuse into the aqueous layer and complex with Gd very slowly, as each are soluble only in their respective layers. As the layers evaporated, the complex slowly crystallized out of solution. The crystals of [Gd(PDALC)]$(NO_3)_2$ were separated and dried under vacuum. IR analysis and X-ray crystallography experiments were performed on the [Gd(PDALC)]$(NO_3)_2$ crystals.

[Mg(PDALC)]$(ClO_4)_2$ crystal preparation

The synthesis of [Mg(PDALC)]$(ClO_4)_2$ crystals was carried out by first dissolving 0.0200 g of PDALC (0.08324 mmol) in *n*-butanol in a 50 mL beaker. Then 83 μL of 0.9983 *M* $Mg(ClO_4)_2$ was added along with enough DI H_2O to make the two layers approximately equal in volume. The beaker was covered with parafilm with just the lip of the beaker uncovered. This allowed for PDALC to diffuse into the aqueous layer and complex with Mg very slowly as each are soluble in their respective layers. As the layers evaporated, the complex slowly crystallized out of solution. The crystals of [Mg(PDALC)]$(ClO_4)_2$ were separated and dried under vacuum. IR analysis and X-ray crystallography were performed on the [Mg(PDALC)]$(ClO_4)_2$ crystals.

[Ni(PDALC)]Cl_2 crystal preparation

The synthesis of [Ni(PDALC)]Cl_2 crystals was carried out by first dissolving 0.0209 g of PDALC (0.08699 mmol) in *n*-butanol in a 50 mL beaker. Then 873 μL of 0.09969 *M* $NiCl_2$ was added along with enough DI H_2O to make the two layers approximately equal in volume. The beaker was covered with parafilm with just the lip of the beaker uncovered. This allowed for PDALC to diffuse into the aqueous layer and complex with Ni very slowly, as each are soluble only in their respective layers. As the layers evaporated, the complex slowly crystallized out of solution. The crystals of [Ni(PDALC)]Cl_2 were separated and dried under vacuum. IR analysis and X-ray crystallography were performed on the [Ni(PDALC)]Cl_2 crystals.

[Pb(PDALC)$(ClO_4)_2$]·H_2O crystal preparation

The synthesis of [Pb(PDALC)$(ClO_4)_2$]·H_2O crystals was carried out by first dissolving 0.0154 g of PDALC (0.06410 mmol) in *n*-butanol in a 50 mL beaker. Then 1.933 mL of

0.03316 *M* $Pb(ClO_4)_2$ was added along with enough DI H_2O to make the two layers approximately equal in volume. The beaker was covered with parafilm with just the lip of the beaker uncovered. This approach allowed for PDALC to diffuse into the aqueous layer and complex with Pb very slowly, as each are soluble only in their respective layers. As the layers evaporated, the complex slowly crystallized out of solution. The crystals of $[Pb(PDALC)(ClO_4)_2]\cdot H_2O$ were separated and dried under vacuum. IR analysis and X-ray crystallography were performed on the $[Pb(PDALC)(ClO_4)_2]\cdot H_2O$ crystals.

$[Zn(PDALC)](ClO_4)_2$ crystal preparation

The synthesis of $[Zn(PDALC)](ClO_4)_2$ crystals was carried out by first dissolving 0.0308 g of PDALC (0.1282 mmol) in *n*-butanol in a 50 mL beaker. Then 3.847 mL of 0.03332 *M* $Zn(ClO_4)_2$ was added along with enough DI H_2O to make the two layers approximately equal in volume. The beaker was covered with parafilm with just the lip of the beaker uncovered. This approach allowed for PDALC to diffuse into the aqueous layer and complex with Zn very slowly, as each are soluble only in their respective layers. As the layers evaporated, the complex slowly crystallized out of solution. The crystals of $[Zn(PDALC)](ClO_4)_2$ were separated and dried under vacuum. IR analysis and X-ray crystallography were performed on the $[Zn(PDALC)](ClO_4)_2$ crystals.

RESULTS AND DISCUSSION

Synthesis of PDALC

The synthesis used in the preparation of 1,10-phenanthroline-2,9-bis(hydroxymethyl) (PDALC) was not efficient in producing pure product. The first step, synthesizing 1,10-

phenanthroline-2,9-dicarboxaldehyde (PDALD) resulted in an impure mixture. The synthesis produced a 28.3% yield of impure product. This recovery is fairly low compared to the 45.5% recovery by Darren Melton[29] and 70% recovery reported by Chandler, *et. al.*,[28] and indicates that some of the product was lost somewhere in the recovery process. The selenium dioxide was effective in oxidizing 2,9-dimethyl-1,10-phenanthroline monohydrate into PDALD, as the ^{1}H-NMR spectrum shows this to be the major product as shown in Figure 4. The ^{1}H-NMR spectrum showed a peak for the aldehyde proton at 10.35 ppm, as well as the aromatic hydrogens on the phenanthroline ring at 8.29 (H5,6, singlet), 8.31 (H 3,8, doublet), and 8.80 (H4,7, doublet) ppm. Chandler, *et. al.*[28] report values of 10.45 ppm for the aldehyde proton and 8.25, 8.30, and 8.75 ppm, respectively, for the aromatic hydrogens. The IR spectrum of PDALD, shown in Figure 5, yielded a C=O stretch for the aldehyde at 1703 cm^{-1}. There was also a peak at 1737 cm^{-1} that closely matched the C=O stretch for 1,10-phenanthroline-2,9-dicarboxylic acid (PDA). A C=O stretch of 1720 cm^{-1} for PDALD was reported by Chandler, *et. al.*,[28] which is not in agreement with the IR data obtained for this synthesis. The final step in the synthesis involved using sodium borohydride, which was used to reduce the aldehyde groups to alcohol groups.

The target ligand of this synthesis is PDALC, which was prepared from impure PDALD. The second step of the synthesis produced a yield of 45.1% of pure PDALC after recrystallization from H_2O which is again lower than the reported recovery of 68% by Chandler, *et. al*.[28] The melting point of the fine, very pale pink needles was 196-197 °C compared to the literature value[11] which was reported as 197-198 °C with decomposition. The sodium borohydride was effective in reducing PDALD into PDALC, as shown by the ^{1}H-NMR spectrum in Figure 6. The ^{1}H-NMR spectrum showed a peak for the alcohol proton at 5.64 ppm (triplet), a peak for the -CH_2- protons at 4.88 ppm (doublet), as well as the aromatic

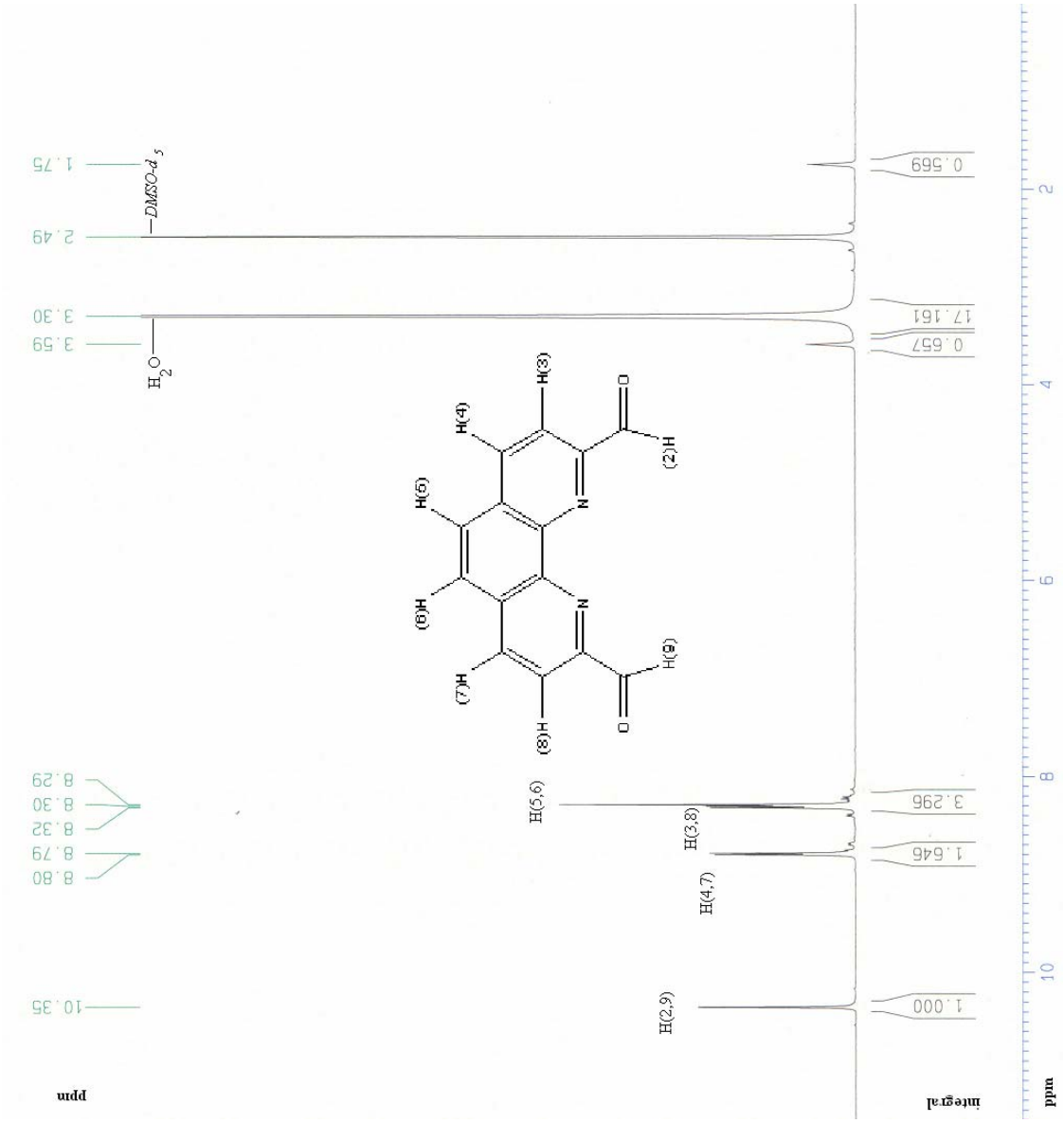

Figure 4: The ^{1}H-NMR spectrum of impure 1,10-phenanthroline-2,9-dicarboxaldehyde in DMSO-d_6.

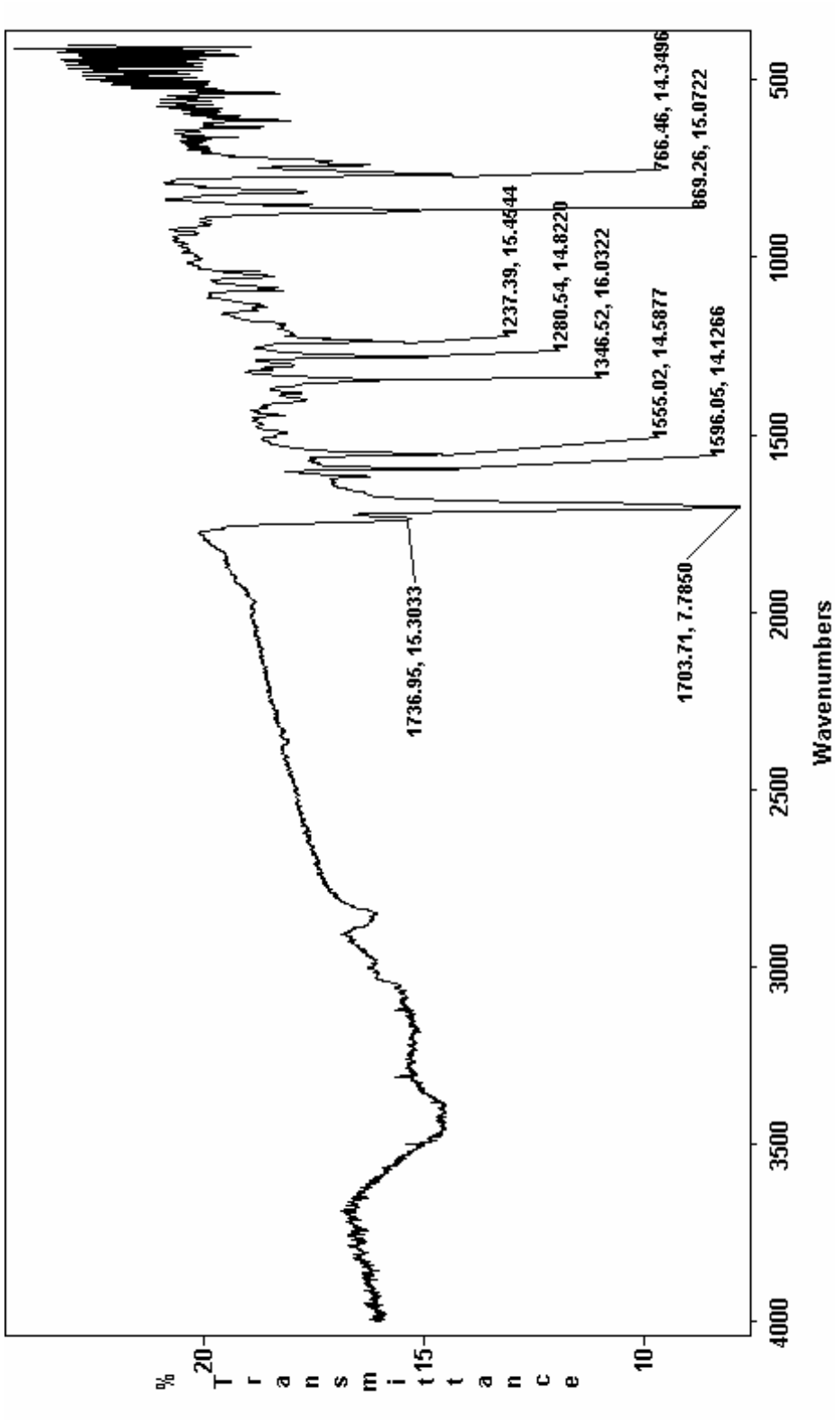

Figure 5: IR spectrum of 1,10-phenanthroline-2,9-dicarboxaldehyde.

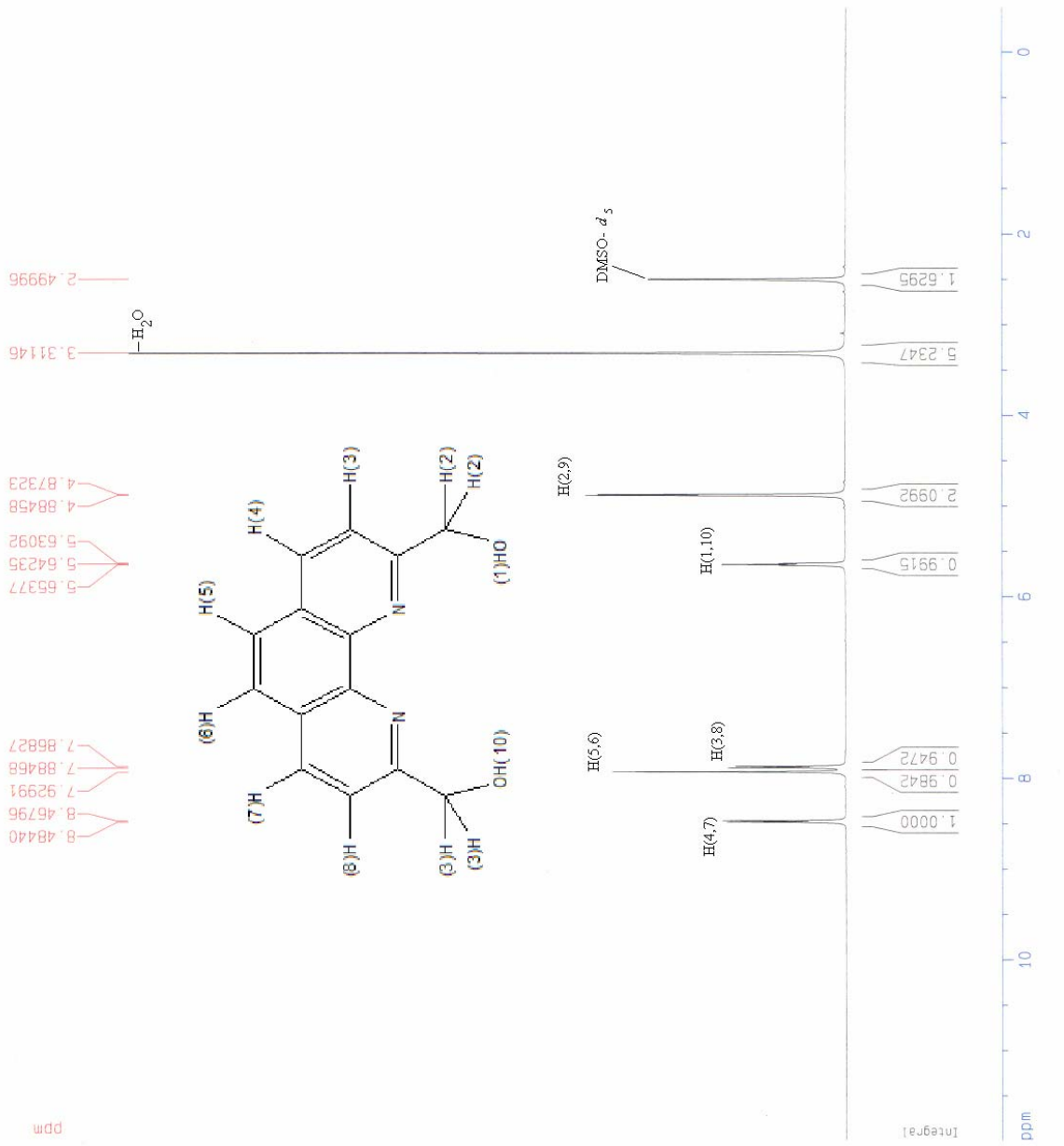

Figure 6: The ^{1}H-NMR spectrum of 2,9-Bis(hydroxymethyl)-1,10-phenanthroline in DMSO-d_6.

protons on the phenanthroline ring at 7.87 (H3,8, doublet), 7.92 (H 5,6, singlet), and 8.47 (H4,7, doublet) ppm. Chandler, *et. al*.[28] report values of 5.65 ppm for the alcohol proton, 4.95 for the -CH_2- proton, and 7.90, 7.95, and 8.50 ppm, respectively, for the aromatic hydrogens. The IR spectrum of PDALC, shown in Figure 7, yielded an O-H stretch for the alcohol at 3000-3500 cm^{-1}. The peaks at 1703 and 1737 cm^{-1} that closely matched the C=O stretch for PDALD and PDA were not present in the IR spectrum. An OH stretch of 3000-3600 cm^{-1} for PDALC was reported by Chandler, *et. al.*,[28] which is in agreement with the IR data obtained for this synthesis. The likely impurity from the synthesis of PDALD was overoxidation of the aldehyde groups to carboxylic acid groups. Upon reaction with sodium borohydride, the carboxylic acid groups would form a carboxylate salt which would be soluble in H_2O, making it simple to separate from PDALC when recrystallized in H_2O.

UV-Vis spectrophotometric titrations Involving PDALC

The titrations were carried out using UV/Vis spectroscopy as an analytical tool to detect metal complex formation involving PDALC. Absorbance scans were recorded from 190 to 350 nm for each titrant addition of $HClO_4$. Absorbance data were taken at selected wavelengths of 228, 237, 260, 271, 279, and 293 nm. Absorbance maxima were shown at 228 and 271 nm for the free PDALC. Upon complexation of PDALC with a metal ion, a peak shift from 271 to 279 nm was observed.

In order to determine the protonation constants for the ligand, PDALC, titrations were carried out at 25.0 ± 0.1 °C in 0.10 *M* $NaClO_4$ to maintain ionic strength at 0.1. Figure 8 shows absorbance versus wavelength (nm) scans at different pH values for the titration of PDALC. Absorbances at 228, 237, 260, and 271 nm for each spectrum were used to generate plots of absorbance versus pH. The best plots, those which experienced a large change in absorption

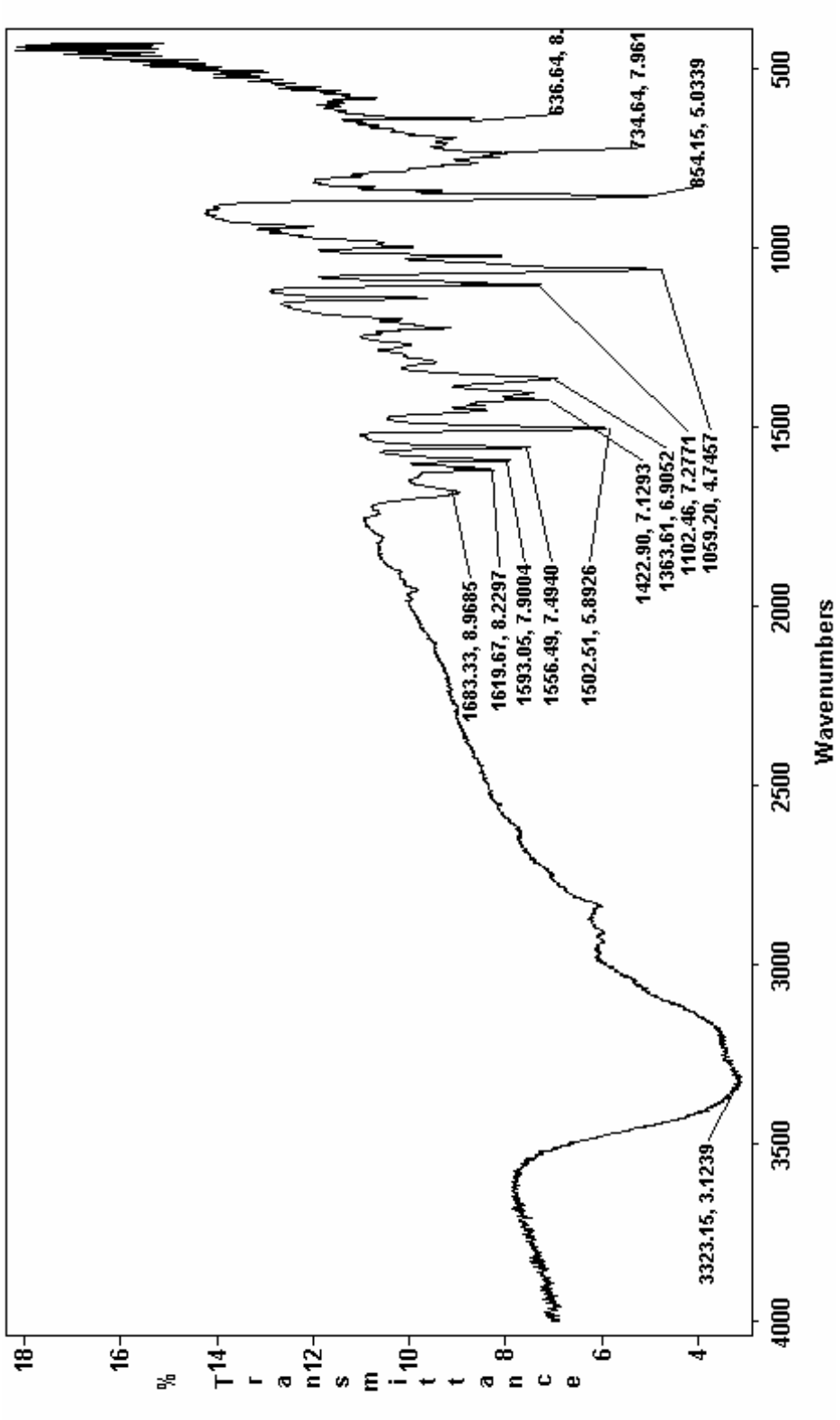

Figure 7: IR spectrum of 2,9-Bis(hydroxymethyl)-1,10-phenanthroline.

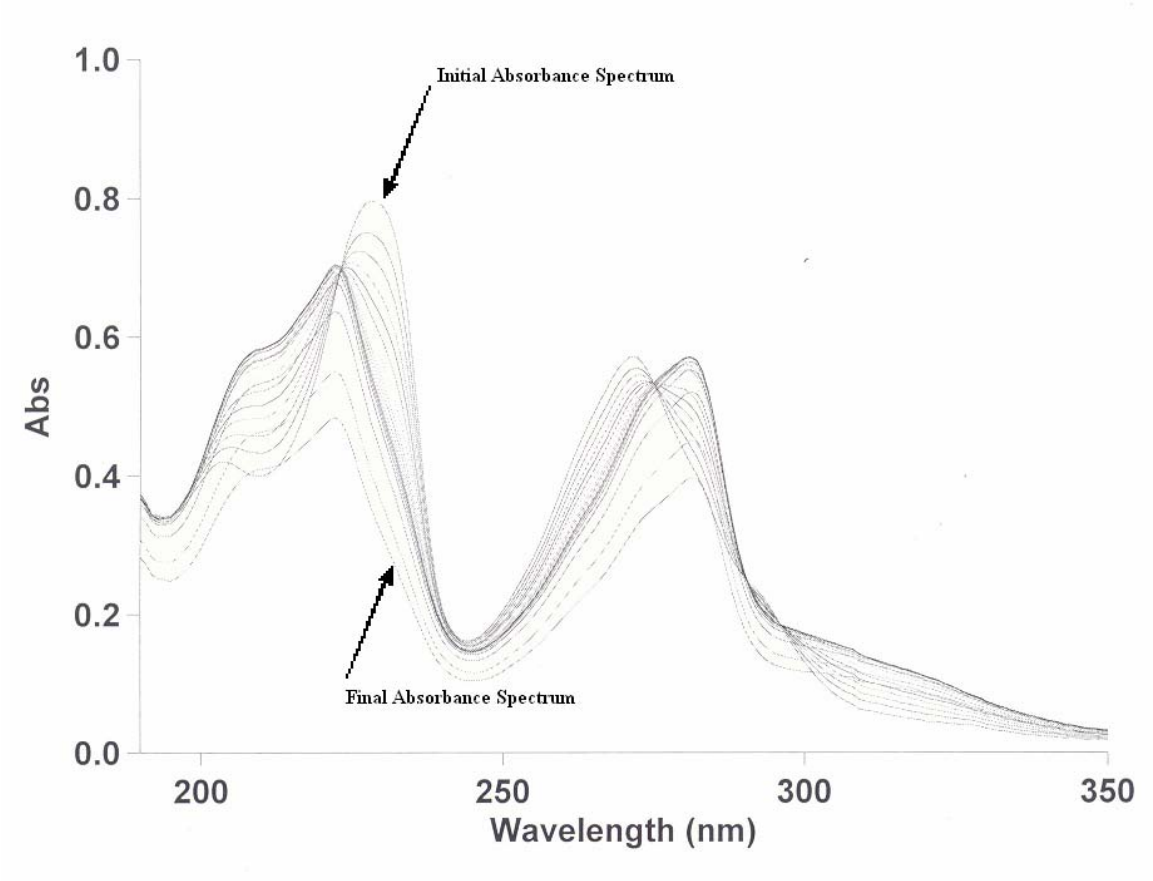

Figure 8: Absorbance versus wavelength (nm) spectra from the titration experiment conducted at 25.0 ± 0.1 °C for PDALC in 0.10 *M* $NaClO_4$ at pH values ranging from an initial pH of 5.29 to a final pH of 1.42.

during the titration, were observed from the data taken at these wavelengths for the absorbance spectra. The titration of PDALC (L in equation 1 below) with no metals present was monitored as a function of absorbance versus pH, and as dissociation occurs following Equation 1.

$$LH^+ \leftrightarrows L + H^+ \quad (1)$$

For each titration experiment, absorbance values were monitored as a function of pH. Corrected absorbance values were plotted versus pH at the selected wavelengths (Figure 9) using EXCEL. Using Equation (2), recorded absorbance values were corrected for dilution after each addition of titrant.

$$\text{Corrected Absorbance} = \frac{\text{Absorbance} \cdot V_{total}}{V_{initial}} \quad (2)$$

The absorbances of the plots were constant at lower pH values, where only the free-PDALC ligand occurs. As the pH was increased, the peak shifted due to the formation of the deprotonated form of PDALC, as shown in Equation 1. This crossover produced a slope for which a pH_{50} value was obtained. The 'SOLVER' module of EXCEL was used to fit a theoretical $\bar{n}$ *vs.* pH curve to fit Figure 9, which gave a pK_a for $PDALCH^+$ of 4.65 ± 0.01. The pH_{50} value is an inflection point in the slope where an equal distribution of the metal ion exists between the free metal and PDALC-metal complex. In the presence of a metal ion, complex-formation displaces the pH_{50} to lower pH, from which the log K_1 for the metal ion can be calculated. In order to obtain the pH_{50}, pH and absorbance values of 228, 237, 260, 271, 279, and 293 nm were selected for the slope for the metal ion. An $\bar{n}$ calculation was performed for the slope using Equation (3). In this equation, Abs_{ini} is the corrected absorbance for $PDALCH^+$ and Abs_{inf} is the corrected absorbance of PDALC.

$$\bar{n} = \frac{Abs - Abs_{ini}}{Abs_{inf} - Abs_{ini}} \quad (3)$$

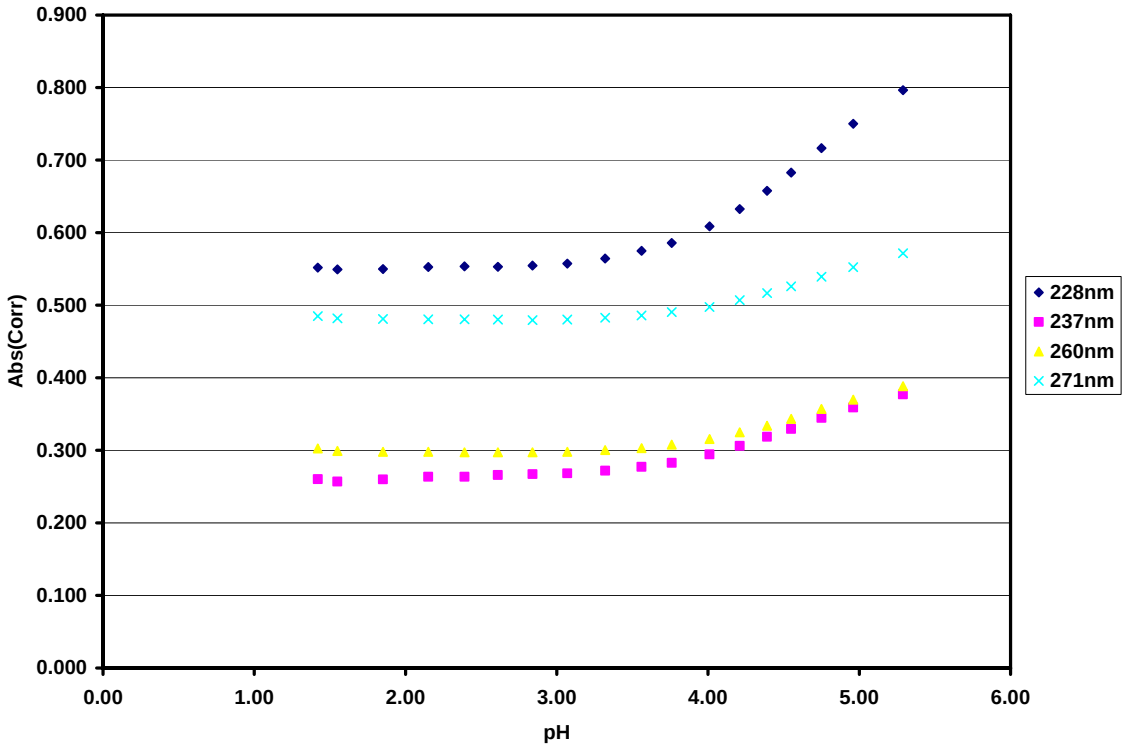

Figure 9: Combined plot of corrected absorbance data versus pH for wavelengths 228 nm, 237 nm, 260 nm, and 271 nm for determining the protonation constant of PDALC of 4.65 in 0.1 *M* $NaClO_4$ at 25 ± 0.1 °C.

The total ligand concentration, $[L]_{total}$, in the sample solution was also calculated using Equation (4) which corrects the initial ligand concentration for dilution from the titration additions.

$$[L]_{total} = \frac{[L]_{ini} \cdot V_{ini}}{V_{total}} \quad (4)$$

After the $\bar{n}$ values and the total ligand concentrations were known, the distribution between the complexed ligand, [ML] and the free ligand, [L], was calculated using Equations (5) and (6) where $\bar{n}$ is the ratio of the metal complexed to the free metal in solution.

$$[ML] = \bar{n} \cdot [L]_{total} \quad (5)$$

$$[L] = [L]_{total} - [ML] \quad (6)$$

The total hydrogen ion concentration, $[H^+]$, in the sample solution was calculated using Equation (7).

$$[H^+] = 10^{-pH} \quad (7)$$

The values obtained from Equations (5), (6), and (7) were used to calculate pH_{50} in Equation (8), where L is PDALC.

$$pH_{50} = \frac{[ML]}{[L][H^+]} \quad (8)$$

The stability constant, log K_1, was calculated for each metal ion with PDALC using Equation (9) where $p[metal]_{50}$ is the negative of the log of the concentration of free metal in solution after half of the ligands in solution are complexed.

$$\text{Log K (PDALC-M)} = \Delta\ pK_a + p[metal]_{50} \quad (9)$$

The protonation constant for PDALC was calculated using the absorbance data and pH values from these plots. The protonation constant (pK_a) for $PDALCH^+$ was measured here to be 4.65 ± 0.01. The species distribution diagram of PDALC, shown in Figure 10, gives the fraction

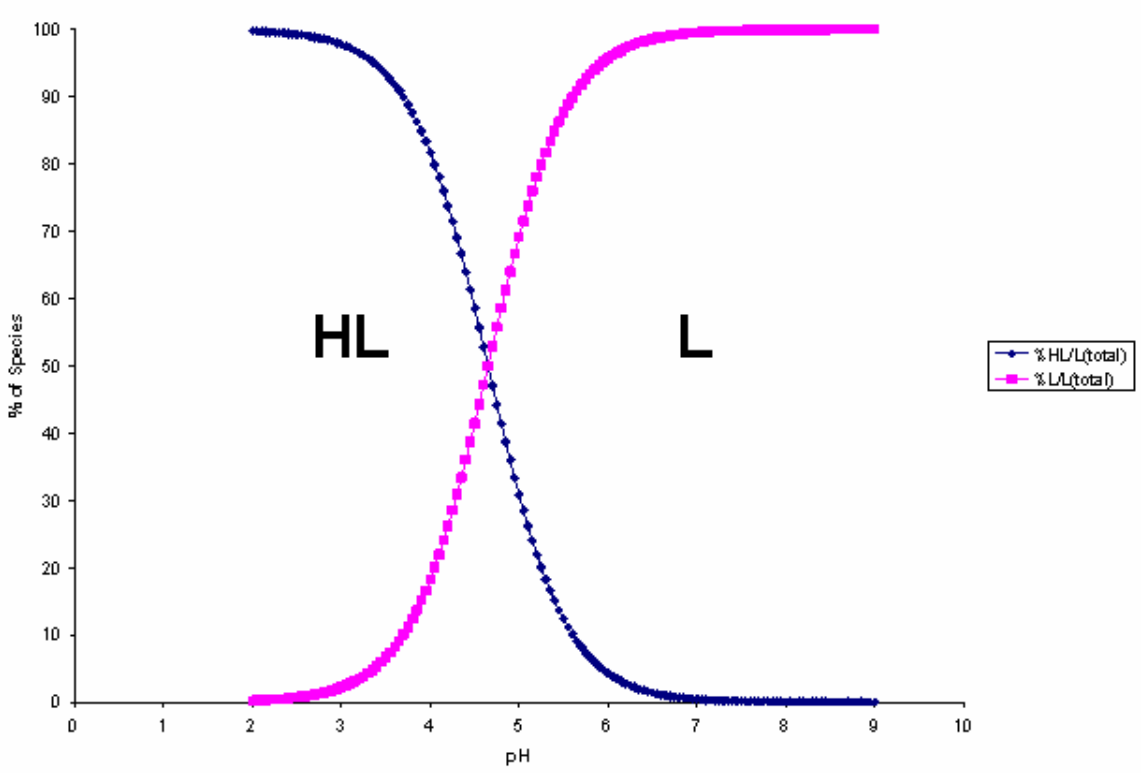

Figure 10: Species distribution diagram for protonation of PDALC with respect to pH.

of LH and L relative to pH, where L is the unprotonated PDALC. An illustration of the proposed site of protonation of PDALC in the protonation equilibrium is shown in Figure 11.

UV-Vis spectrophotometric titrations involving metals with PDALC

The formation constants for each metal ion with PDALC were determined by first calculating a new pK_a (Equation 1-8) and taking the difference of the pK_a values relative to that of the free ligand, and then adding the negative of the log of the concentration of free metal when half of the ligand is complexed, p[metal]$_{50}$ (Equation 9). The titration experiment provided absorbance values that varied as a function of pH for the metal ion with PDALC. For most metal ions, the protonation of the ligand was still observable within an effective pH range.

For some metal ions, the new protonation of the PDALC in the presence of a metal ion was found to be too low. If the log K_1 values for the metal ions with PDALC were too high it was difficult to drive out the metal ion from a PDALC complex with a direct titration experiment with acid. In order to solve this problem, a second titration was carried out in which PDALC and the ligand EGTA which would compete for the metal ion with PDALC. EGTA is a octadentate ligand that has log K_1 values that are slightly higher than the tetradentate ligand, PDALC. The equilibrium being studied is given by Equation (10).

$$M^{n+}(EGTA)^{4-} + PDALC + H^+ \leftrightarrows M^{n+}(PDALC) + [(EGTA)H]^{3-} \qquad (10)$$

PDALC is able to compete with EGTA in equation 10 because of the much higher pK_a values[28] of 9.32 and 8.71, compared to only 4.65 for PDALC. Equation 10 shows the exchange equilibrium of the metal ion between PDALC and EGTA as a function of pH. The equilibrium was readily studied by monitoring absorbance since EGTA does not have a significant absorption band in the UV region due to a lack of conjugation in the molecule. The titration

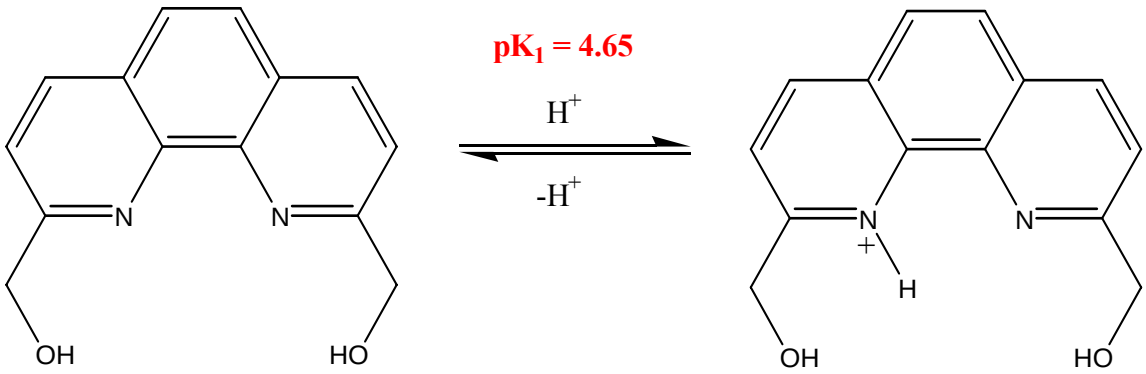

Figure 11: Diagram showing the proposed protonation event of PDALC.

experiment provided absorbance values as a function of pH for the competition of EGTA and PDALC for the metal ion. As the pH of the solution was lowered, a transition was observed where Equation (1) shifts from left to right. The pK_1, first protonation constant, for EGTA is 9.32 at an ionic strength of 0.10 *M* $NaClO_4$.[21] PDALC is a weaker proton base and has a much lower pK_1 at 4.65 for an ionic strength of 0.10 *M* $NaClO_4$. These large differences in pK_1 values allow PDALC to complex the metal ion strongly at lower pH values relative to EGTA. The direct titration experiment of PDALC with the metal ion was used only as a reference for competition reactions involving PDALC and EGTA with a metal ion, useful for determining the log*K* values of the MLOH of MLH_{-1}. For some metal-PDALC complexes, a proton can be lost from either a coordinated water molecule or from an alcohol group of PDALC. This is referred to as MLOH when the water molecule loses a proton and MLH_{-1} when the ligand loses a proton. For the studies here, it is unknown which event actually happens, so the two terms are used to refer to a proton being lost from the complex.

For these competition experiments, a new calculation was necessary. For these experiments, the competing ligand needed to factor into the stability constant calculation from the equilibrium shown in Equation (10) is shown in Equation (11)

$$\log K_1\,(\text{PDALC}) = \log K_1\,(\text{EGTA}) - \text{p}K_1\,(\text{EGTA}) + \text{pH}_{50} \qquad (11)$$

The formation constants (log K_1) values determined here for PDALC are shown in Table 1, along with log K_1 values for EDDE and 1,10-phenanthroline for comparison.

The best size of metal ion for coordination with PDALC can be determined by molecular mechanics (MM).[30] The strain energy (U) of a generalized PDALC complex can be calculated as a function of metal ion size, and the minimum in such a curve indicates the best-fit size of metal ion for coordinating with PDALC. MM calculations using HyperChem5.11 showed an

energy minimum for PDALC with metal ions of ionic radius around 1.20 Å, such as Sr(II) and Pb(II). For metal ions around this size, very low steric strain was observed. As the size of the metal ion was increased, such as with Ba(II), the steric strain increased slightly. As the size of the metal ion was decreased, such as with Zn(II), the steric strain also increased, but much more quickly. Calculations with MM produced energy ($kcal \cdot mol^{-1}$) which was plotted versus the metal-nitrogen (M-N) bond length as illustrated in Figure 12. The stability constants, log K_1 values, measured here for PDALC showed that the metal ion selectivity is more complicated than simply the size of the metal ion because the increase in complex formation strength is not a linear relationship with ionic radius. This complication could be due to the flexibility of the hydroxymethyl groups of PDALC which reduces the preorganization and allows complexation with metal ions that do not fit the ideal size.

The stability constants showed that the addition of the hydroxymethyl groups to the 1,10-phenanthroline ligand produced increased stability for metal ions closer to 1.00 Å. When PDALC is compared with EDDE (N,N'-bis(2-hydroxyethyl)-ethylenediamine), the unpreorganized precursor of PDALC, an increase in stability is observed with metal ions that are also closer to 1.00 Å. Table 1 displays the stability constants for PDALC, EDDE, and 1,10-phenanthroline.

PDALC-barium(II) results

Barium(II) has an ionic radius of 1.36 Å and is the largest of the metal ions chosen for study. The UV absorbance spectrum for the titration of Ba(II) with PDALC is shown in Figure 13. The plot of corrected absorbance versus pH for Ba(II) is shown in Figure 14. In addition, observed and calculated $\bar{n}$ versus pH plots are shown in Figure 15. From the selected

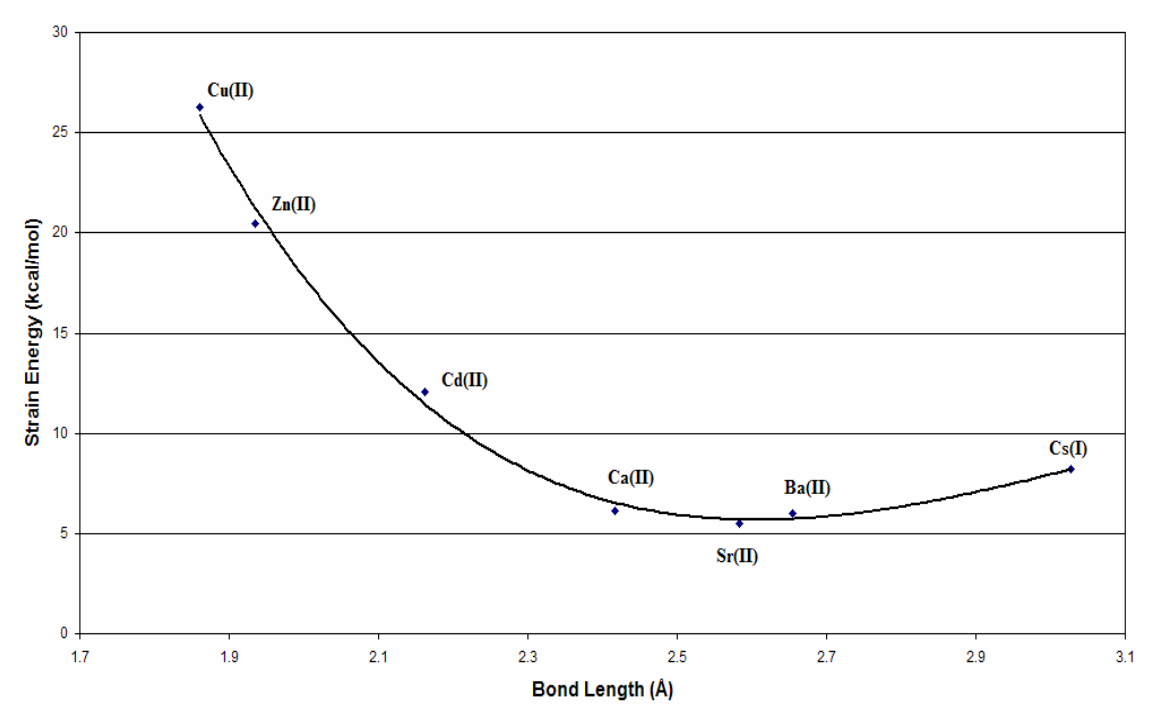

Figure 12: Calculated strain energy (kcal·mol^{-1}) versus metal-nitrogen bond length (Å) for M^{n+}-PDALC complexes using Hyperchem embedded MM+ calculations.

Table 1: a.) Comparison of log K_1 data for metal ions with PDALC, EDDE, and 1,10-phenanthroline (log K_1 data for EDDE and 1,10-phenanthroline from reference 16, except for Ca(II), La(III), and Mg(II) with EDDE (this work)) and b.) List of MLOH values for PDALC.

a.)

Metal	**Ionic Radius (Å)**	**log K_1 PDALC**	**log K_1 EDDE**	**Δ log K_1**	**log K_1 1,10-phen**	**Δ log K_1**
Ba(II)	1.36	2.02			0.4[16]	+1.6
Pb(II)	1.19	7.26	6.12[16]	+1.14	4.6[16]	+2.7
Sr(II)	1.18	2.40			0.7[16]	+1.7
La(III)	1.061	5.29	4.30	+0.99	2.1[16]	+3.2
Bi(III)	1.03	6.04			5.6[16]	+0.4
Ca(II)	0.99	3.68	1.08	+2.60	1.0[16]	+2.7
Cd(II)	0.97	7.28	5.10[16]	+2.18	5.4[16]	+1.9
Gd(III)	0.938	6.10				
In(II)	0.8	5.43			6.5[16]	-1.1
Co(II)	0.745	6.31	5.10[16]	+1.21	7.1[16]	-0.8
Zn(II)	0.74	6.51	4.80[16]	+1.71	6.4[16]	+0.1
Mg(II)	0.74	1.70	1.24	+0.46	1.5[16]	+0.2
Zr(IV)	0.72	7.89			6.6[16]	+1.3
Ni(II)	0.69	8.63	6.70[16]	+1.93	8.7[16]	-0.1
Cu(II)	0.57	7.46	9.70[16]	-2.24	9.7[16]	-2.2

b.)

Metal	**MLOH**	**$ML(OH)_2$**	**$ML(OH)_3$**	**$ML(OH)_4$**
Bi(III)	7.64	9.54	----	----
Cd(II)	8.54	----	----	----
Cu(II)	7.50	11.15	----	----
Pb(II)	8.08	9.70	----	----
Zr(IV)	4.07	6.42	7.56	9.95

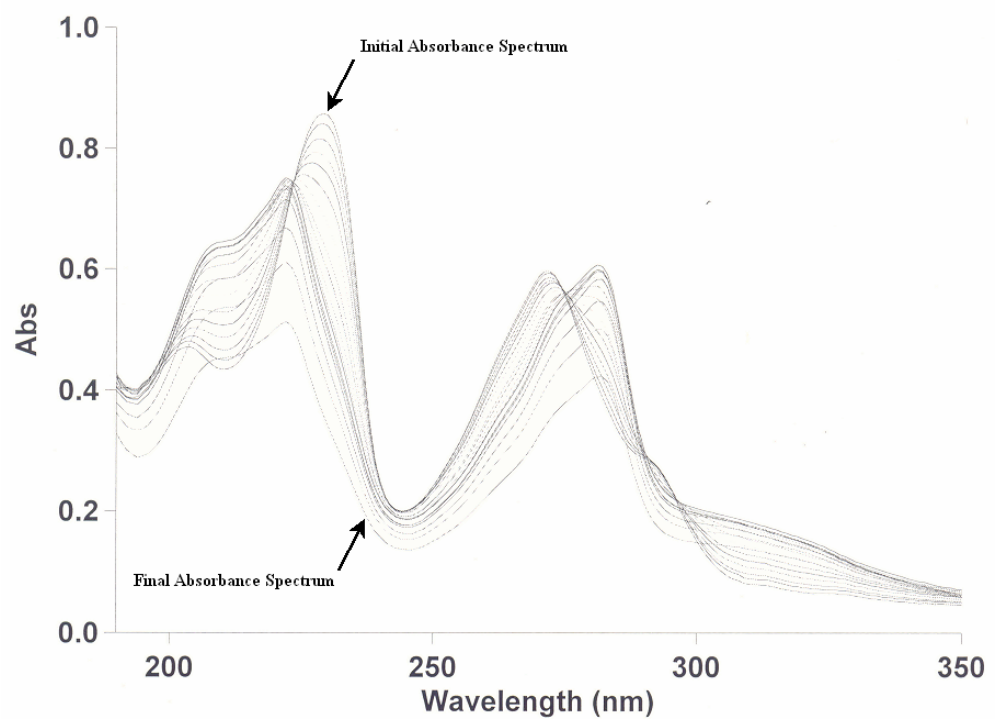

Figure 13: UV absorbance spectra for the titration of Ba(II) (0.0333 *M*) and PDALC ($2x10^{-5}$ *M*) and pH values ranging from 5.48 to 1.52 in 0.1 *M* $NaClO_4$ at 25 ± 0.1 °C.

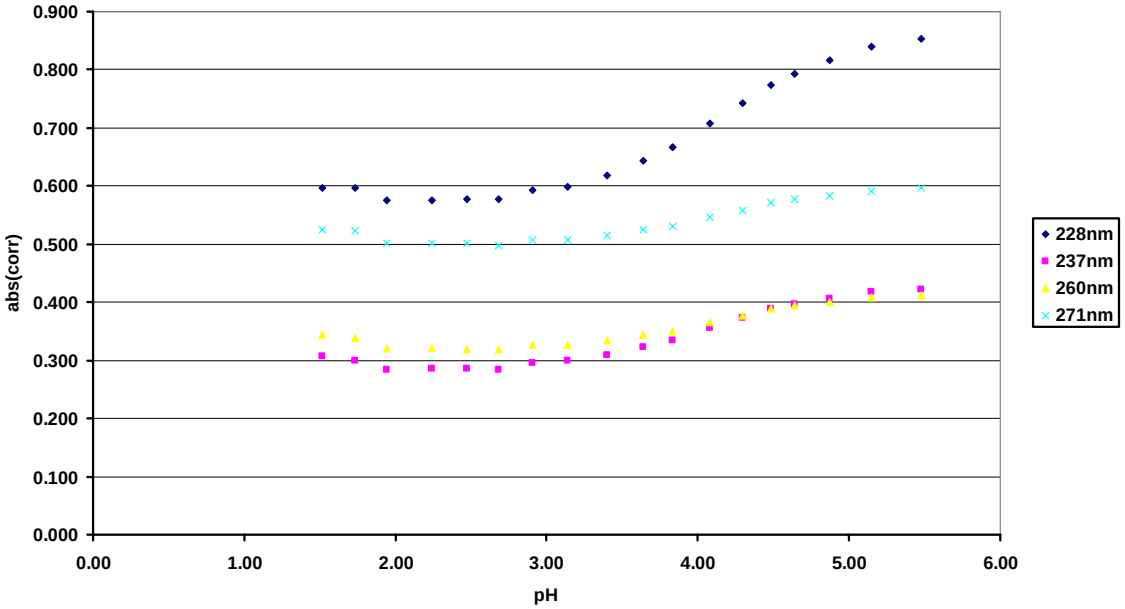

Figure 14: Combined plot of corrected absorbance data versus pH for wavelengths 228 nm, 237 nm, 260 nm, and 271 nm for the titration of PDALC ($2x10^{-5}$ *M*) with Ba(II) (0.0333 *M*) in 0.1 *M* $NaClO_4$ at 25 ± 0.1 °C.

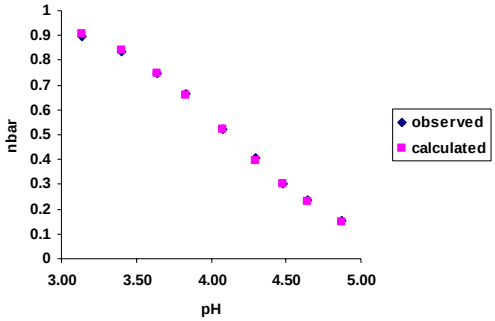

a.)

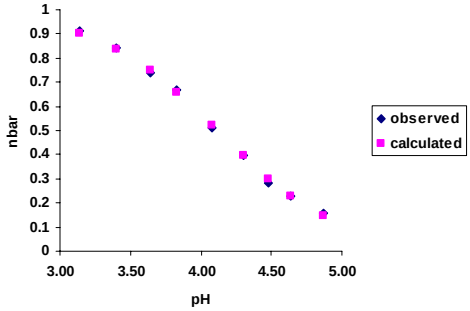

b.)

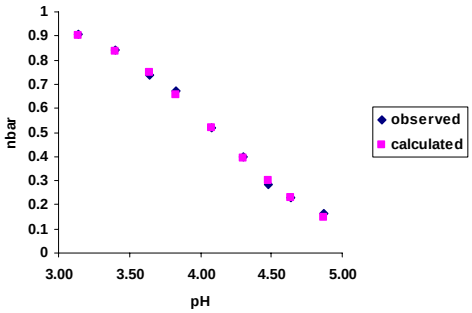

c.)

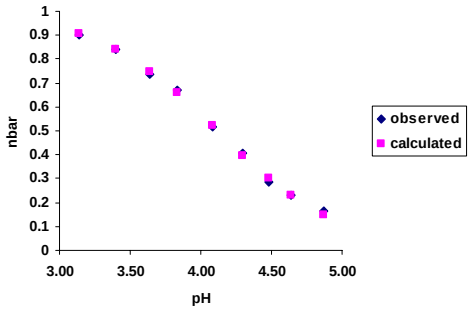

d.)

Figure 15: Comparison of $\bar{n}$ observed versus $\bar{n}$ calculated with respect to pH at wavelengths of a.) 228 nm, b.) 237 nm, c.) 260 nm and d.) 271 nm for the titration of PDALC ($2x10^{-5}$ *M*) with Ba(II) (0.0333 *M*) in 0.1 *M* $NaClO_4$ at 25 ± 0.1 °C. The theoretical curves were calculated from an apparent pK_a of 4.11.

wavelengths described above, an apparent pK_a of 4.11 and a log K_1 of 2.02 was calculated from the absorbance data using Equations (1-9). The UV absorbance spectrum appears to show a formation of a new species, but as shown in the plot of the corrected absorbance versus pH, this loss of an isosbestic point is due to dilution. When compared to the log K_1 of 1,10 phenanthroline, which is 0.4, PDALC showed an increase in complex stability.[21] This gives a Δ log K_1 of 1.6, between the log K_1 values of the PDALC and the 1,10 phenanthroline complex with Ba(II). There was no log K_1 reported for EDDE with Ba(II) to compare to PDALC with and due to the weakness of the PDALC complex with Ba(II), the log K_1 of EDDE with Ba(II) would probably not be large enough to measure with the techniques available.

PDALC-bismuth(III) results

Bismuth(III) has an ionic radius of 1.03 Å, and is a very acidic metal ion[16] which was expected to show a great affinity for the deprotonated oxygens of the alcoholic O-donor atoms in PDALC. The UV absorbance spectra are shown in Figure 16 for the titrations of Bi(III) with PDALC. An example plot of corrected absorbance versus pH for Bi(III) is shown in Figure 17. In addition, observed and calculated $\bar{n}$ versus pH plots are shown in Figure 18. From the selected wavelengths described above, a log K_1 of 6.04 was calculated for Bi(III) with PDALC using Equations (1-9). When compared to the log K_1 of 1,10 phenanthroline, which is 5.6, PDALC showed a slight increase in complex stability.[21] A Δ log K_1 of about 0.4 shows a quantitative difference in stability between the PDALC complex and the 1,10 phenanthroline complex of Bi(III). There was no log K_1 reported for EDDE with Bi(III) to compare PDALC with and because of the acidic nature of the Bi(III) and its low solubility, the log K_1 of EDDE could not be measured with the techniques available. In addition to the protonation event at 3.61

a.)

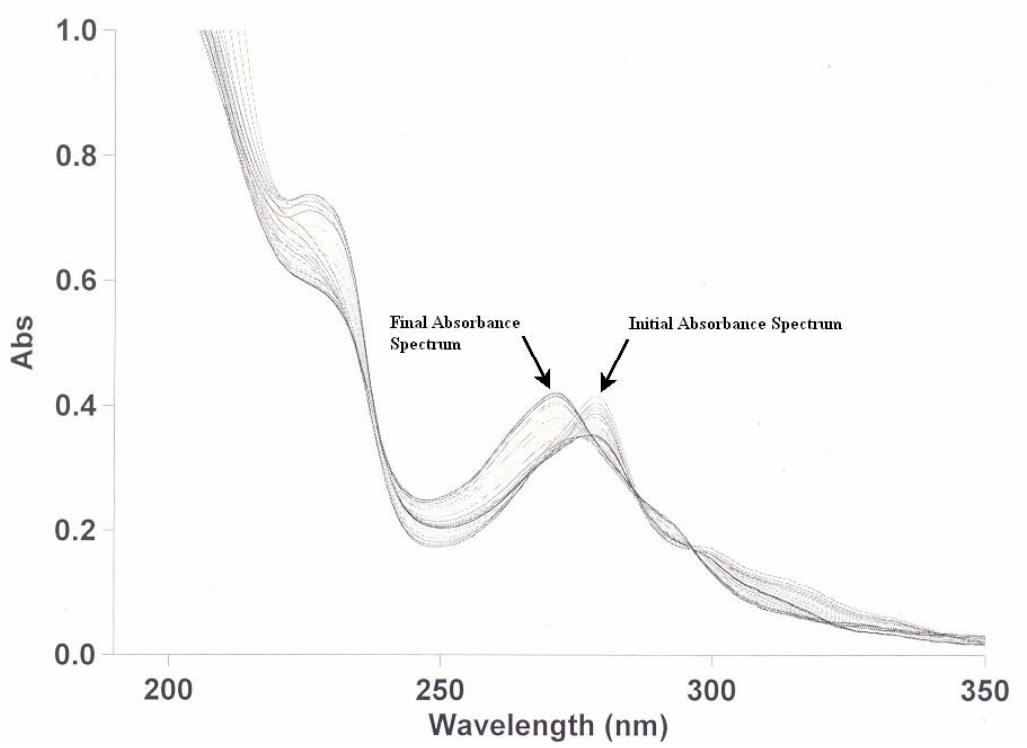

b.)

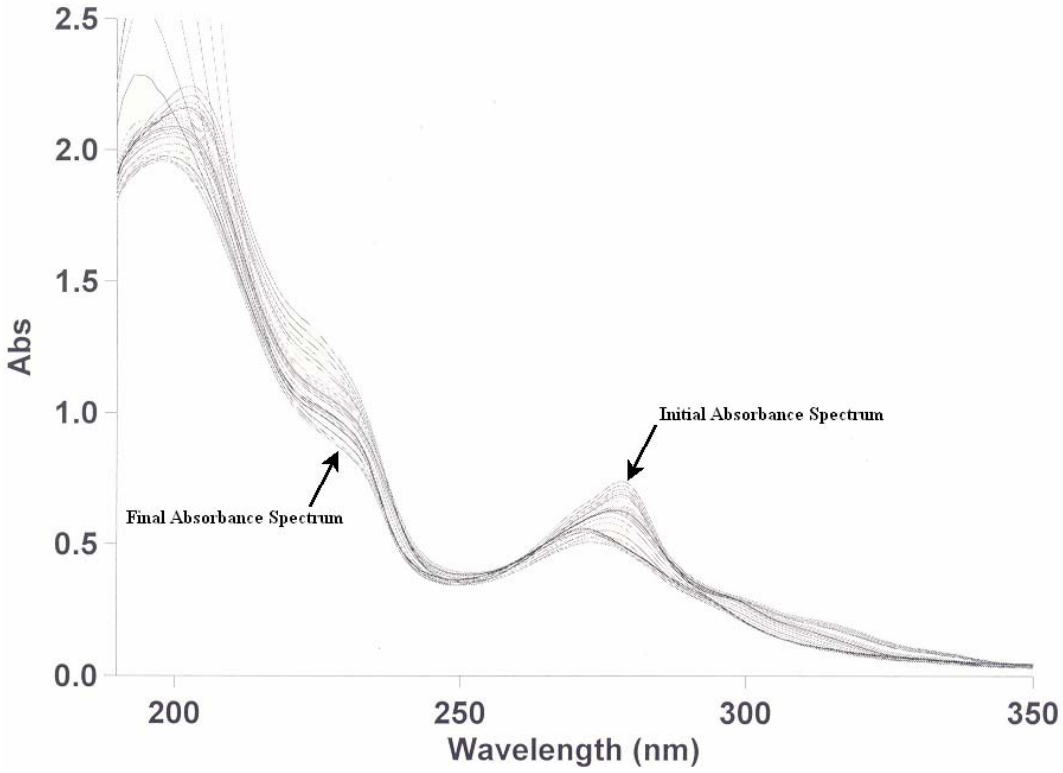

Figure 16: UV absorbance spectra for the titration of a.) 1:1 Bi(III) and PDALC at $2x10^{-5}$ *M* with the pH ranging from 2.28 to 11.67 and b.) 1:1 Bi(III) and PDALC at $4x10^{-5}$ *M* with the pH ranging from 2.24 to 11.78 in 0.1 *M* $NaClO_4$ at 25 ± 0.1 °C.

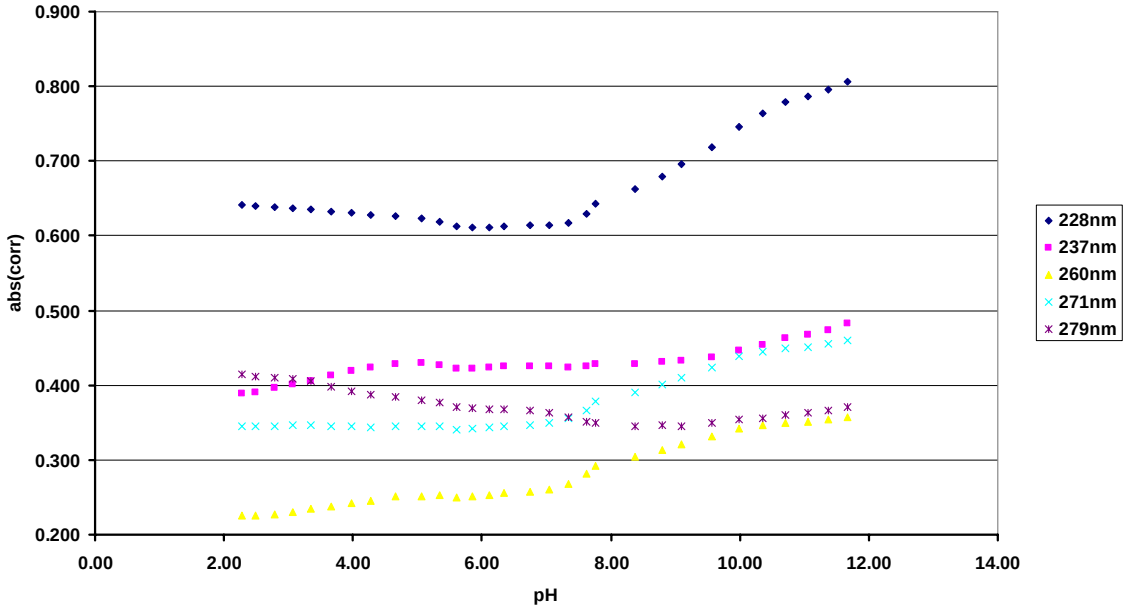

Figure 17: Combined plot of corrected absorbance data versus pH for wavelengths 228 nm, 237 nm, 260 nm, 271 nm, and 279 nm for the titration of PDALC ($2x10^{-5}$ *M*) with Bi(III) ($2x10^{-5}$ *M*) in 0.1 *M* $NaClO_4$ at 25 ± 0.1 °C.

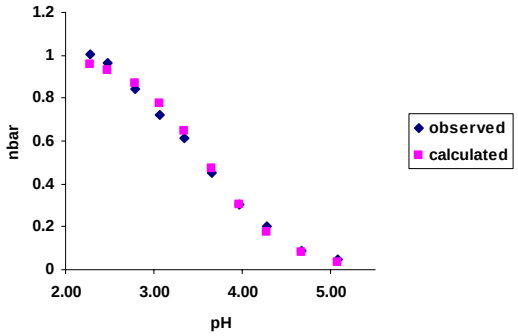

a.)

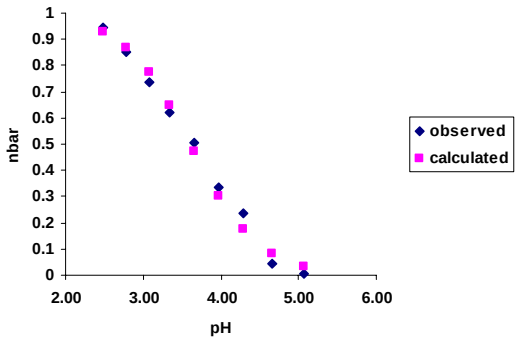

b.)

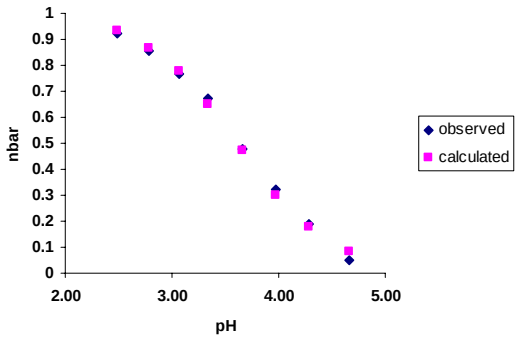

c.)

Figure 18: Comparison of $\bar{n}$ observed versus $\bar{n}$ calculated with respect to pH at wavelengths of a.) 237 nm, b.) 260 nm, and c.) 293 nm for the titration of PDALC (2×10^{-5} *M*) with Bi(III) (2×10^{-5} *M*) in 0.1 *M* $NaClO_4$ at 25 ± 0.1 °C. The theoretical curves were calculated from an apparent pK_a of 3.61.

which corresponded to demetallation of the ligand, other events were observed at pH 7.64 and 9.54 which are proposed to correspond to deprotonation of the coordinated alcoholic groups. These values were calculated as deprotonation events using the same calculations as for the deprotonation of the protonated ligand. The following equations show the protonation and deprotonation events of the Bi-PDALC complex:

$$[Bi(PDALC)]^{3+} + H^{+} \leftrightarrows Bi^{3+} + PDALCH^{+} \qquad pK = 3.61$$

$$[Bi(PDALC)]^{3+} \leftrightarrows H^{+} + [Bi(PDALC)H_{-1}]^{2+} \qquad pK = 7.64$$

$$[Bi(PDALC)H_{-1}]^{2+} \leftrightarrows H^{+} + [Bi(PDALC)H_{-2}]^{1+} \qquad pK = 9.54$$

PDALC-cadmium(II) results

Cadmium(II) has an ionic radius of 0.95 Å, and is a acidic metal ion which was expected to show a great affinity for the oxygens of the alcohol donor atoms in PDALC. The UV absorbance spectra are shown in Figure 19 for the titration of Cd(II) with PDALC. A example plot of corrected absorbance versus pH for Cd(II) is shown in Figure 20. In addition, observed and calculated $\bar{n}$ versus pH plots are shown in Figure 21 for the log K_1 and Figure 22 for MLOH. From the selected wavelengths described above, a log K_1 of 7.28 was calculated for Cd(II) with PDALC using Equations (1-9). When compared to the log K_1 of EDDE, which is 5.10, PDALC showed an increase in complex stability.[21] A Δ log K_1 of about 2.18 shows a quantitative difference in stability between the PDALC complex and the EDDE complex of Cd(II). When compared to the log K_1 of 1,10 phenanthroline, which is 5.4, PDALC showed an increase in complex stability with Cd(II).[21] A Δ log K_1 of about 1.9 shows a quantitative difference in stability between the PDALC complex and the 1,10 phenanthroline complex of

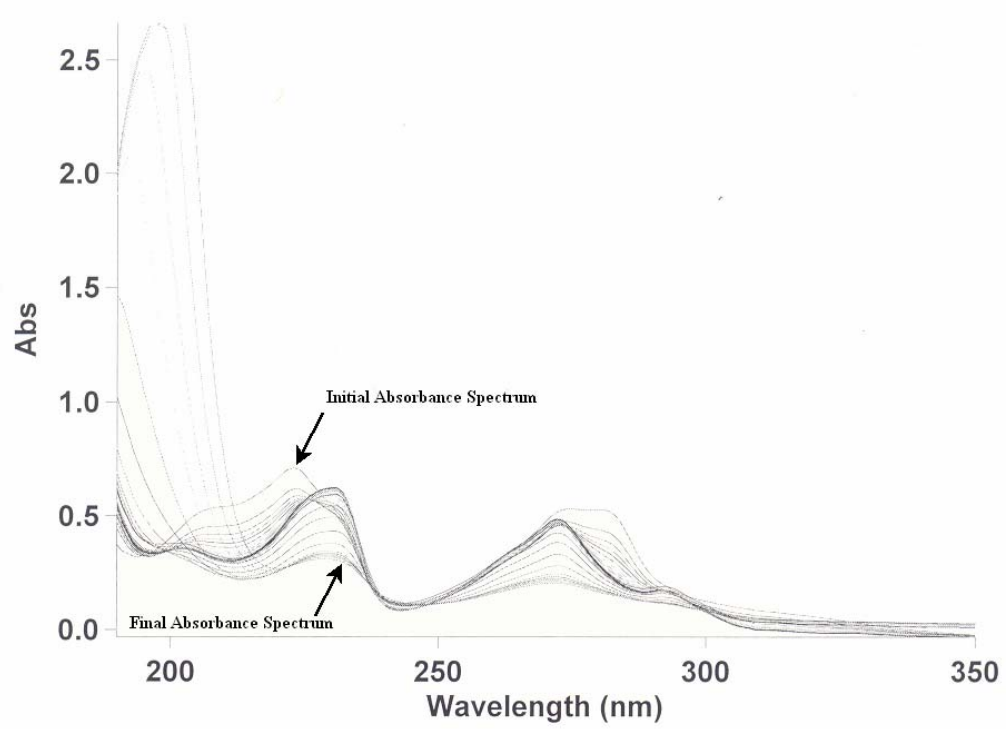

Figure 19: UV absorbance spectra for the titration of 1:1 Cd(II) and PDALC at $2x10^{-5}$ *M* with the pH ranging from 1.55 to 11.55 in 0.1 *M* $NaClO_4$ at 25 ± 0.1 °C.

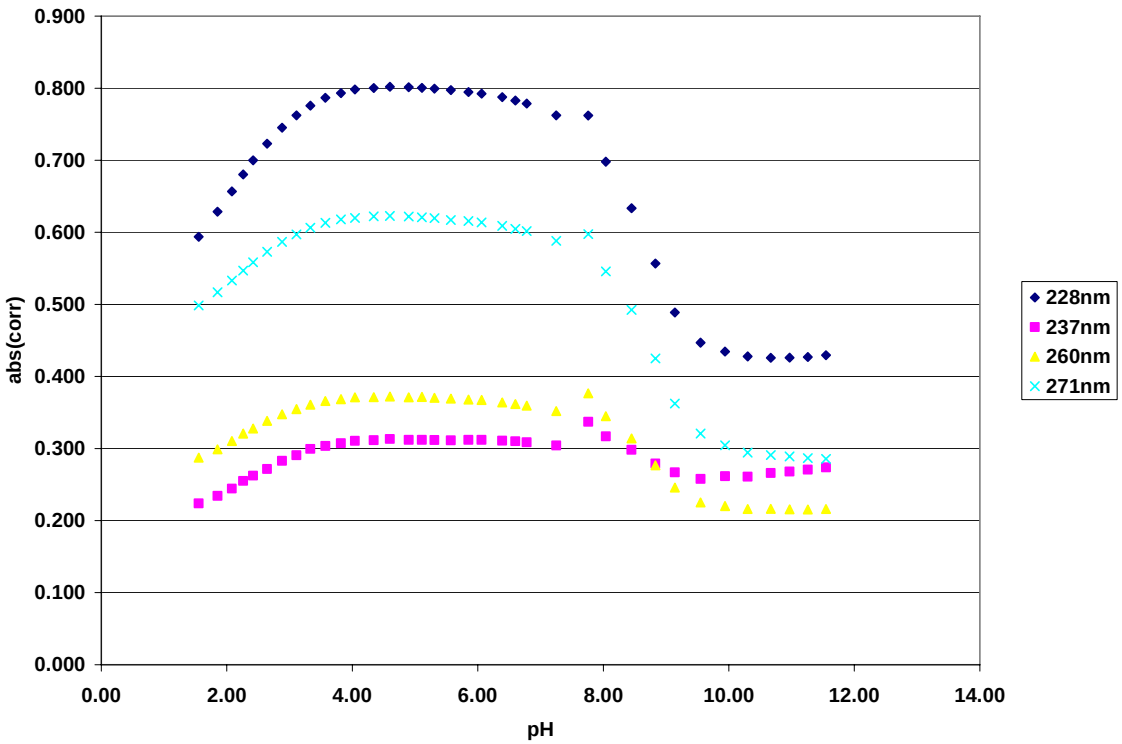

Figure 20: The combined plot of corrected absorbance data versus pH for wavelengths 228 nm, 237 nm, 260 nm, and 271 nm for the titration of PDALC ($2x10^{-5}$ *M*) with Cd(II) ($2x10^{-5}$ *M*) in 0.1 *M* $NaClO_4$ at 25 ± 0.1 °C.

a.)

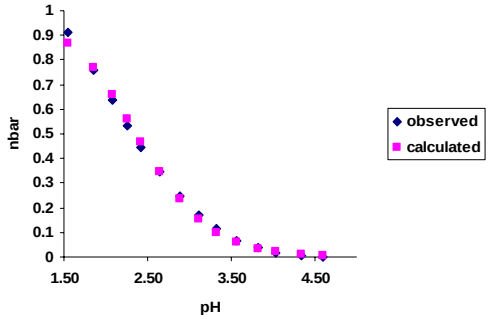

b.)

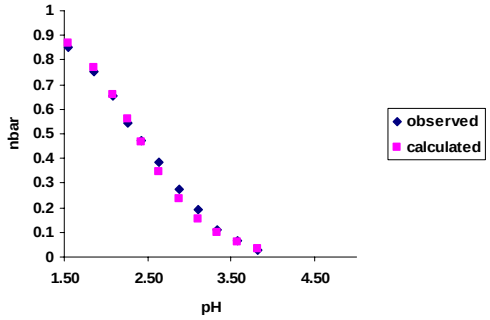

c.)

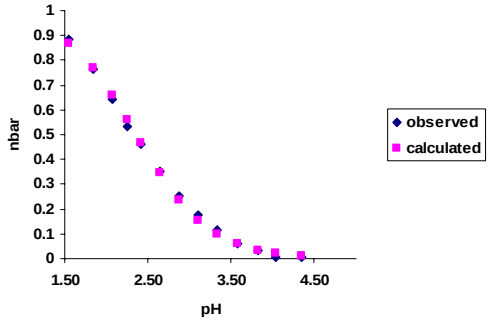

d.)

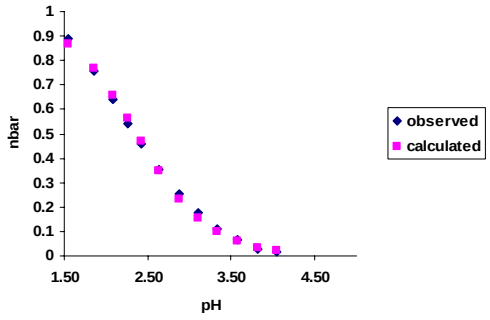

Figure 21: The comparison of $\bar{n}$ observed versus $\bar{n}$ calculated with respect to pH at wavelengths of a.) 228 nm, b.) 237 nm, c.) 260 nm, and d.) 271 nm for the titration of PDALC (2×10^{-5} *M*) with Cd(II) (2×10^{-5} *M*) in 0.1 *M* $NaClO_4$ at 25 ± 0.1 °C for determining the log*K* value. The theoretical curves were calculated from an apparent pK_a of 2.37.

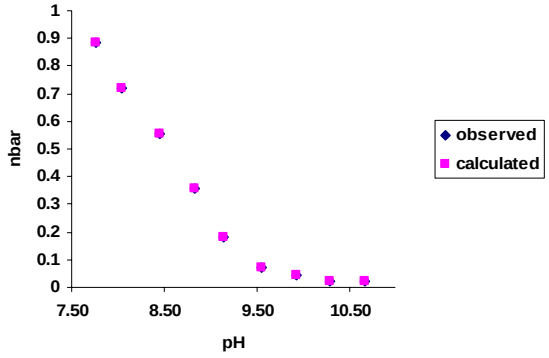

a.)

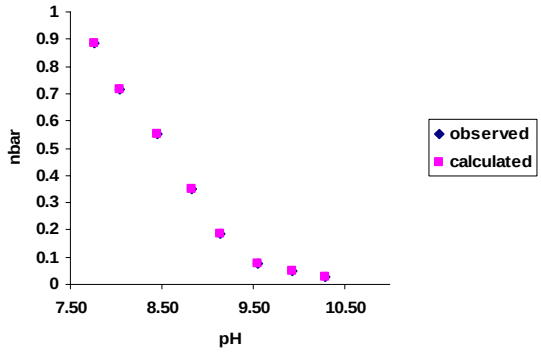

b.)

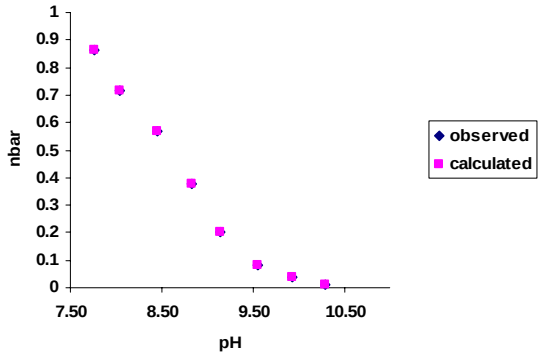

c.)

Figure 22: The comparison of $\bar{n}$ observed versus $\bar{n}$ calculated with respect to pH at wavelengths of a.) 228 nm, b.) 260 nm, and c.) 271 nm for the titration of PDALC ($2x10^{-5}$ *M*) with Cd(II) ($2x10^{-5}$ *M*) in 0.1 *M* $NaClO_4$ at 25 ± 0.1 °C for determining the MLOH value. The theoretical curves were calculated from an apparent pK_a of 8.54.

Cd(II). In addition, formation of MLOH was calculated for PDALC with Cd(II) to occur at pH = 8.54.

$$[Cd(PDALC)H_{-1}]^{+} + H^{+} \leftrightarrows [Cd(PDALC)]^{2+} \quad pK = 8.54$$

PDALC-calcium(II) results

Calcium(II) has an ionic radius of 1.00 Å, which lies in the middle of the range of metals tested. The UV absorbance spectra are shown in Figure 23 for the titration of Ca(II) with PDALC. An example plot of corrected absorbance versus pH for Ca(II) is shown in Figure 24. In addition, observed and calculated $\bar{n}$ versus pH plots are shown in Figure 25. From the selected wavelengths described above, an apparent pK_a of 2.45 and a log K_1 of 3.68 was calculated for Ca(II) with PDALC using Equations (1-9). When compared to the log K_1 of EDDE, which is 1.08 (results below), PDALC showed an increase in complex stability.[21] A Δ log K_1 of about 2.60 shows a quantitative difference in stability between the PDALC complex and the EDDE complex of Ca(II). When compared to the log K_1 of 1,10 phenanthroline, which is 1.0, PDALC showed an increase in complex stability with Ca(II).[21] A Δ log K_1 of about 2.7 shows a quantitative difference in stability between the PDALC complex and the 1,10 phenanthroline complex of Ca(II).

PDALC-cobalt(II) results

Cobalt(II) has an ionic radius of 0.745 Å, which is one of the smaller metals tested. The UV absorbance spectra are shown in Figure 26 for the titration of Co(II) with PDALC. An example plot of corrected absorbance versus pH for Co(II) is shown in Figure 27. In addition, observed and calculated $\bar{n}$ versus pH plots are shown in Figure 28. From the selected

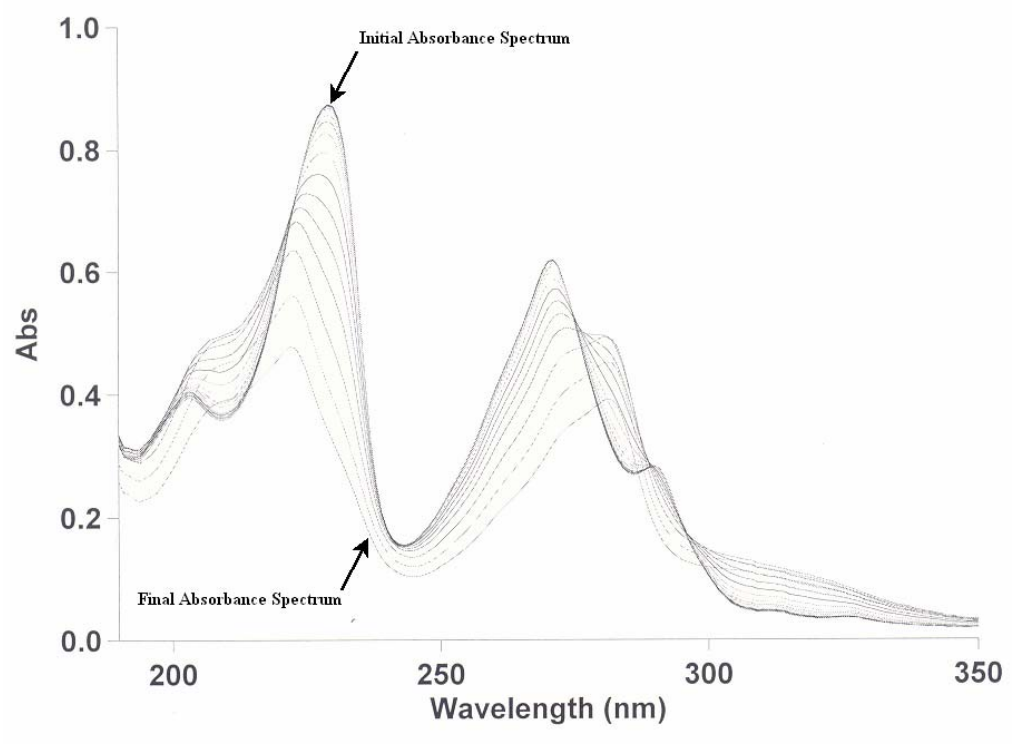

Figure 23: UV absorbance spectra for the titration of Ca(II) (0.0333 *M*) and PDALC ($2x10^{-5}$ *M*) with the pH ranging from 5.42 to 1.42 in 0.1 *M* $NaClO_4$ at 25 ± 0.1 °C.

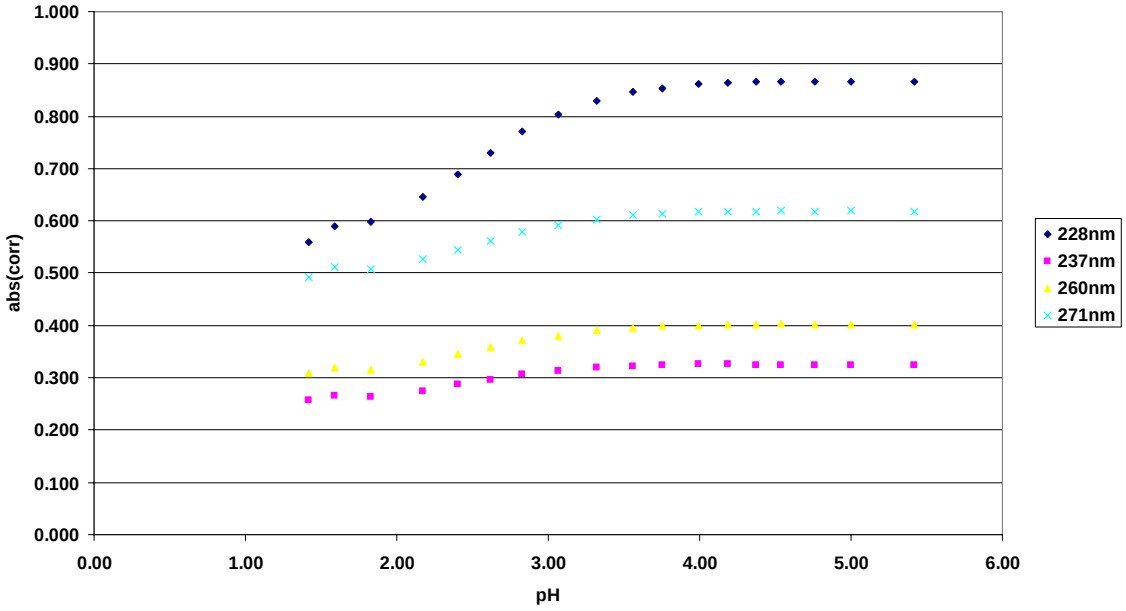

Figure 24: Combined plot of corrected absorbance data versus pH for wavelengths 228 nm, 237 nm, 260 nm, and 271 nm for the titration of PDALC ($2x10^{-5}$ *M*) with Ca(II) (0.0333 *M*) in 0.1 *M* $NaClO_4$ at 25 ± 0.1 °C.

a.)

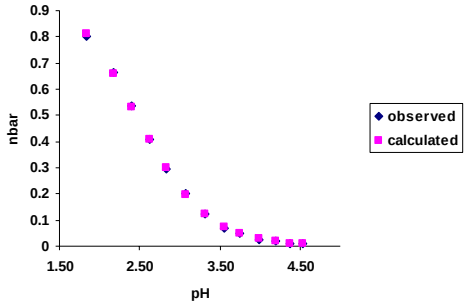

b.)

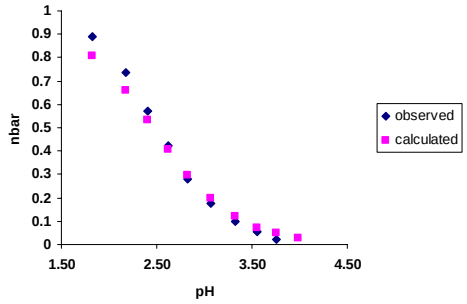

c.)

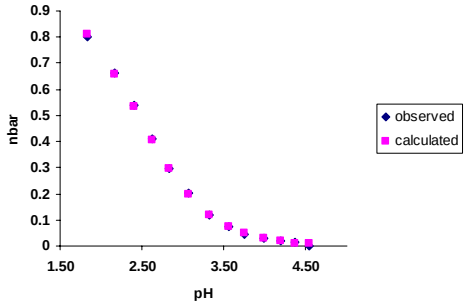

d.)

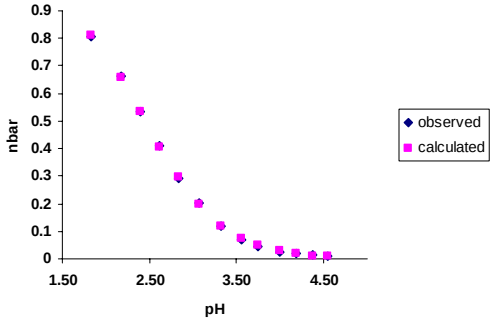

Figure 25: Comparison of $\bar{n}$ observed versus $\bar{n}$ calculated with respect to pH at wavelengths of a.) 228 nm, b.) 237 nm, c.) 260 nm, and d.) 271 nm for the titration of PDALC ($2x10^{-5}$ *M*) with Ca(II) (0.0333 *M*) in 0.1 *M* $NaClO_4$ at 25 ± 0.1 °C for determining the log*K* value. The theoretical curves were calculated from an apparent pK_a of 2.45.

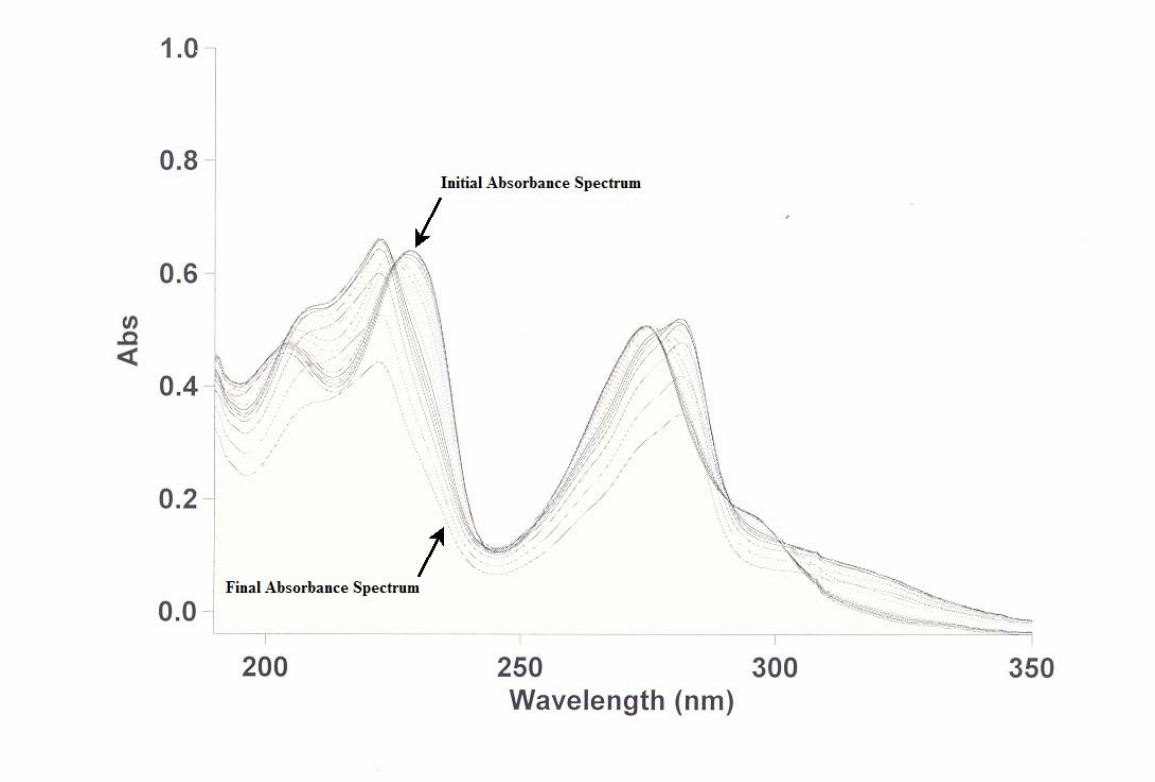

Figure 26: UV absorbance spectra for the titration of 1:1 Co(II) and PDALC at $2x10^{-5}$ *M* with the pH ranging from 5.52 to 1.52 in 0.1 *M* $NaClO_4$ at 25 ± 0.1 °C.

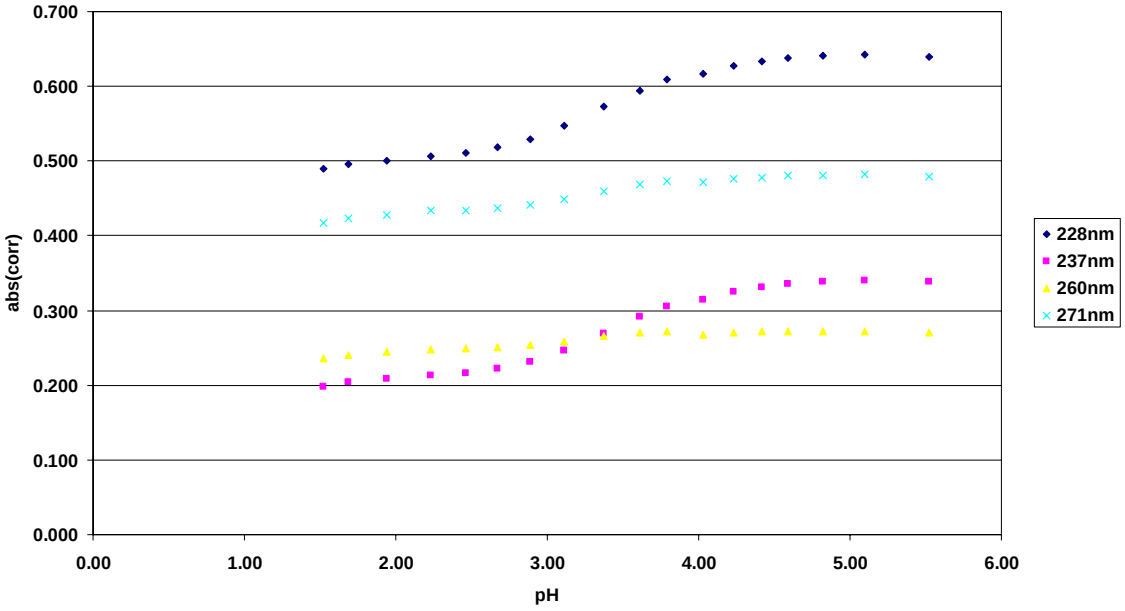

Figure 27: Combined plot of corrected absorbance data versus pH for wavelengths 228 nm, 237 nm, 260 nm, and 271 nm for the titration of PDALC ($2x10^{-5}$ *M*) with Co(II) ($2x10^{-5}$ *M*) in 0.1 *M* $NaClO_4$ at 25 ± 0.1 °C.

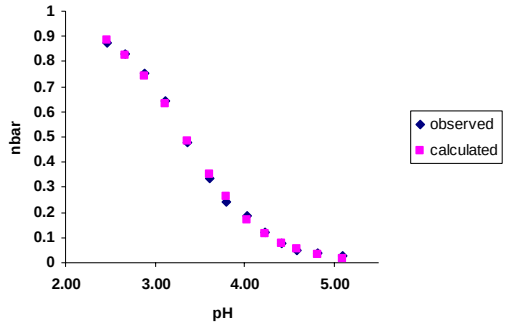

a.)

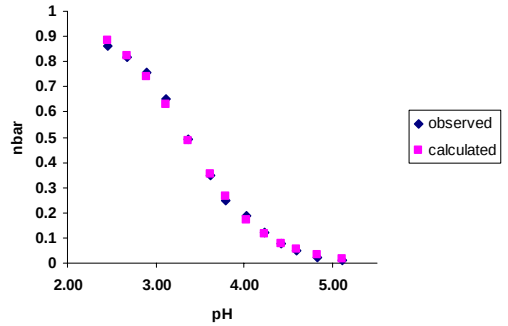

b.)

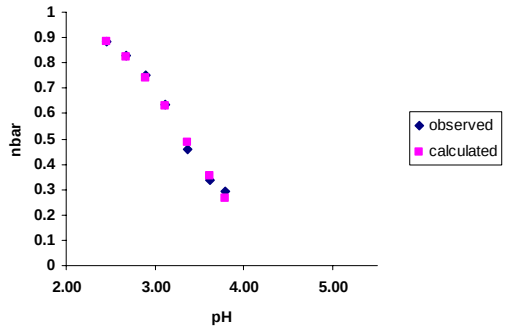

c.)

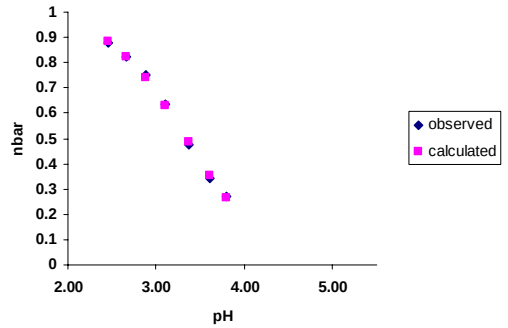

d.)

Figure 28: Comparison of $\bar{n}$ observed versus $\bar{n}$ calculated with respect to pH at wavelengths of a.) 228 nm, b.) 237 nm, c.) 260 nm, and d.) 271 nm for the titration of PDALC ($2x10^{-5}$ *M*) with Co(II) ($2x10^{-5}$ *M*) for determining the log*K* value. The theoretical curves were calculated from an apparent pK_a of 3.34.

wavelengths described above, an apparent pK_a of 3.34 and a log K_1 of 6.31 was calculated for Co(II) with PDALC using Equations (1-9). When compared to the log K_1 of EDDE, which is 5.10, PDALC showed an increase in complex stability.[21] A Δ log K_1 of about 1.21 shows a quantitative difference in stability between the PDALC complex and the EDDE complex of Co(II). When compared to the log K_1 of 1,10 phenanthroline, which is 7.1, PDALC showed a decrease in complex stability with Co(II).[21] A Δ log K_1 of about -0.8 shows a quantitative difference in stability between the PDALC complex and the 1,10 phenanthroline complex of Co(II).

PDALC-copper(II) results

Copper(II) has an ionic radius of 0.57 Å, which is one of the smaller metals tested. The UV absorbance spectra are shown in Figure 29 for the titration of Cu(II) with PDALC at 2×10^{-5} *M* and 4×10^{-5} *M*. An example plot of corrected absorbance versus pH for Cu(II) is shown in Figure 30. In addition, observed and calculated $\bar{n}$ versus pH plots for log K_1, MLOH, and $ML(OH)_2$ are shown in Figures 31, 32, 33. From the selected wavelengths described above, an apparent pK_a of 2.19 and a log K_1 of 7.46 was calculated for Cu(II) with PDALC using Equations (1-9). When compared to the log K_1 of EDDE, which is 9.70, PDALC showed an decrease in complex stability.[21] A Δ log K_1 of about -2.24 shows a quantitative difference in stability between the PDALC complex and the EDDE complex of Cu(II). When compared to the log K_1 of 1,10 phenanthroline, which is 9.7, PDALC showed an decrease in complex stability with Cu(II).[21] A Δ log K_1 of about -2.2 shows a quantitative difference in stability between the PDALC complex and the 1,10 phenanthroline complex of Cu(II).

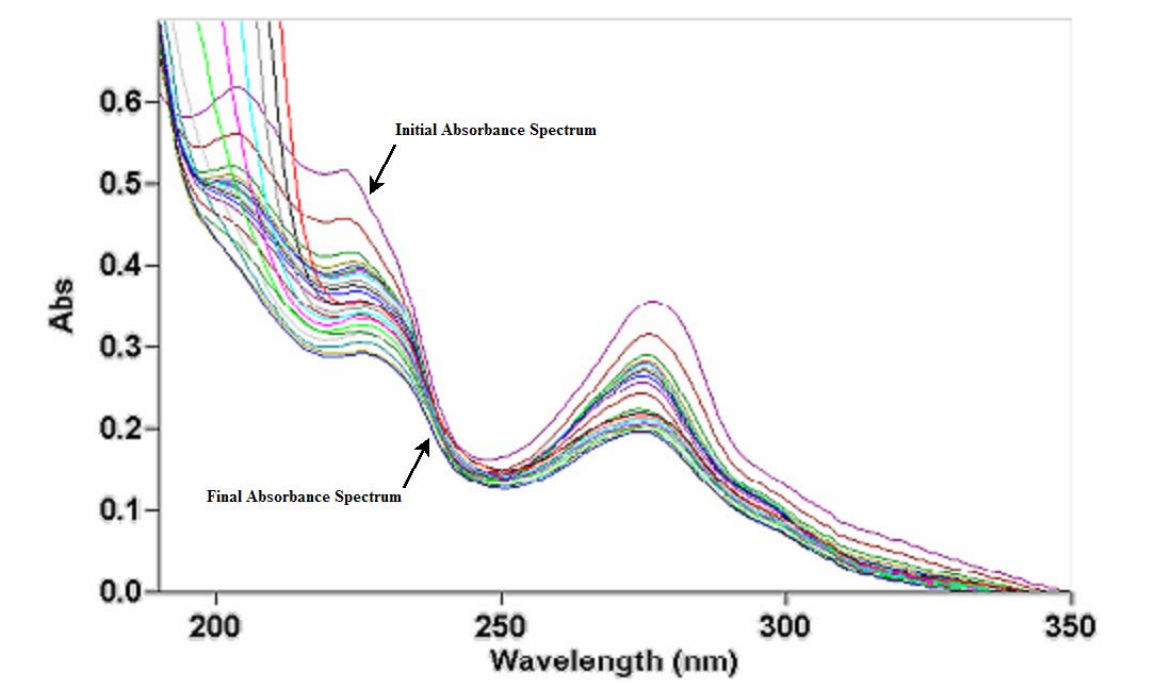

a.)

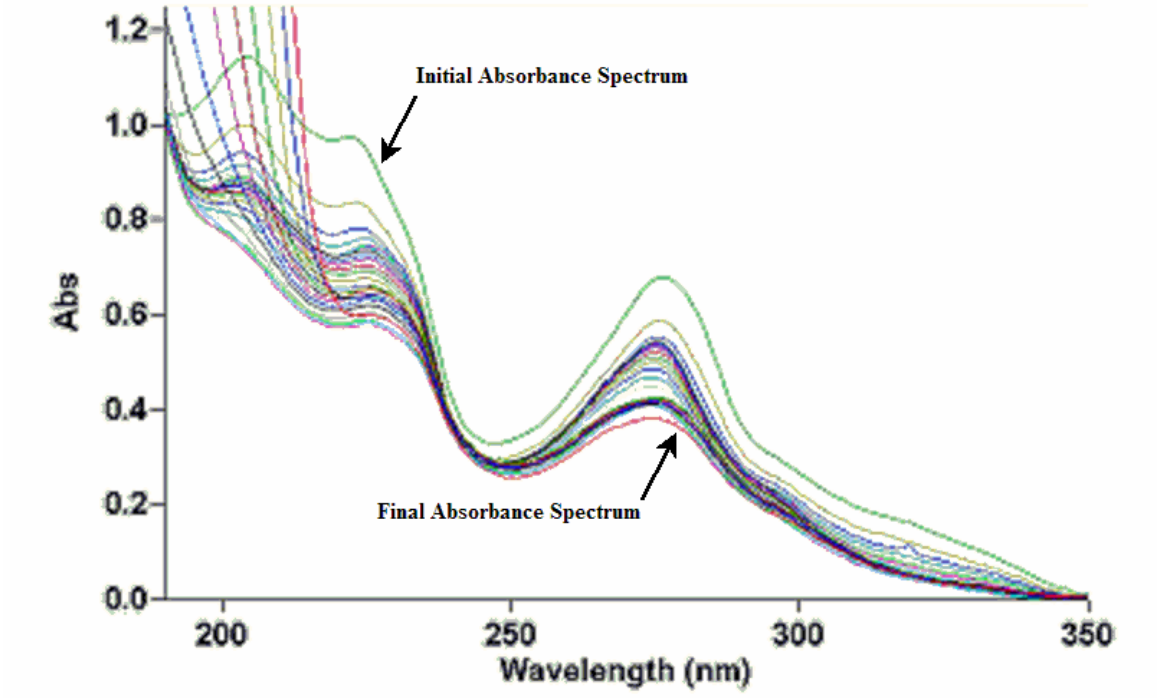

b.)

Figure 29: UV absorbance spectra for the titration of a.) 1:1 Cu(II) and PDALC at $2x10^{-5}$ *M* with the pH ranging from 1.50 to 11.55 and b.) 1:1 Cu(II) and PDALC at $4x10^{-5}$ *M* with the pH ranging from 1.52 to 11.97 in 0.1 *M* $NaClO_4$ at 25 ± 0.1 °C.

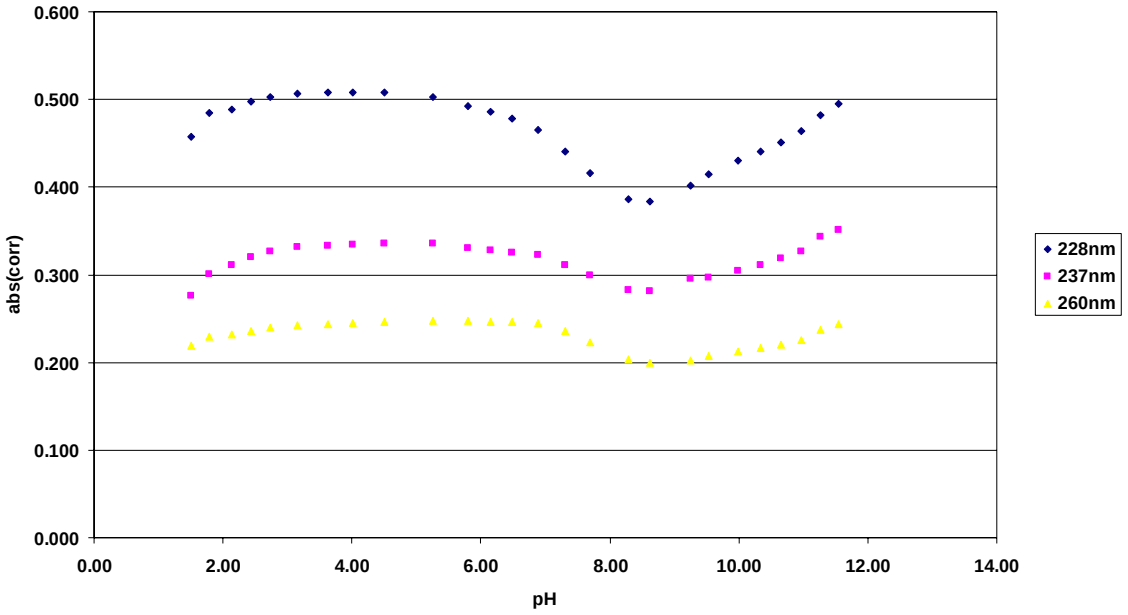

Figure 30: Combined plot of corrected absorbance data versus pH for wavelengths 228 nm, 237 nm, and 260 nm for the titration of PDALC ($2x10^{-5}$ *M*) with Cu(II) ($2x10^{-5}$ *M*) in 0.1 *M* $NaClO_4$ at 25 ± 0.1 °C.

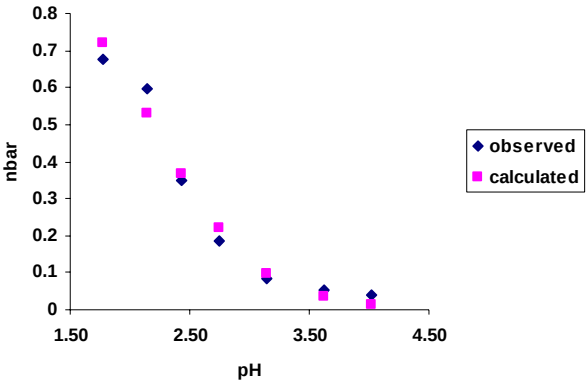

a.)

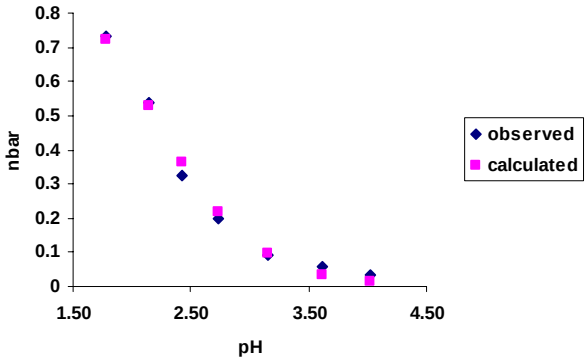

b.)

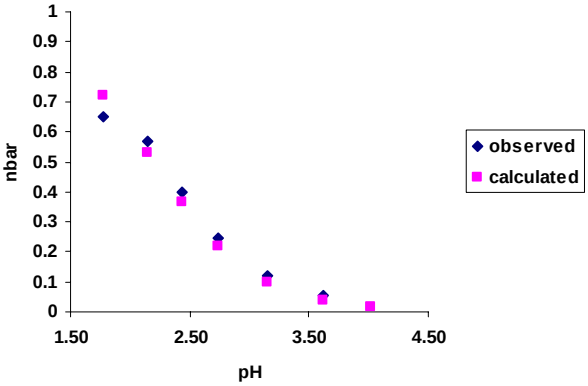

c.)

Figure 31: The comparison of $\bar{n}$ observed versus $\bar{n}$ calculated with respect to pH at wavelengths of a.) 228 nm, b.) 237 nm, and c.) 260 nm for the titration of PDALC ($2x10^{-5}$ *M*) with Cu(II) ($2x10^{-5}$ *M*) for determining the log*K* value. The theoretical curves were calculated from an apparent pK_a of 2.19.

a.)

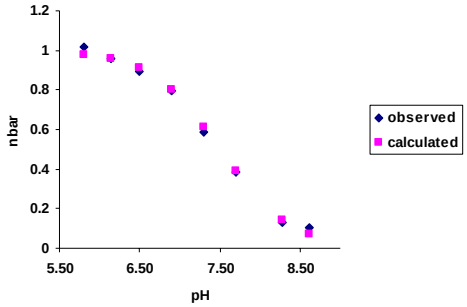

b.)

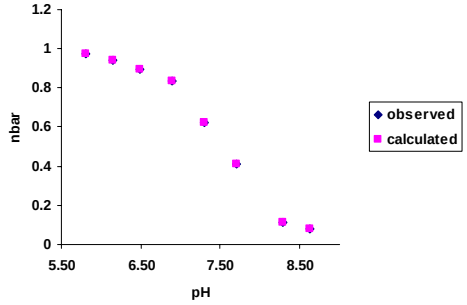

c.)

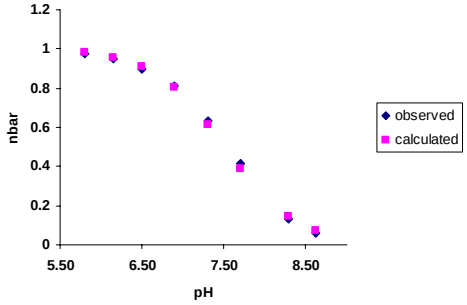

d.)

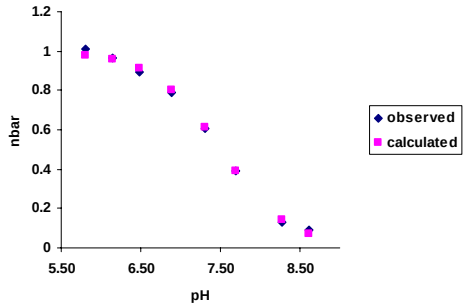

Figure 32: Comparison of $\bar{n}$ observed versus $\bar{n}$ calculated with respect to pH at wavelengths of a.) 228 nm, b.) 237 nm, c.) 271 nm, and d.) 279 nm for the titration of PDALC ($2x10^{-5}$ *M*) with Cu(II) ($2x10^{-5}$ *M*) for determining the MLOH value. The theoretical curves were calculated from an apparent pK_a of 7.50.

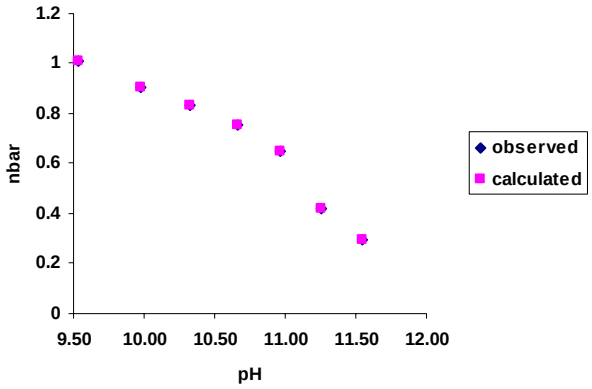

a.)

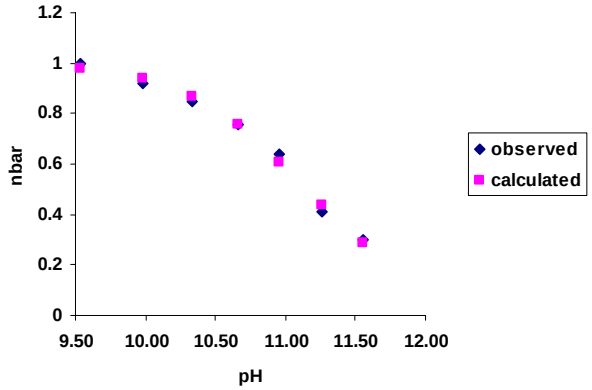

b.)

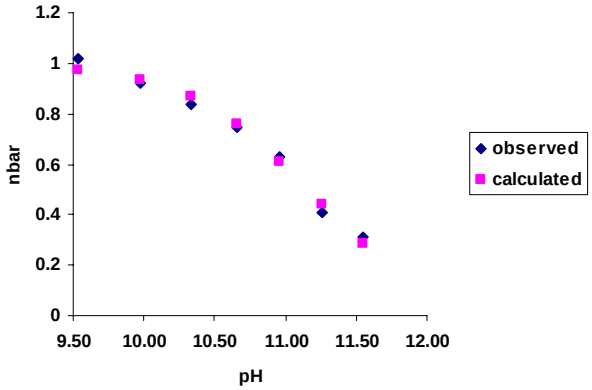

c.)

Figure 33: Comparison of $\bar{n}$ observed versus $\bar{n}$ calculated with respect to pH at wavelengths of a.) 260 nm, b.) 271 nm, and c.) 279 nm for the titration of PDALC ($2x10^{-5}$ *M*) with Cu(II) ($2x10^{-5}$ *M*) for determining the $ML(OH)_2$ value. The theoretical curves were calculated from an apparent pK_a of 11.15.

PDALC-gadolinium(III) results

Gadolinium(III) has an ionic radius of 0.93 Å, which lies in the middle of the range of sizes of metals tested. The UV absorbance spectra are shown in Figure 34 for the titration of Gd(III) with PDALC. An example plot of corrected absorbance versus pH for Gd(III) is shown in Figure 35. In addition, observed and calculated $\bar{n}$ versus pH plots are shown in Figure 36. From the selected wavelengths described above, an apparent pK_a of 3.55 and a log K_1 of 6.10 was calculated for Gd(III) with PDALC using Equations (1-9). There was no log K_1 reported for EDDE with Gd(III) to compare PDALC with and due to the weakness of the PDALC complex with Gd(III), the log K_1 of EDDE with Gd(III) would probably not be large enough to measure with the techniques available. There was also no reported log K_1 value for 1,10 phenanthroline with Gd(III) to compare PDALC with.

PDALC-indium(III) results

Indium(III) has an ionic radius of 0.8 Å, which is one of the smaller metals tested. The UV absorbance spectra are shown in Figure 37 for the titration of In(III) with PDALC. A example plot of corrected absorbance versus pH for In(III) is shown in Figure 38. In addition, observed and calculated $\bar{n}$ versus pH plots are shown in Figure 39. From the selected wavelengths described above, an apparent pK_a of 4.22 and a log K_1 of 5.43 was calculated for In(III) with PDALC using Equations (1-9). When compared to the log K_1 of 1,10 phenanthroline, which is 6.5, PDALC showed a decrease in complex stability.[21] A Δ log K_1 of about -1.1 shows a quantitative difference in stability between the PDALC complex and the 1,10 phenanthroline complex of In(III). There was no log K_1 reported for EDDE with In(III) to compare PDALC with and due to the weakness of the PDALC complex with In(III), the log K_1

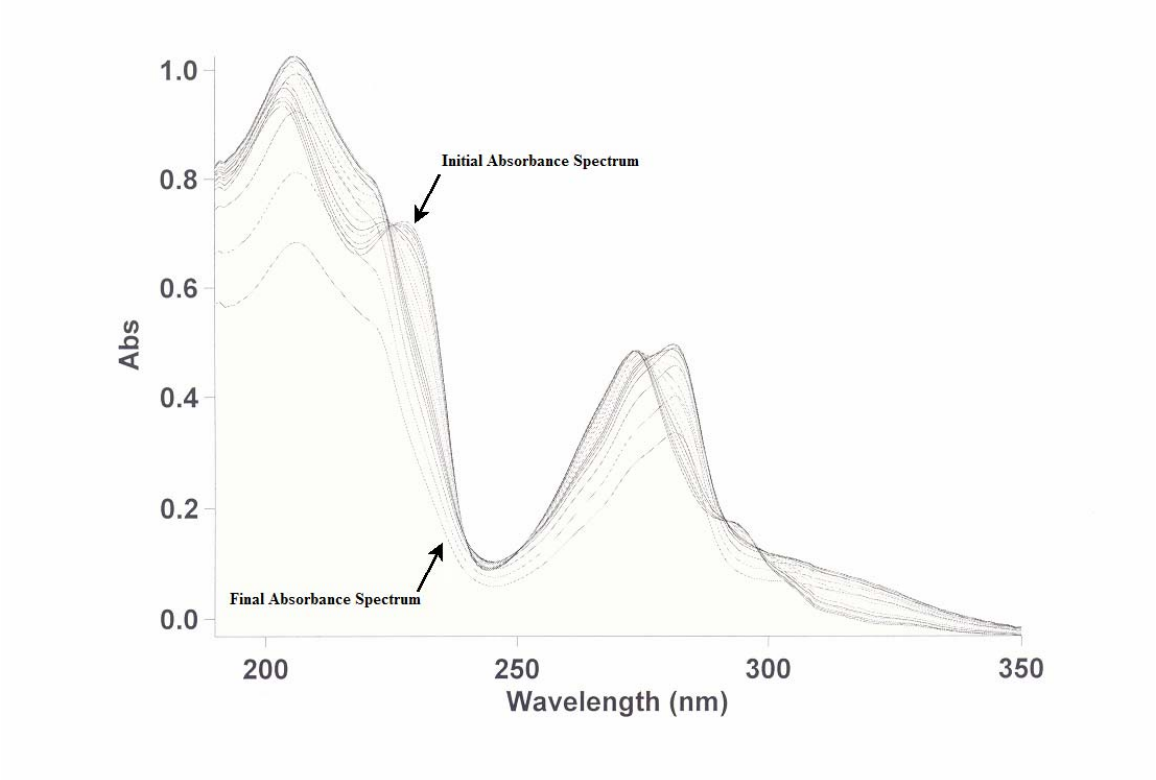

Figure 34: UV absorbance spectra for the titration of 1:1 Gd(III) and PDALC at $2x10^{-5}$ *M* with the pH ranging from 5.19 to 1.41in 0.1 *M* $NaClO_4$ at 25 ± 0.1 °C.

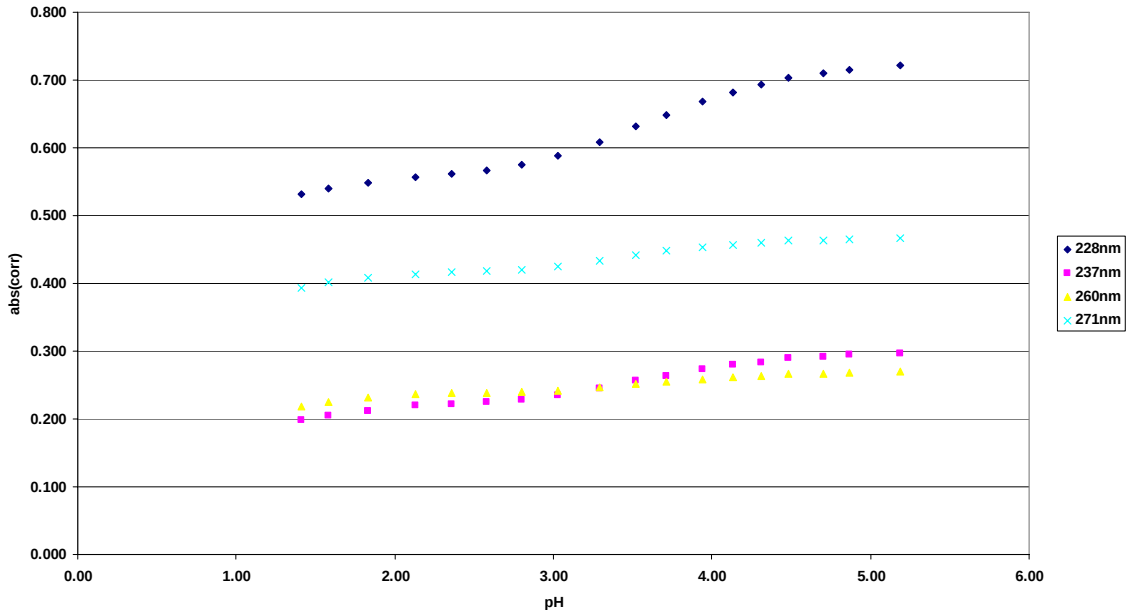

Figure 35: Combined plot of corrected absorbance data versus pH for wavelengths 228 nm, 237 nm, 260 nm, and 271 nm for the titration of PDALC ($2x10^{-5}$ *M*) with Gd(III) ($2x10^{-5}$ *M*) in 0.1 *M* $NaClO_4$ at 25 ± 0.1 °C.

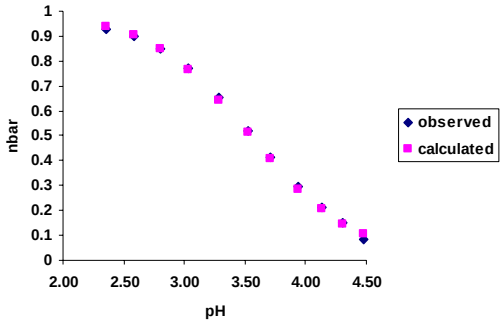

a.)

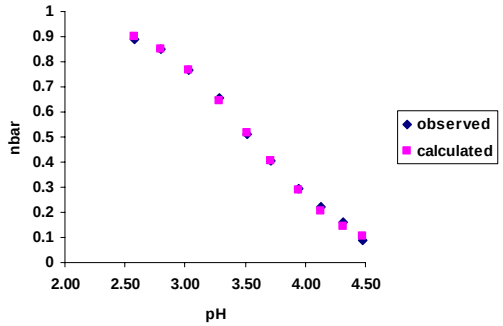

b.)

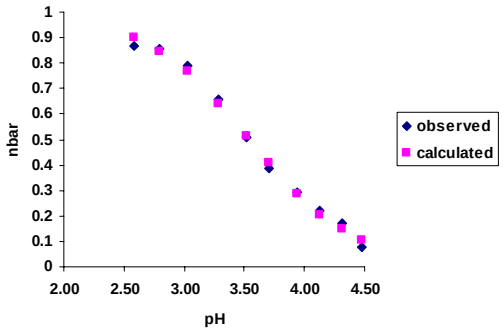

c.)

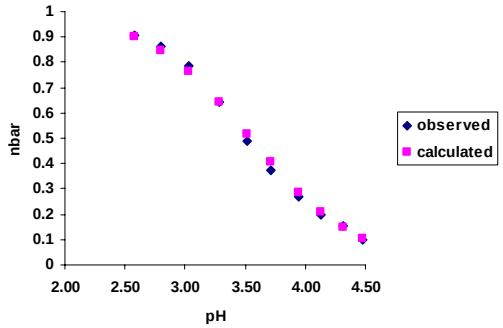

d.)

Figure 36: Comparison of $\bar{n}$ observed versus $\bar{n}$ calculated with respect to pH at wavelengths of a.) 228 nm, b.) 237 nm, c.) 260 nm, and d.) 271 nm for the titration of PDALC ($2x10^{-5}$ *M*) with Gd(III) ($2x10^{-5}$ *M*) for determining the log*K* value. The theoretical curves were calculated from an apparent pK_a of 3.55.

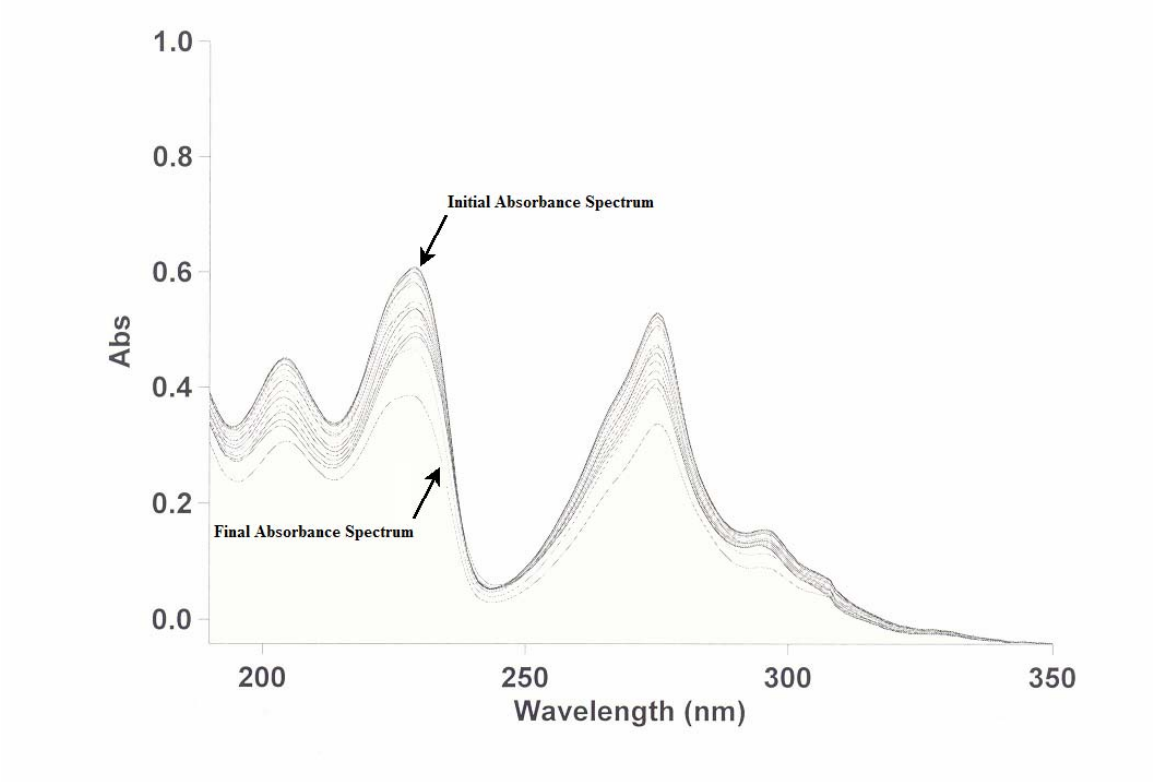

Figure 37: UV absorbance spectra for the titration of 1:1 In(III) and PDALC at $2x10^{-5}$ *M* with the pH ranging from 5.28 to 1.51 in 0.1 *M* $NaClO_4$ at 25 ± 0.1 °C.

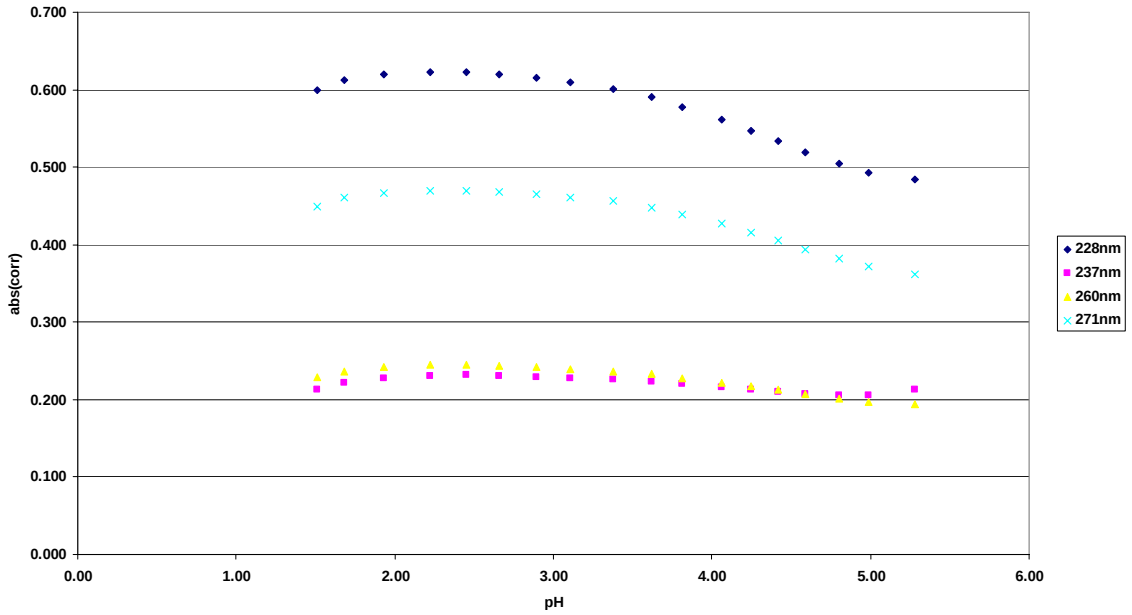

Figure 38: Combined plot of corrected absorbance data versus pH for wavelengths 228 nm, 237 nm, 260 nm, and 271 nm for the titration of PDALC ($2x10^{-5}$ *M*) with In(III) ($2x10^{-5}$ *M*) in 0.1 *M* $NaClO_4$ at 25 ± 0.1 °C.

a.)

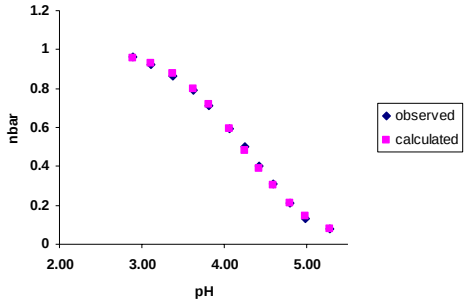

b.)

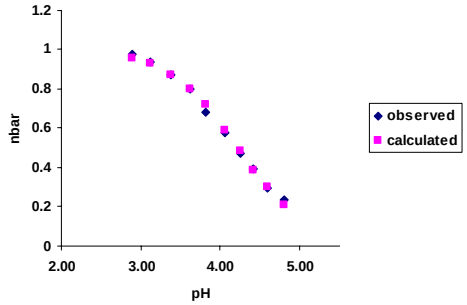

c.)

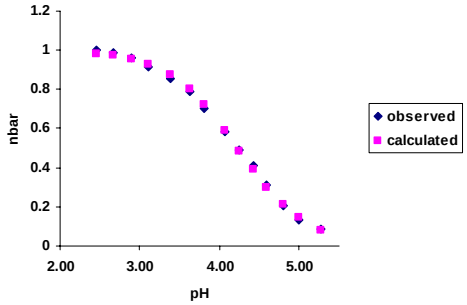

d.)

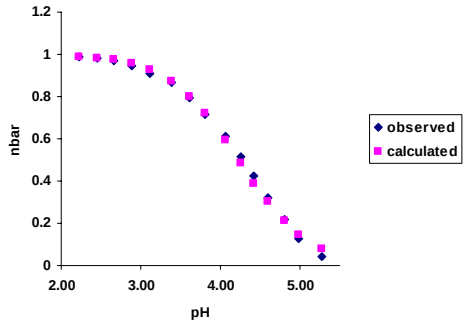

Figure 39: Comparison of $\bar{n}$ observed versus $\bar{n}$ calculated with respect to pH at wavelengths of a.) 228 nm, b.) 237 nm, c.) 260 nm, and d.) 271 nm for the titration of PDALC ($2x10^{-5}$ *M*) with In(III) ($2x10^{-5}$ *M*) for determining the log*K* value. The theoretical curves were calculated from an apparent pK_a of 4.22.

of EDDE with In(III) would probably not be large enough to measure with the techniques available.

PDALC-lanthanum(III) results

Lanthanum(III) has an ionic radius of 1.03 Å, which lies in the middle of the range of metals tested. The UV absorbance spectra are shown in Figure 40 for the titration of La(III) with PDALC. An example plot of corrected absorbance versus pH for La(III) is shown in Figure 41. In addition, observed and calculated $\bar{n}$ versus pH plots are shown in Figure 42. From the selected wavelengths described above, an apparent pK_a of 4.36 and a log K_1 of 5.29 was calculated for La(III) with PDALC using Equations (1-9). When compared to the log K_1 of EDDE, which is 4.30 (results below), PDALC showed an increase in complex stability. A Δ log K_1 of about 0.99 shows a quantitative difference in stability between the PDALC complex and the EDDE complex of La(III). When compared to the log K_1 of 1,10 phenanthroline, which is 2.1, PDALC showed an increase in complex stability.[21] A Δ log K_1 of about 3.2 shows a quantitative difference in stability between the PDALC complex and the 1,10 phenanthroline complex of La(III).

PDALC-lead(II) results

Lead(II) has an ionic radius of 1.19 Å, which is one of the larger metals tested. The UV absorbance spectra are shown in Figure 43 for the titration of Pb(II) with PDALC. An example plot of corrected absorbance versus pH for Pb(II) is shown in Figure 44. In addition, observed and calculated $\bar{n}$ versus pH plots are shown in Figures 45, 46, and 47 for log K_1, MLOH, and $ML(OH)_2$. From the selected wavelengths described above, an apparent pK_a of 2.39 and a log K_1

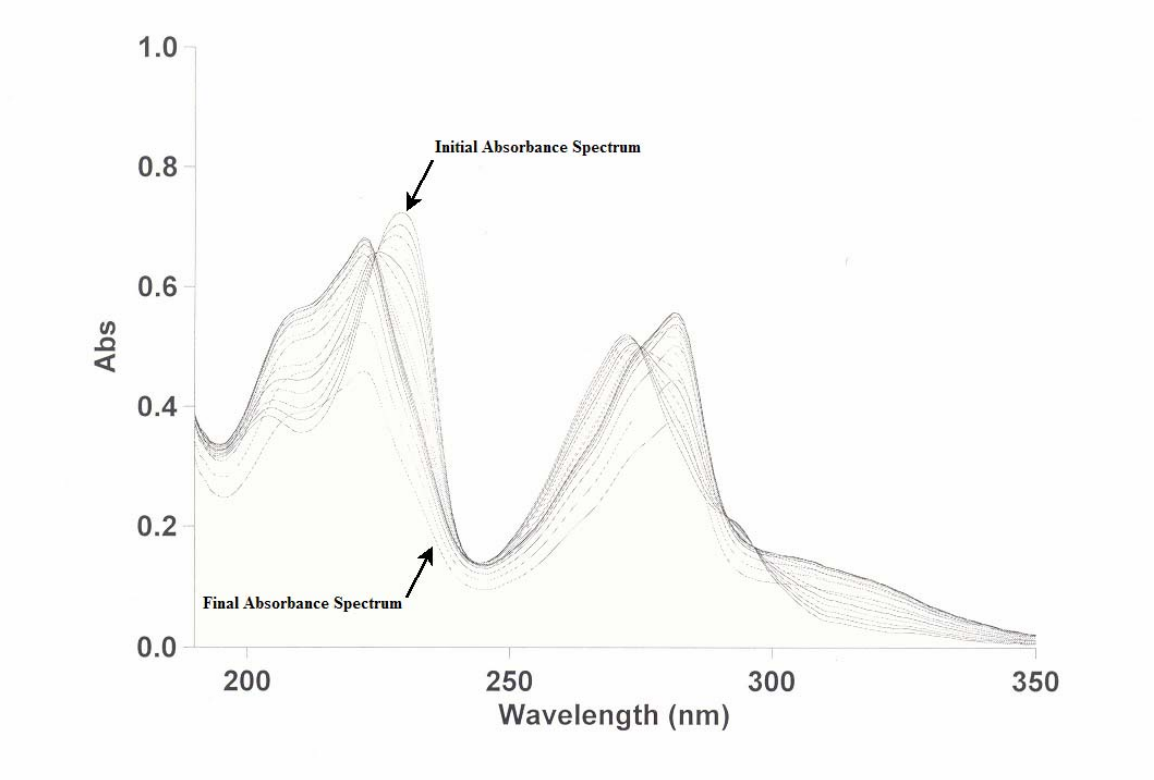

Figure 40: UV absorbance spectra for the titration of 1:1 La(III) and PDALC at $2x10^{-5}$ *M* with the pH ranging from 5.52 to 1.52 in 0.1 *M* $NaClO_4$ at 25 ± 0.1 °C.

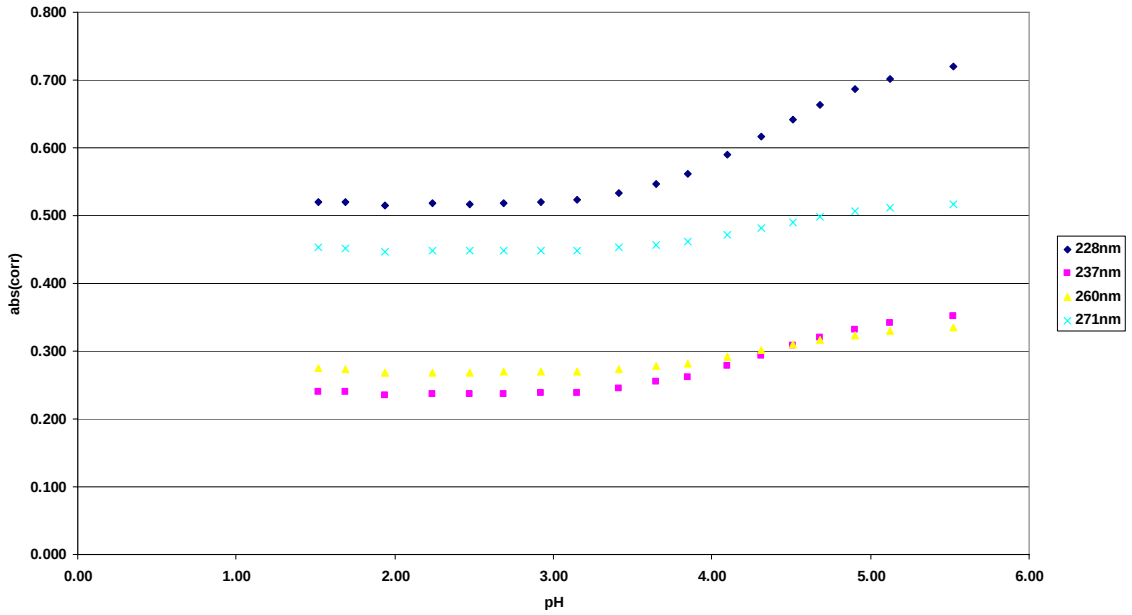

Figure 41: Combined plot of corrected absorbance data versus pH for wavelengths 228 nm, 237 nm, 260 nm, and 271 nm for the titration of PDALC ($2x10^{-5}$ *M*) with La(III) ($2x10^{-5}$ *M*) in 0.1 *M* $NaClO_4$ at 25 ± 0.1 °C.

a.)

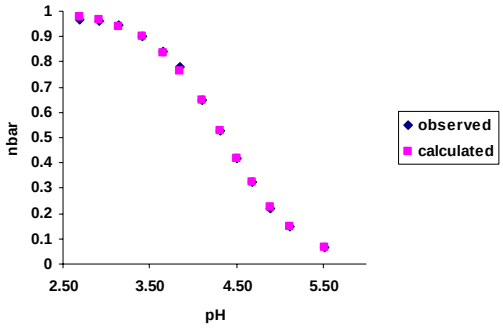

b.)

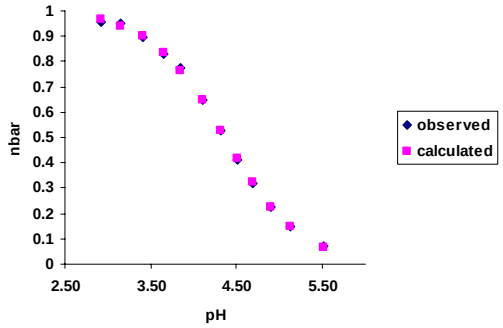

c.)

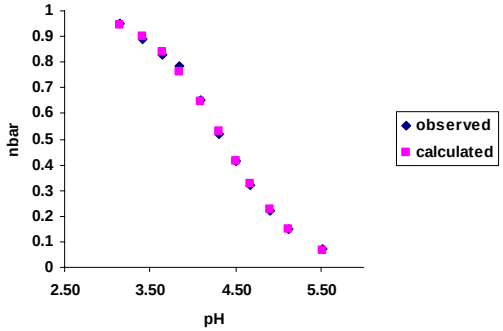

d.)

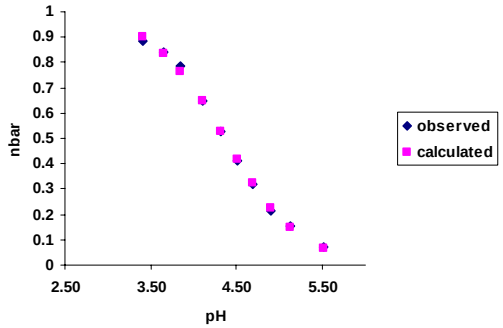

Figure 42: Comparison of $\bar{n}$ observed versus $\bar{n}$ calculated with respect to pH at wavelengths of a.) 228 nm, b.) 237 nm, c.) 260 nm, and d.) 271 nm for the titration of PDALC ($2x10^{-5}$ *M*) with La(III) ($2x10^{-5}$ *M*) for determining the log*K* value. The theoretical curves were calculated from an apparent pK_a of 4.36.

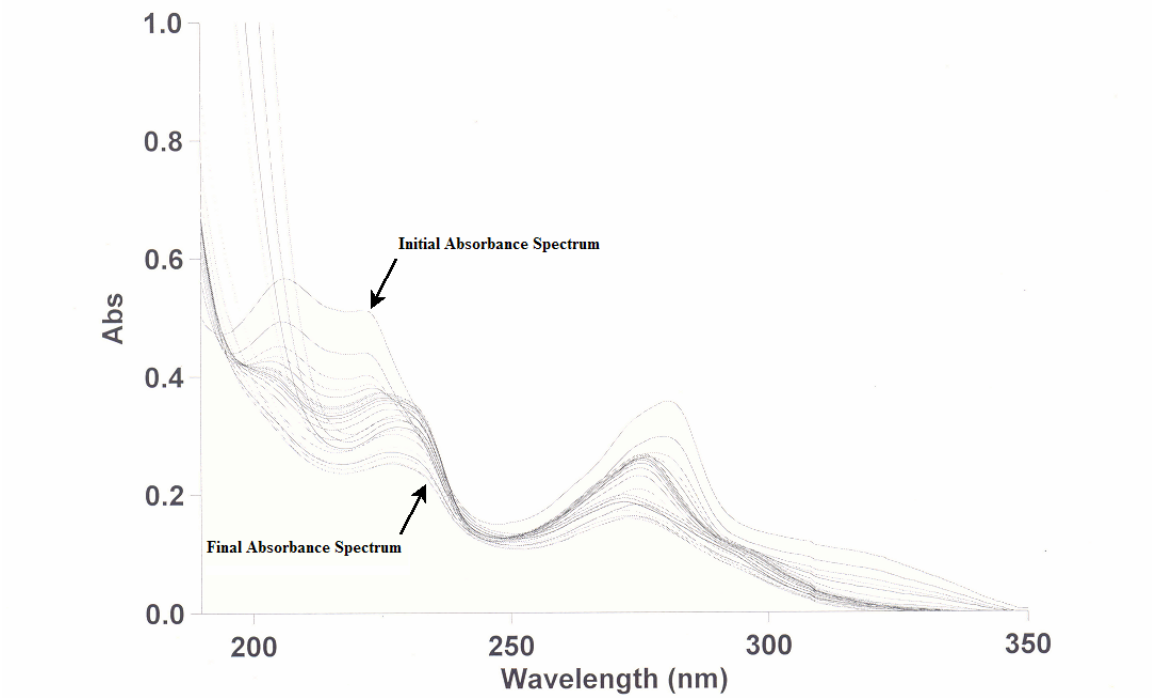

a.)

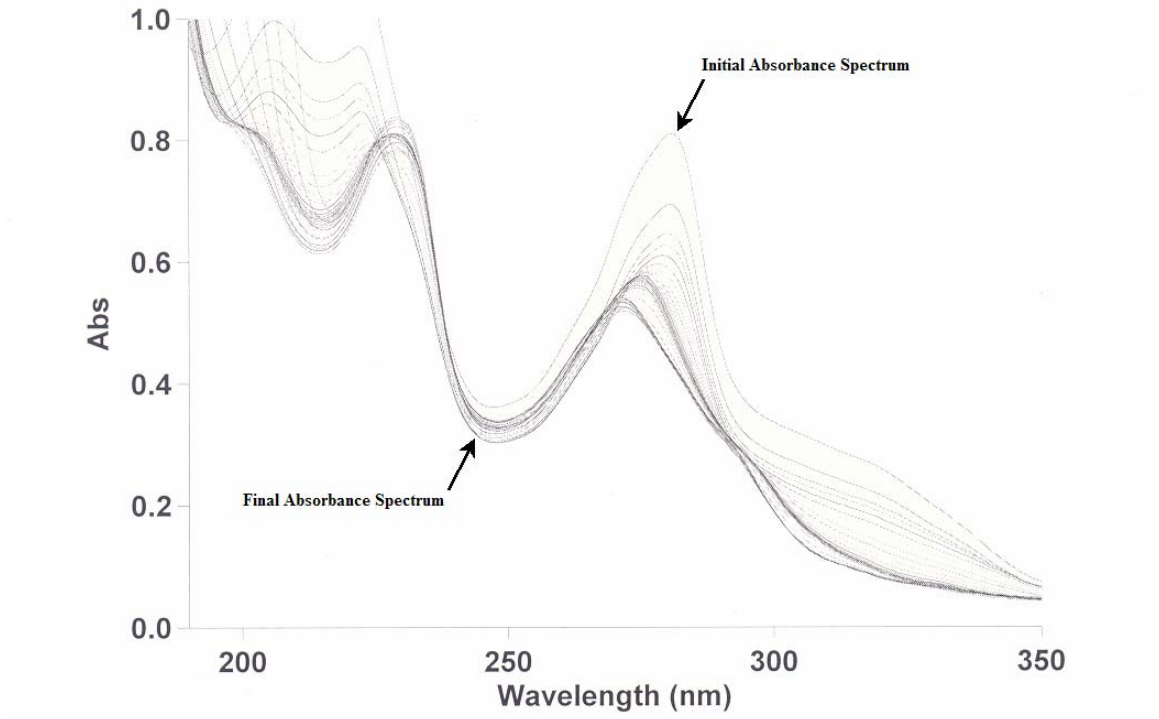

b.)

Figure 43: UV absorbance spectra for the titration of a.) 1:1 Pb(II) and PDALC at $2x10^{-5}$ *M* with the pH ranging from1.36 to 11.03 and b.) 1:1 Pb(II) and PDALC at $4x10^{-5}$ *M* with the pH ranging from 1.39 to 11.36 in 0.1 *M* $NaClO_4$ at 25 ± 0.1 °C.

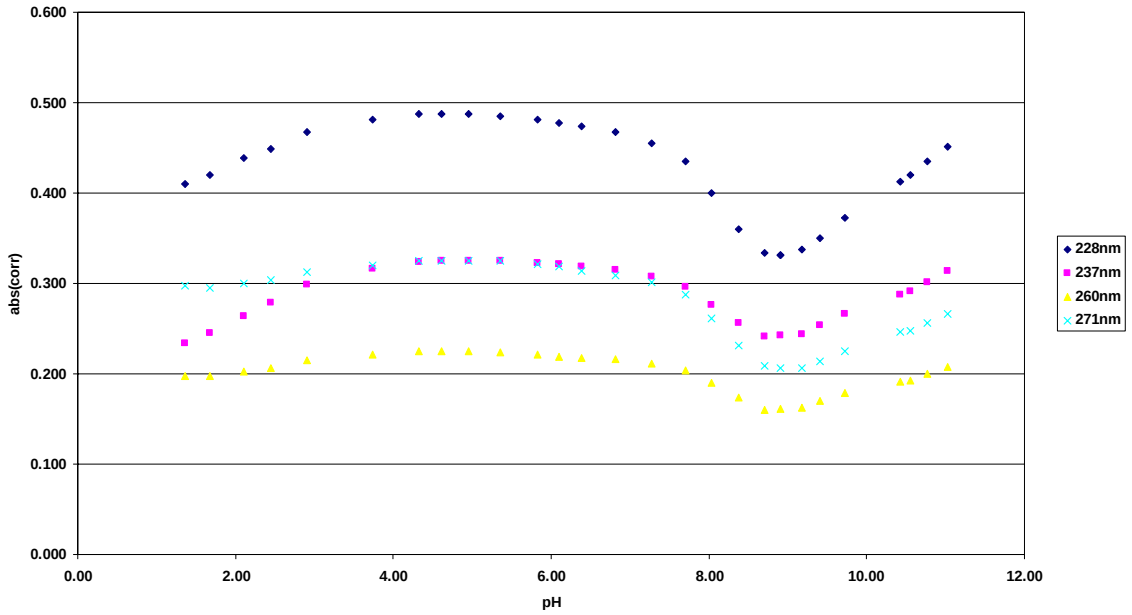

Figure 44: Combined plot of corrected absorbance data versus pH for wavelengths 228 nm, 237nm, 260 nm, and 271 nm for the titration of PDALC ($2x10^{-5}$ *M*) with Pb(II) ($2x10^{-5}$ *M*) in 0.1 *M* $NaClO_4$ at 25 ± 0.1 °C.

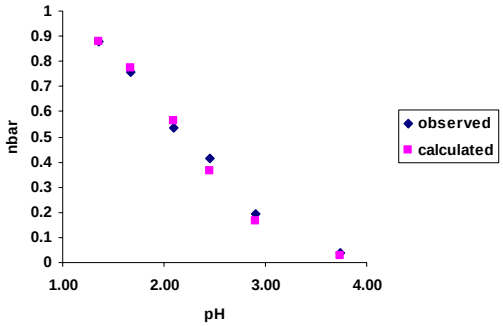

a.)

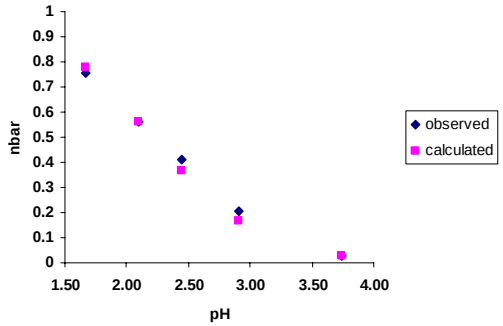

b.)

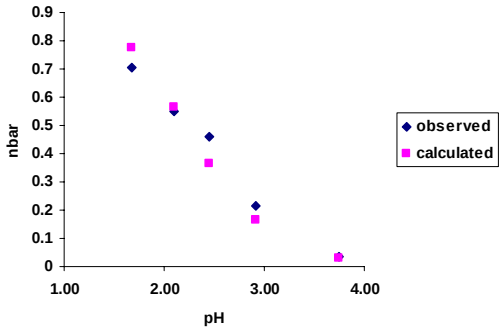

c.)

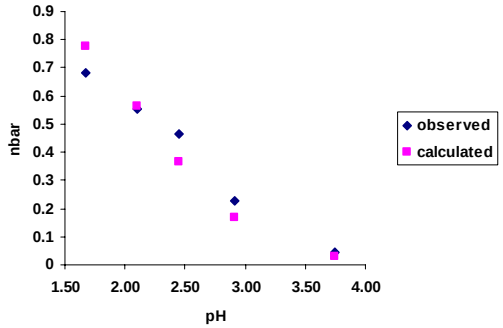

d.)

Figure 45: Comparison of $\bar{n}$ observed versus $\bar{n}$ calculated with respect to pH at wavelengths of a.) 228 nm, b.) 237 nm, c.) 260 nm, and d.) 271 nm for the titration of PDALC ($2x10^{-5}$ *M*) with Pb(II) ($2x10^{-5}$ *M*) for determining the log*K* value. The theoretical curves were calculated from an apparent pK_a of 2.39.

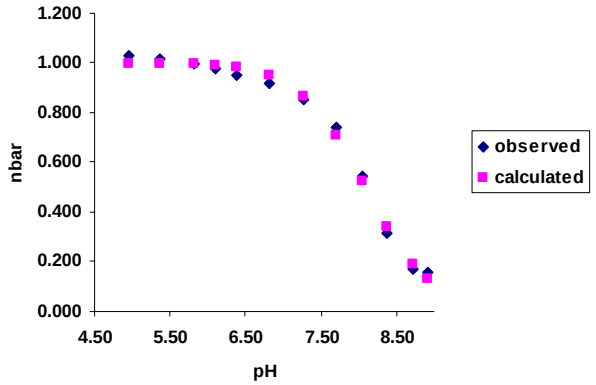

a.)

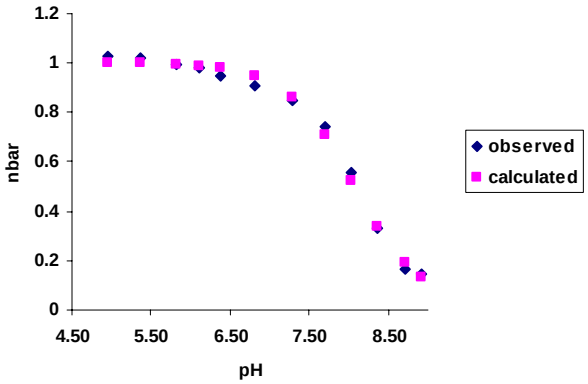

b.)

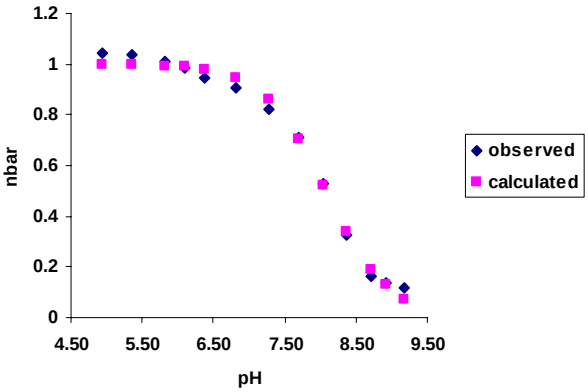

c.)

Figure 46: Comparison of $\bar{n}$ observed versus $\bar{n}$ calculated with respect to pH at wavelengths of a.) 228 nm, b.) 271 nm, and c.) 279 nm for the titration of PDALC ($2x10^{-5}$ *M*) with Pb(II) ($2x10^{-5}$ *M*) for determining the MLOH value. The theoretical curves were calculated from an apparent pK_a of 8.08.

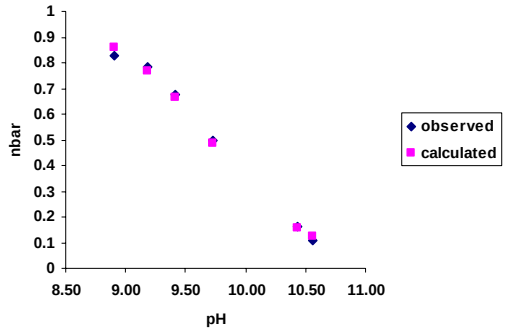

a.)

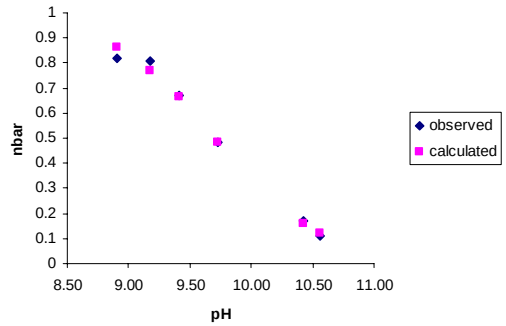

b.)

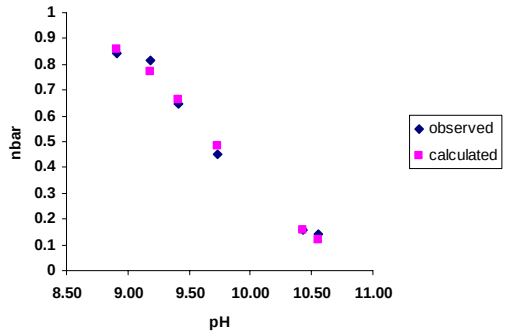

c.)

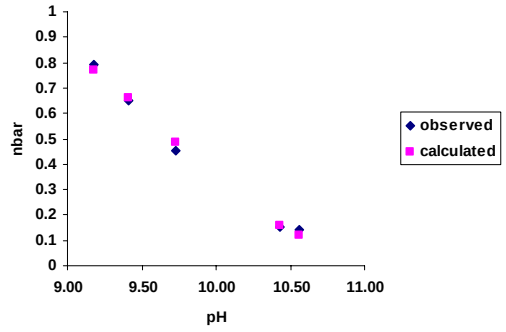

d.)

Figure 47: Comparison of $\bar{n}$ observed versus $\bar{n}$ calculated with respect to pH at wavelengths of a.) 228 nm, b.) 237 nm, c.) 260 nm, and d.) 279 nm for the titration of PDALC ($2x10^{-5}$ *M*) with Pb(II) ($2x10^{-5}$ *M*) for determining the $ML(OH)_2$ value. The theoretical curves were calculated from an apparent pK_a of 9.70.

of 7.26 was calculated for Pb(II) with PDALC using Equations (1-9). When compared to the log K_1 of EDDE, which is 6.12, PDALC showed an increase in complex stability.[21] A Δ log K_1 of about 1.14 shows a quantitative difference in stability between the PDALC complex and the EDDE complex of Pb(II). When compared to the log K_1 of 1,10 phenanthroline, which is 4.6, PDALC showed an increase in complex stability.[21] A Δ log K_1 of about 2.66 shows a quantitative difference in stability between the PDALC complex and the 1,10 phenanthroline complex of Pb(II).

PDALC-magnesium(II) results

Magnesium(II) has an ionic radius of 0.74 Å, which is one of the smaller metals tested. The UV absorbance spectra are shown in Figure 48 for the titration of Mg(II) with PDALC. An example plot of corrected absorbance versus pH for Mg(II) is shown in Figure 49. In addition, observed and calculated $\bar{n}$ versus pH plots are shown in Figure 50. From the selected wavelengths described above, an apparent pK_a of 4.43 and a log K_1 of 1.70 was calculated for Mg(II) with PDALC using Equations (1-9). When compared to the log K_1 of EDDE, which is 1.24 (results below), PDALC showed an increase in complex stability. A Δ log K_1 of about 0.46 shows a quantitative difference in stability between the PDALC complex and the EDDE complex of Mg(II). When compared to the log K_1 of 1,10 phenanthroline, which is 1.5, PDALC showed a slight increase in complex stability.[21] A Δ log K_1 of about 0.2 shows a quantitative difference in stability between the PDALC complex and the 1,10 phenanthroline complex of Mg(II).

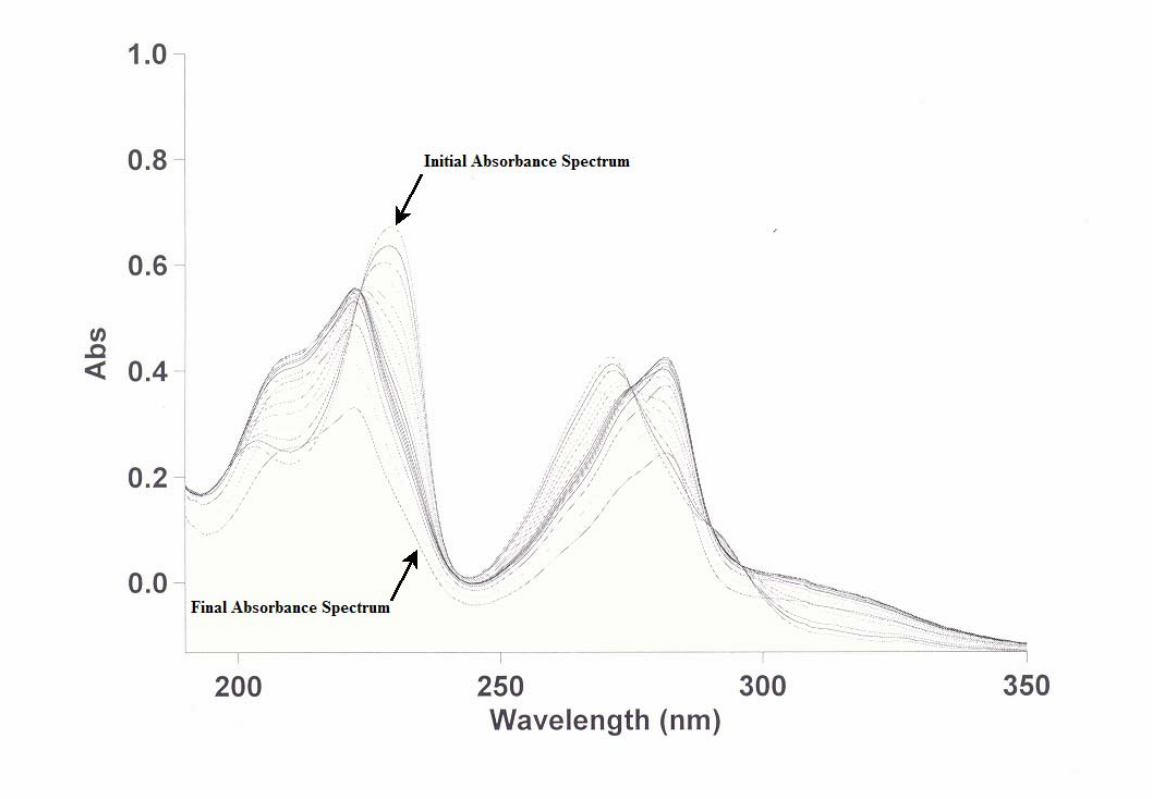

Figure 48: UV absorbance spectra for the titration of 1:1 Mg(II) and PDALC at $2x10^{-5}$ *M* with the pH ranging from 5.48 to 1.51 in 0.1 *M* $NaClO_4$ at 25 ± 0.1 °C.

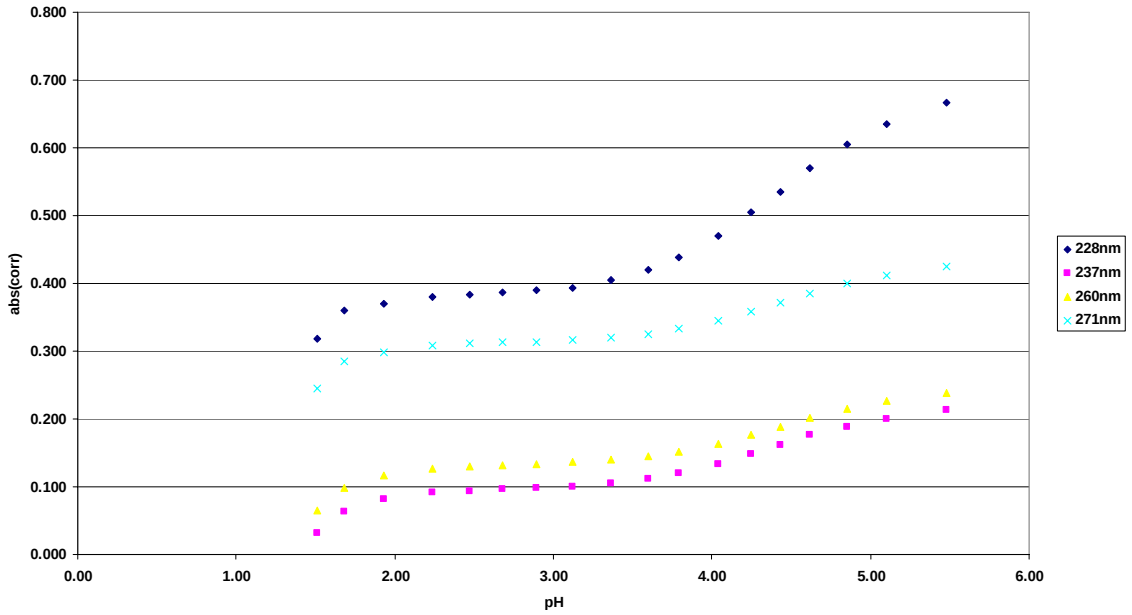

Figure 49: Combined plot of corrected absorbance data versus pH for wavelengths 228 nm, 237 nm, 260 nm, and 271 nm for the titration of PDALC ($2x10^{-5}$ *M*) with Mg(II) ($2x10^{-5}$ *M*) in 0.1 *M* $NaClO_4$ at 25 ± 0.1 °C.

a.)

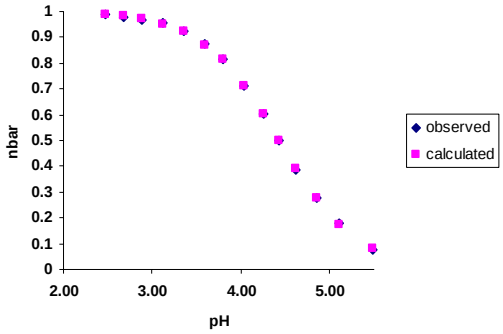

b.)

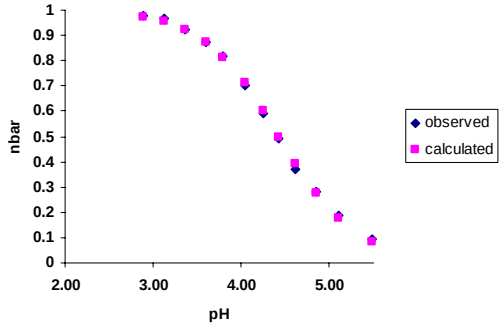

c.)

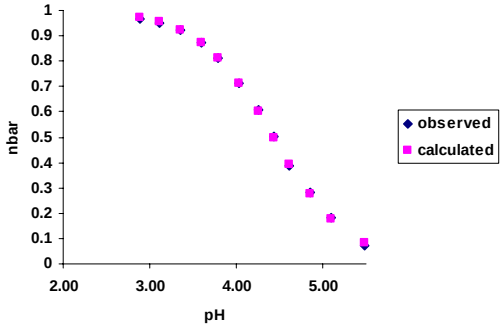

d.)

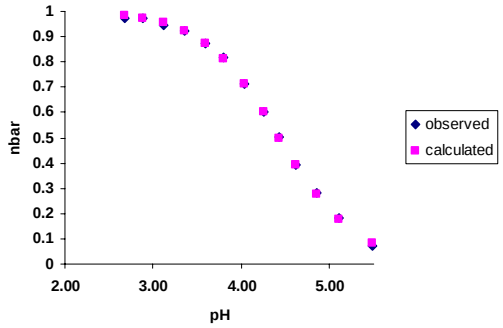

Figure 50: Comparison of $\bar{n}$ observed versus $\bar{n}$ calculated with respect to pH at wavelengths of a.) 228 nm, b.) 237 nm, c.) 260 nm, and d.) 271 nm for the titration of PDALC ($2x10^{-5}$ *M*) with Mg(II) ($2x10^{-5}$ *M*) for determining the log*K* value. The theoretical curves were calculated from an apparent pK_a of 4.43.

PDALC-nickel(II) results

Nickel(II) has an ionic radius of 0.69 Å, which is one of the smaller metals tested. The UV absorbance spectra are shown in Figure 51 for the titration of Ni(II) with PDALC. An example plot of corrected absorbance versus pH for Ni(II) is shown in Figure 52. In addition, observed and calculated $\bar{n}$ versus pH plots are shown in Figure 53. From the selected wavelengths described above, an apparent pK_a of 1.02 and a log K_1 of 8.63 was calculated for Ni(II) with PDALC using Equations (1-9). When compared to the log K_1 of EDDE, which is 6.70, PDALC showed an increase in complex stability.[21] A Δ log K_1 of about 1.93 shows a quantitative difference in stability between the PDALC complex and the EDDE complex of Ni(II). When compared to the log K_1 of 1,10 phenanthroline, which is 8.7, PDALC showed a slight decrease in complex stability.[21] A Δ log K_1 of about -0.1 shows a quantitative difference in stability between the PDALC complex and the 1,10 phenanthroline complex of Ni(II).

PDALC-strontium(II) results

Strontium(II) has an ionic radius of 1.18 Å, which is one of the larger metals tested. The UV absorbance spectra are shown in Figure 54 for the titration of Sr(II) with PDALC. An example plot of corrected absorbance versus pH for Sr(II) is shown in Figure 55. In addition, observed and calculated $\bar{n}$ versus pH plots are shown in Figure 56. From the selected wavelengths described above, an apparent pK_a of 3.73 and a log K_1 of 2.40 was calculated for Sr(II) with PDALC using Equations (1-9). When compared to the log K_1 of 1,10 phenanthroline, which is 0.7, PDALC showed an increase in complex stability.[21] A Δ log K_1 of about 1.7 shows a quantitative difference in stability between the PDALC complex and the 1,10 phenanthroline complex of Pb(II). There was no log K_1 reported for EDDE with Sr(II) to compare to PDALC

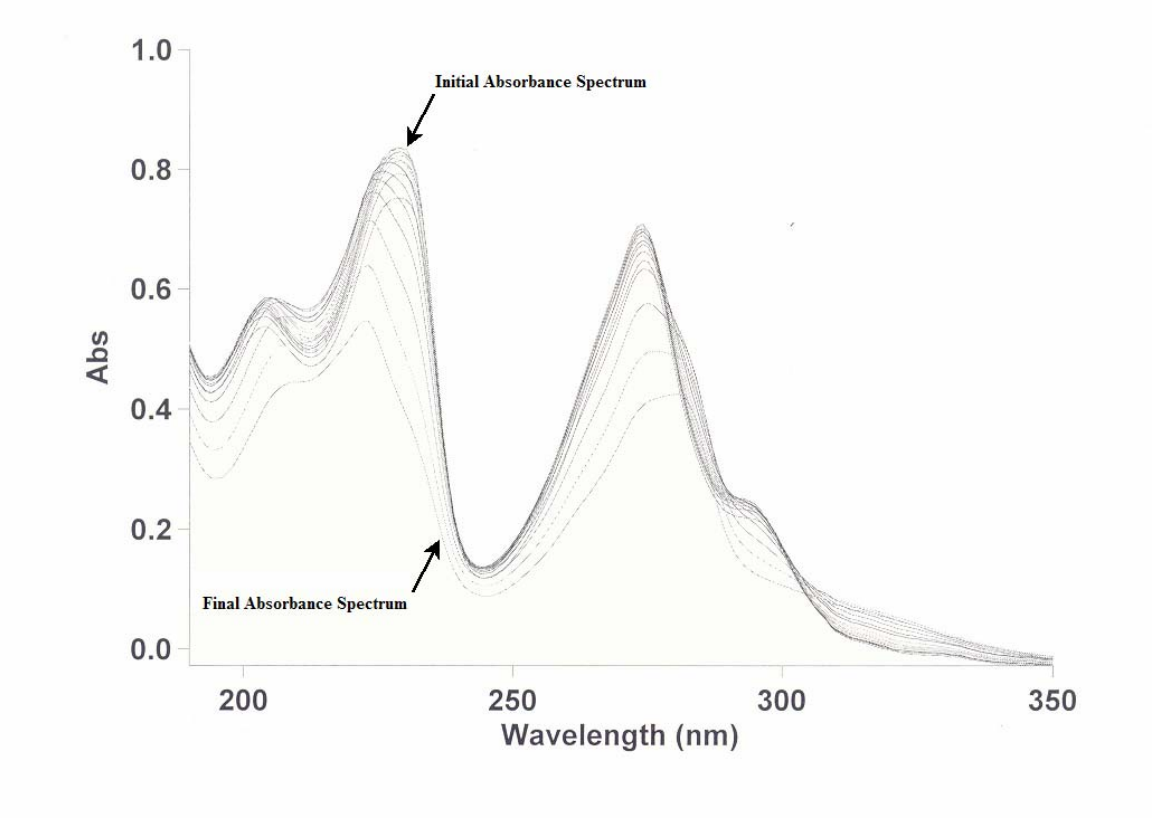

Figure 51: UV absorbance spectra for the titration of 1:1 Ni(II) and PDALC at $2x10^{-5}$ *M* with the pH ranging from 5.94 to 1.51 in 0.1 *M* $NaClO_4$ at 25 ± 0.1 °C.

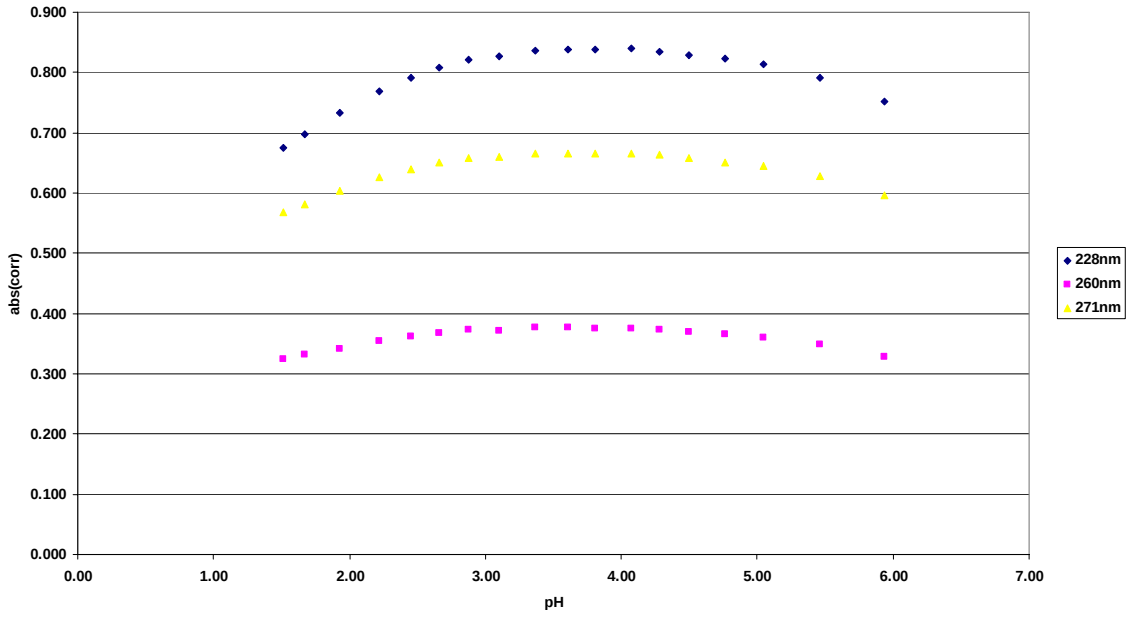

Figure 52: Combined plot of corrected absorbance data versus pH for wavelengths 228 nm, 260 nm, and 271 nm for the titration of PDALC ($2x10^{-5}$ *M*) with Ni(II) ($2x10^{-5}$ *M*) in 0.1 *M* $NaClO_4$ at 25 ± 0.1 °C.

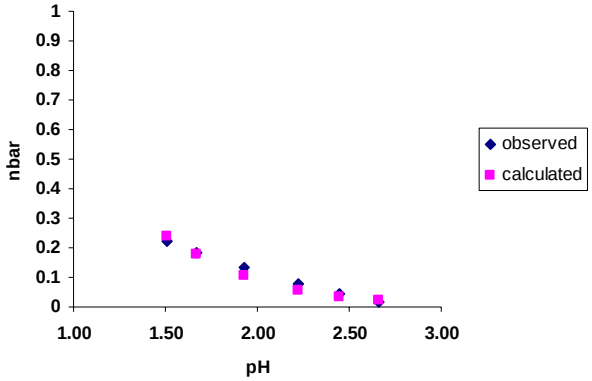

a.)

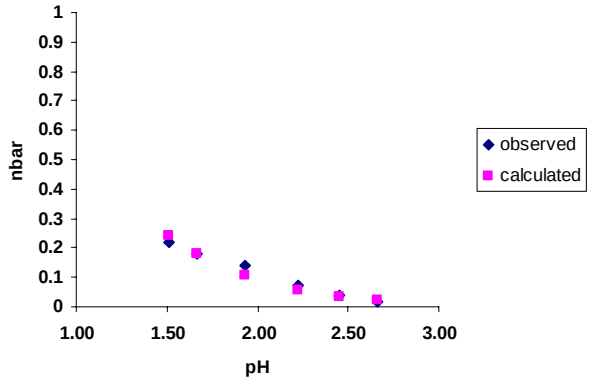

b.)

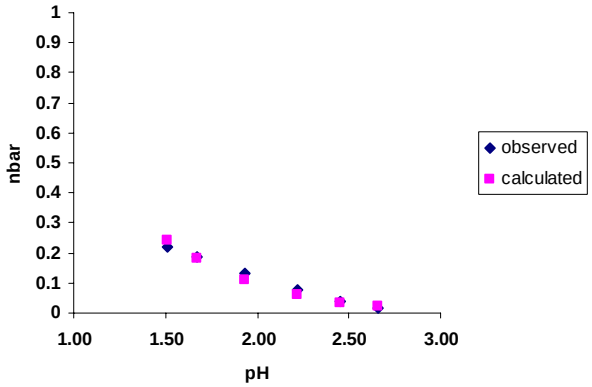

c.)

Figure 53: Comparison of $\bar{n}$ observed versus $\bar{n}$ calculated with respect to pH at wavelengths of a.) 228 nm, b.) 260 nm, and c.) 271 nm for the titration of PDALC ($2x10^{-5}$ *M*) with Ni(II) ($2x10^{-5}$ *M*) for determining the log*K* value. The theoretical curves were calculated from an apparent pK_a of 1.02.

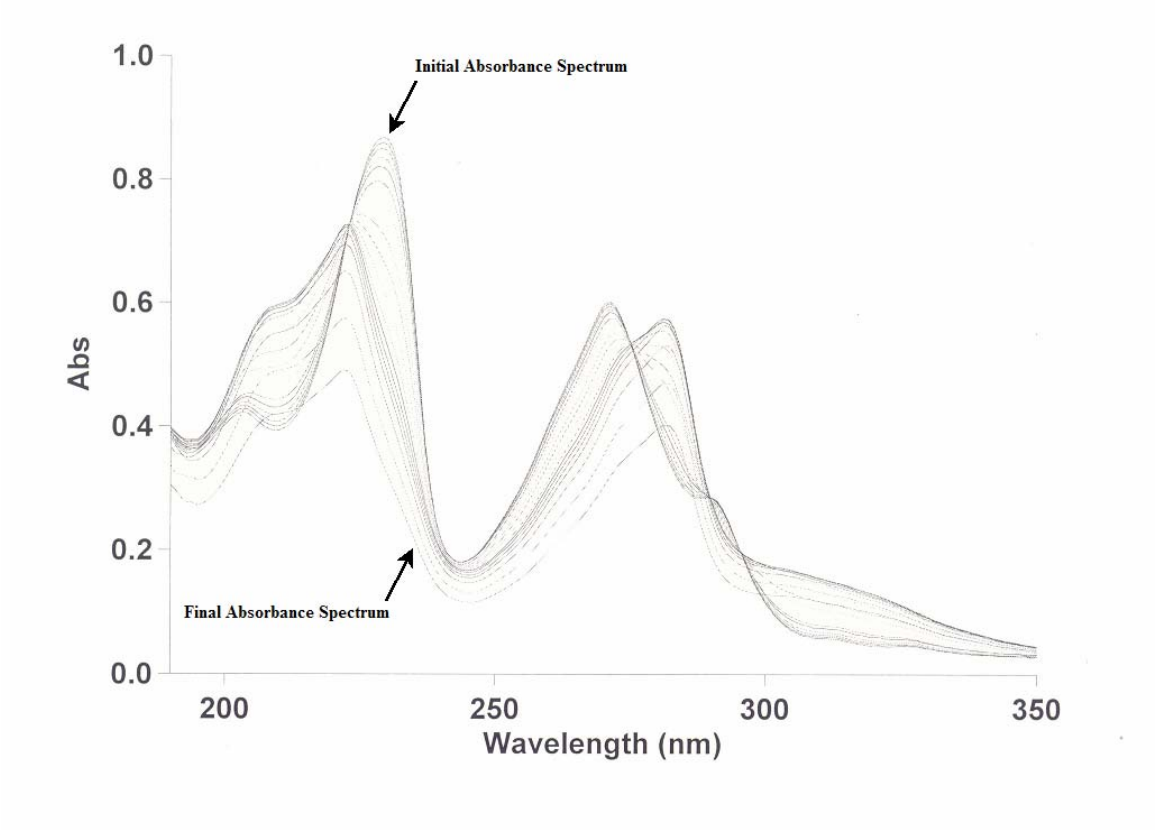

Figure 54: UV absorbance spectra for the titration of 1:1 Sr(II) and PDALC at $2x10^{-5}$ *M* with the pH ranging from 5.33 to 1.45 in 0.1 *M* $NaClO_4$ at 25 ± 0.1 °C.

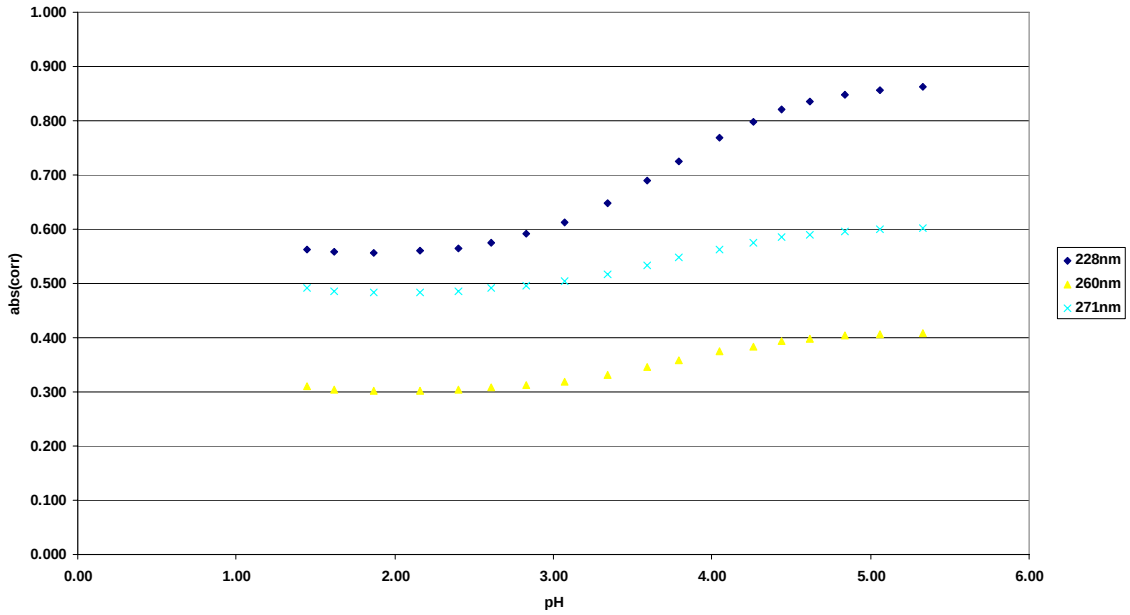

Figure 55: Combined plot of corrected absorbance data versus pH for wavelengths 228 nm, 260 nm, and 271 nm for the titration of PDALC ($2x10^{-5}$ *M*) with Sr(II) ($2x10^{-5}$ *M*) in 0.1 *M* $NaClO_4$ at 25 ± 0.1 °C.

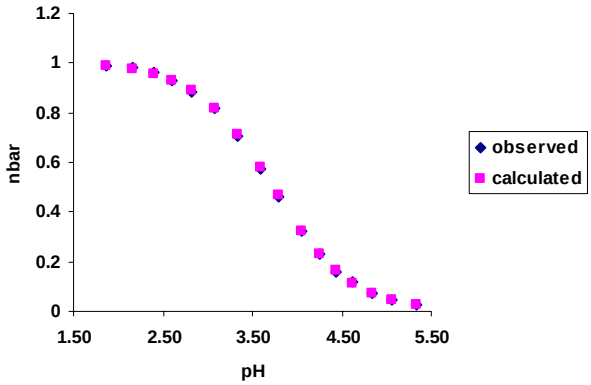

a.)

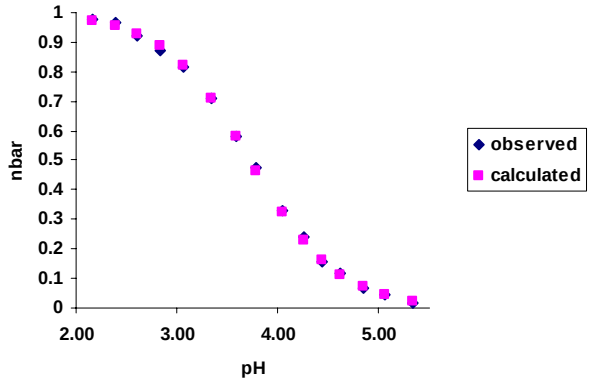

b.)

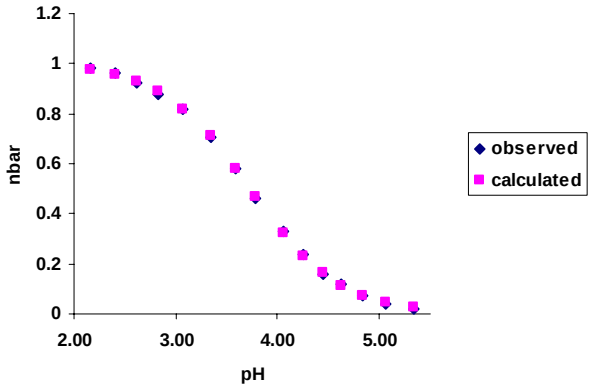

c.)

Figure 56: Comparison of $\bar{n}$ observed versus $\bar{n}$ calculated with respect to pH at wavelengths of a.) 228 nm, b.) 260 nm, and c.) 271 nm for the titration of PDALC ($2x10^{-5}$ *M*) with Sr(II) ($2x10^{-5}$ *M*) for determining the log*K* value. The theoretical curves were calculated from an apparent pK_a of 3.73.

with and due to the weakness of the PDALC complex with Sr(II), the log K_1 of EDDE with Sr(II) would probably not be large enough to measure with the techniques available.

PDALC-zinc(II) results

Zinc(II) has an ionic radius of 0.74 Å, which is one of the smaller metals tested. The UV absorbance spectra are shown in Figure 57 for the titration of Zn(II) with PDALC. An example plot of corrected absorbance versus pH for Zn(II) is shown in Figure 58. In addition, observed and calculated $\bar{n}$ versus pH plots are shown in Figure 59. From the selected wavelengths described above, an apparent pK_a of 3.14 and a log K_1 of 6.51 was calculated for Zn(II) with PDALC using Equations (1-9). When compared to the log K_1 of EDDE, which is 4.8, PDALC showed an increase in complex stability.[21] A Δ log K_1 of about 1.7 shows a quantitative difference in stability between the PDALC complex and the EDDE complex of Zn(II). When compared to the log K_1 of 1,10 phenanthroline, which is 6.4, PDALC showed a slight increase in complex stability.[21] A Δ log K_1 of about 0.1 shows a quantitative difference in stability between the PDALC complex and the 1,10 phenanthroline complex of Zn(II).

PDALC-zirconium(IV) results

Zirconium(IV) has an ionic radius of 0.72 Å, which is one of the smaller metals tested. The UV absorbance spectra are shown in Figure 60 for the titration of Zr(IV) with PDALC. An example plot of corrected absorbance versus pH for Zr(IV) is shown in Figure 61. In addition, observed and calculated $\bar{n}$ versus pH plots are shown in Figures 62, 63, 64, 65, and 66 for calculating log K_1, MLOH, $ML(OH)_2$, $ML(OH)_3$, and $ML(OH)_4$ respectively. From the selected wavelengths described above, an apparent pK_a of 1.76 and a log K_1 of 7.89 was calculated for

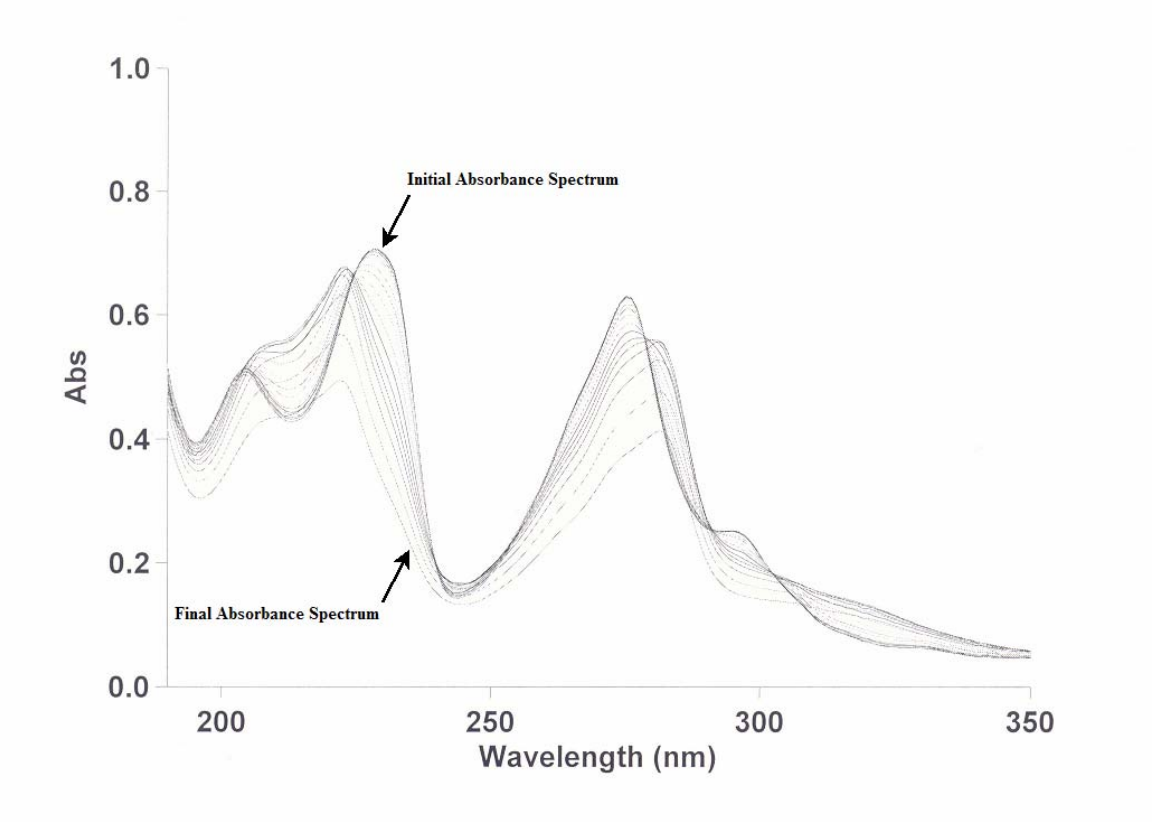

Figure 57: UV absorbance spectra for the titration of 1:1 Zn(II) and PDALC at $2x10^{-5}$ *M* with the pH ranging from 5.28 to 1.45 in 0.1 *M* $NaClO_4$ at 25 ± 0.1 °C.

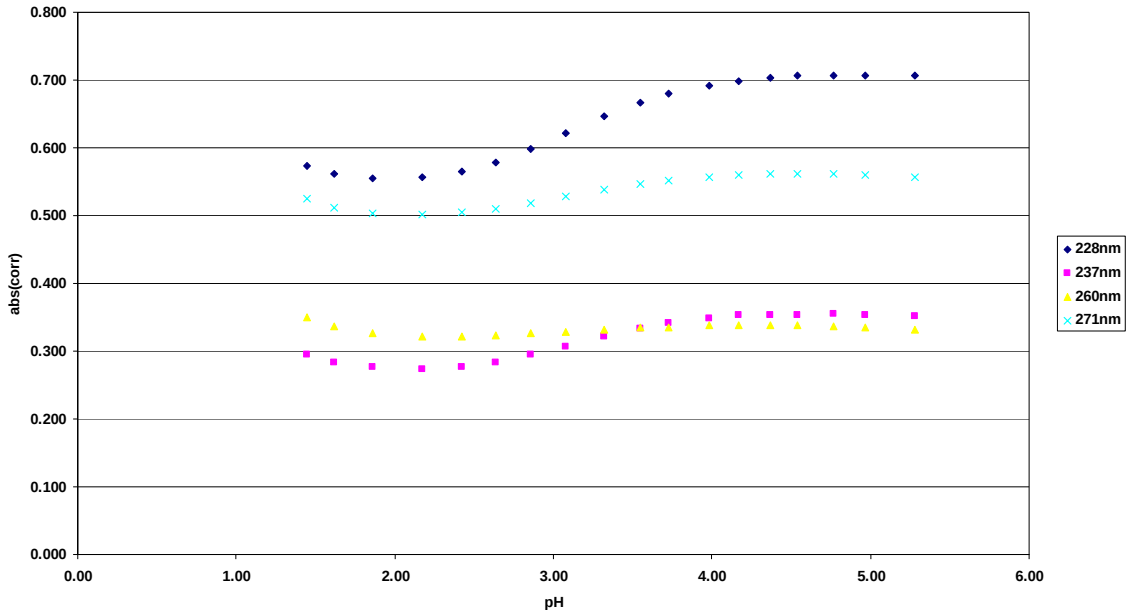

Figure 58: Combined plot of corrected absorbance data versus pH for wavelengths 228 nm, 237 nm, 260 nm, and 271 nm for the titration of PDALC ($2x10^{-5}$ *M*) with Zn(II) ($2x10^{-5}$ *M*) in 0.1 *M* $NaClO_4$ at 25 ± 0.1 °C.

a.)

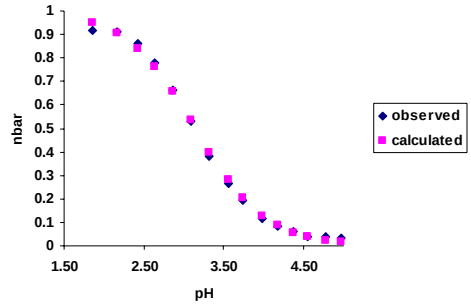

b.)

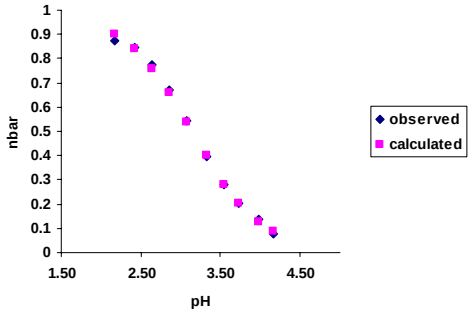

c.)

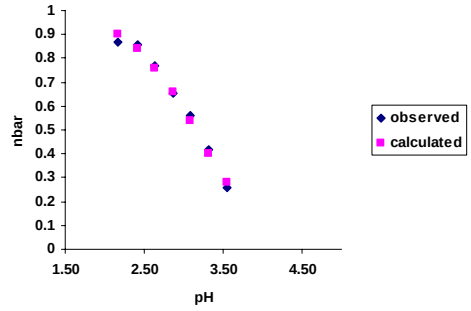

d.)

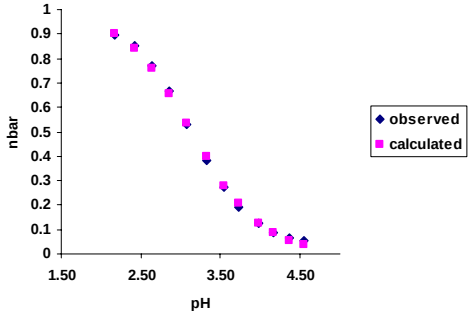

Figure 59: Comparison of $\bar{n}$ observed versus $\bar{n}$ calculated with respect to pH at wavelengths of a.) 228 nm, b.) 237 nm, c.) 260 nm, and d.) 271 nm for the titration of PDALC ($2x10^{-5}$ *M*) with Zn(II) ($2x10^{-5}$ *M*) for determining the log*K* value. The theoretical curves were calculated from an apparent pK_a of 3.14.

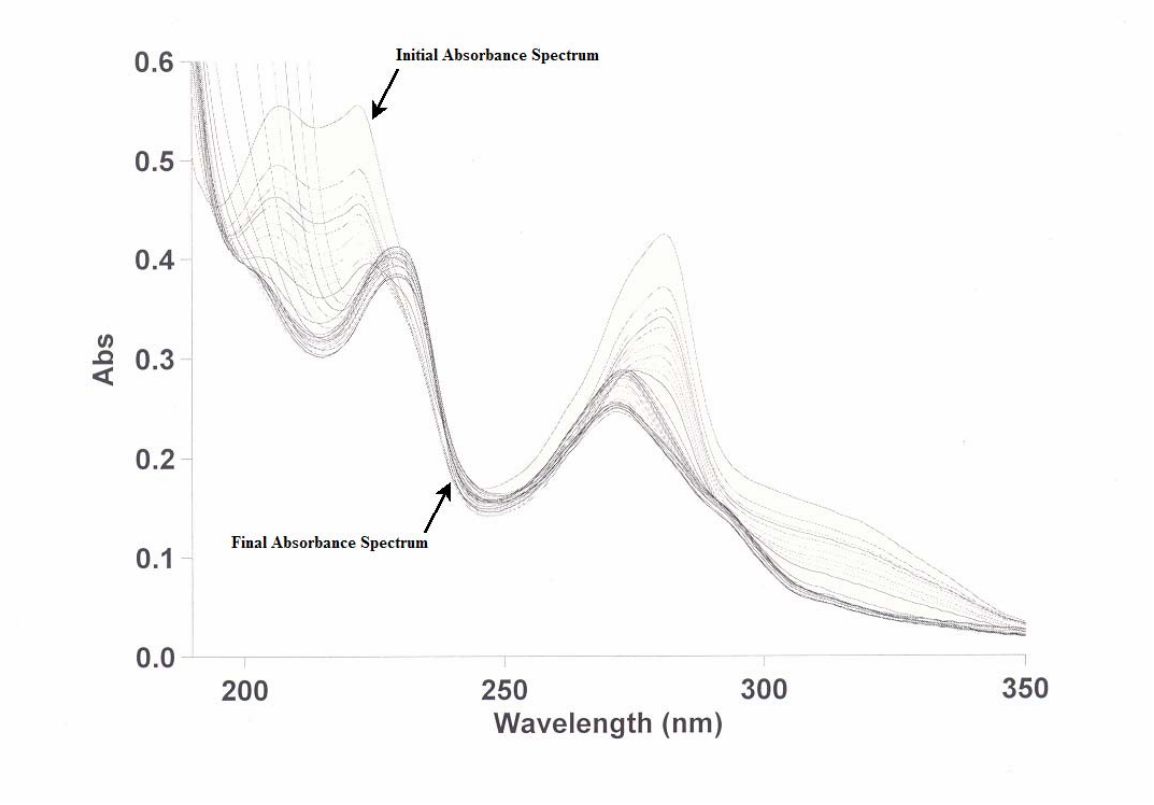

Figure 60: UV absorbance spectra for the titration of 1:2 Zr(IV) ($1x10^{-5}$ *M*) and PDALC ($2x10^{-5}$ *M*) with the pH ranging from 1.53 to 11.71 in 0.1 *M* $NaClO_4$ at 25 ± 0.1 °C.

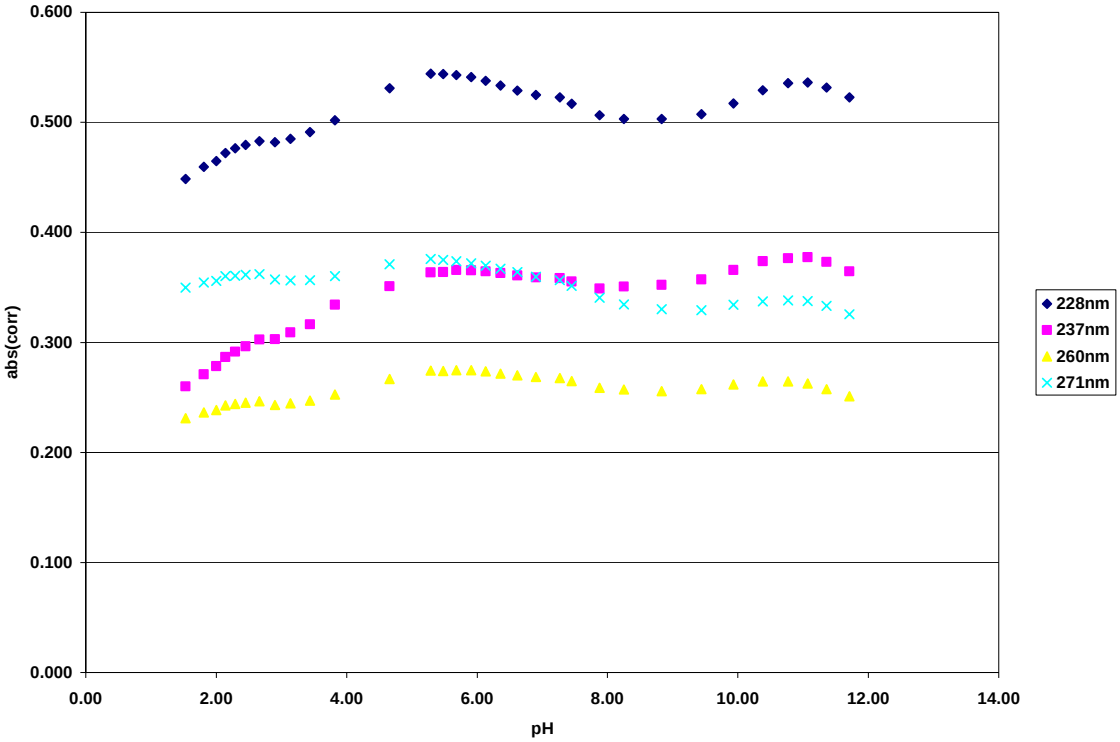

Figure 61: Combined plot of corrected absorbance data versus pH for wavelengths 228 nm, 237 nm, 260 nm, and 271 nm for the titration of PDALC with Zr(IV) ($2x10^{-5}$ *M*) in 0.1 *M* $NaClO_4$ at 25 ± 0.1 °C.

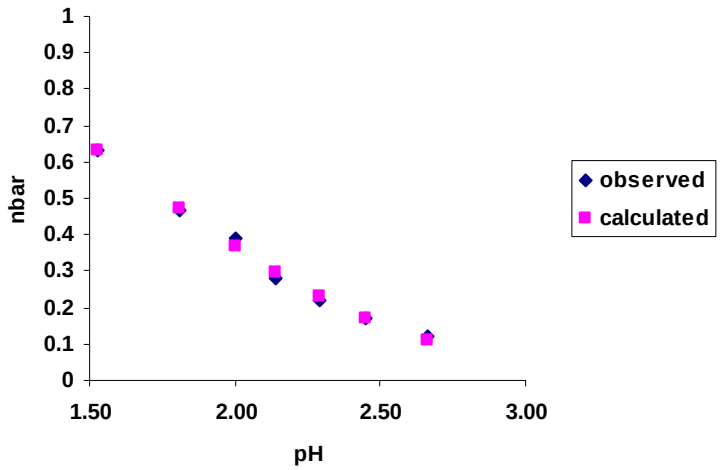

a.)

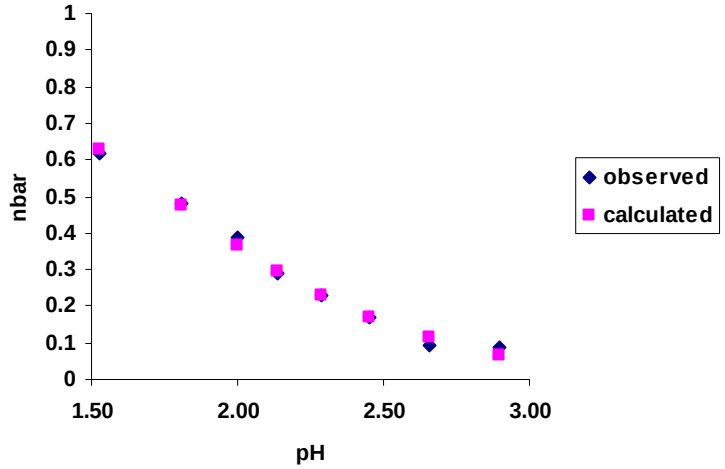

b.)

Figure 62: Comparison of $\bar{n}$ observed versus $\bar{n}$ calculated with respect to pH at wavelengths of a.) 228 nm and b.) 237 nm for the titration of PDALC ($2x10^{-5}$ *M*) with Zr(IV) ($1x10^{-5}$ *M*) for determining the log*K* value. The theoretical curves were calculated from an apparent pK_a of 1.76.

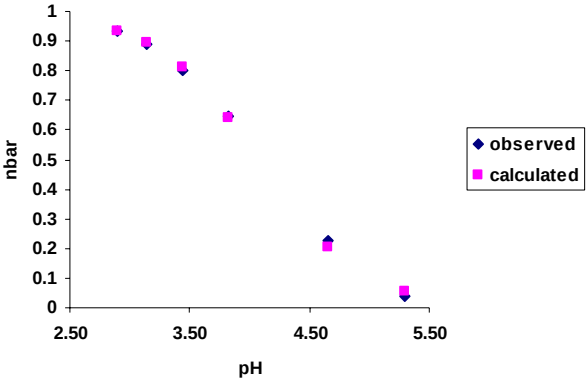

a.)

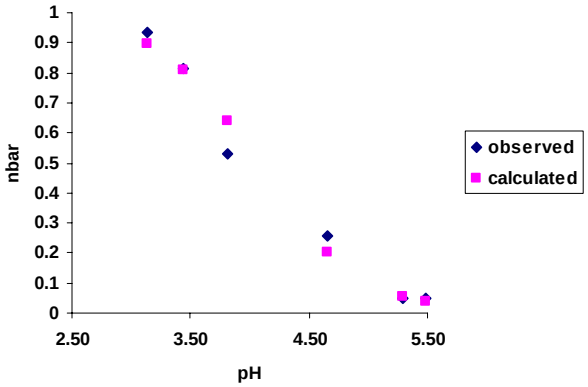

b.)

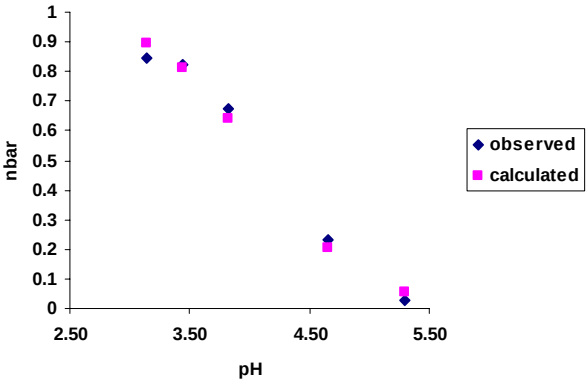

c.)

Figure 63: Comparison of $\bar{n}$ observed versus $\bar{n}$ calculated with respect to pH at wavelengths of a.) 228 nm, b.) 237 nm, and c.) 271 nm for the titration of PDALC (2x10^{-5} *M*) with Zr(IV) (1x10^{-5} *M*) for determining the MLOH value. The theoretical curves were calculated from an apparent pK_a of 4.06.

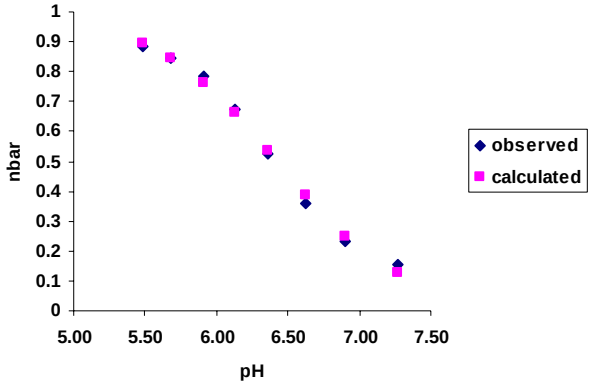

a.)

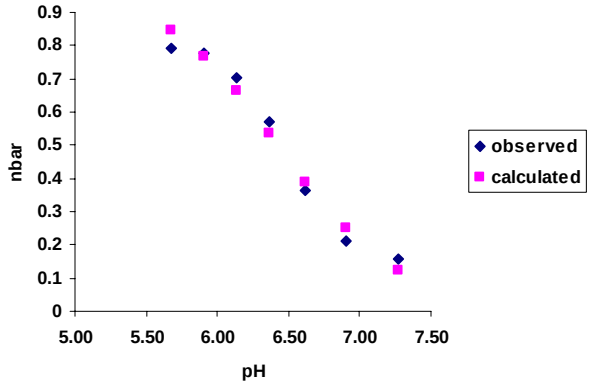

b.)

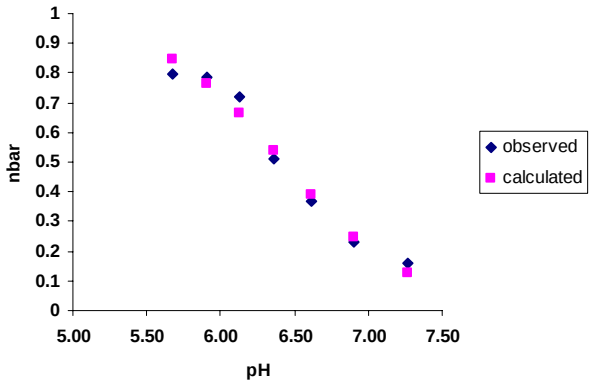

c.)

Figure 64: Comparison of $\bar{n}$ observed versus $\bar{n}$ calculated with respect to pH at wavelengths of a.) 228 nm, b.) 237 nm, and c.) 260 nm for the titration of PDALC ($2x10^{-5}$ *M*) with Zr(IV) ($1x10^{-5}$ *M*) for determining the $ML(OH)_2$ value. The theoretical curves were calculated from an apparent pK_a of 6.42.

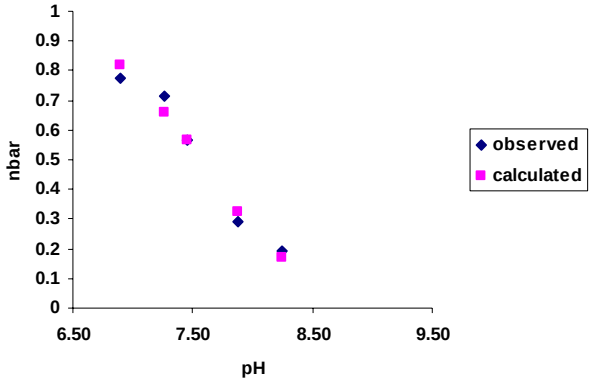

a.)

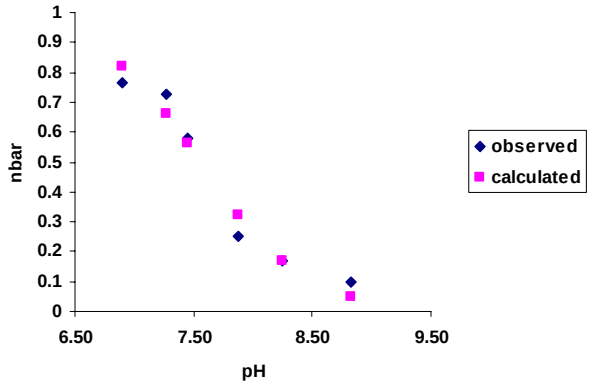

b.)

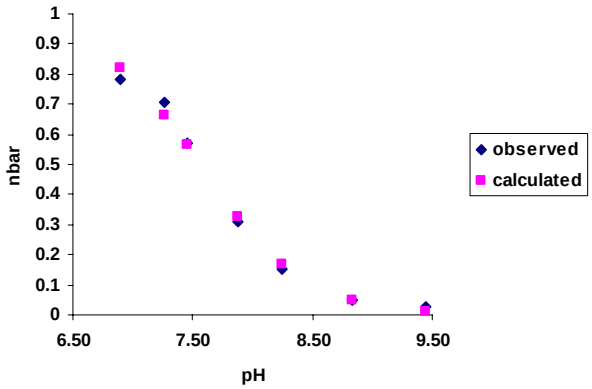

c.)

Figure 65: Comparison of $\bar{n}$ observed versus $\bar{n}$ calculated with respect to pH at wavelengths of a.) 228 nm, b.) 260 nm, and c.) 271 nm for the titration of PDALC ($2x10^{-5}$ *M*) with Zr(IV) ($1x10^{-5}$ *M*) for determining the $ML(OH)_3$ value. The theoretical curves were calculated from an apparent pK_a of 7.56.

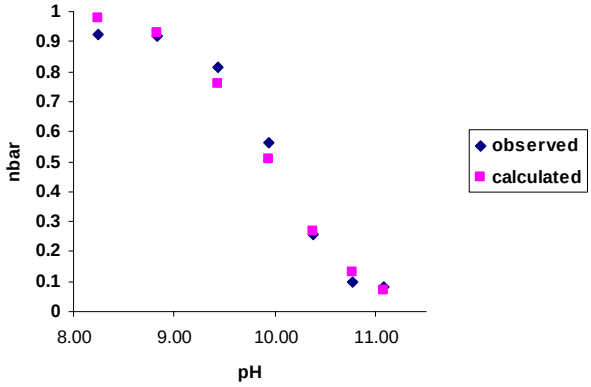

a.)

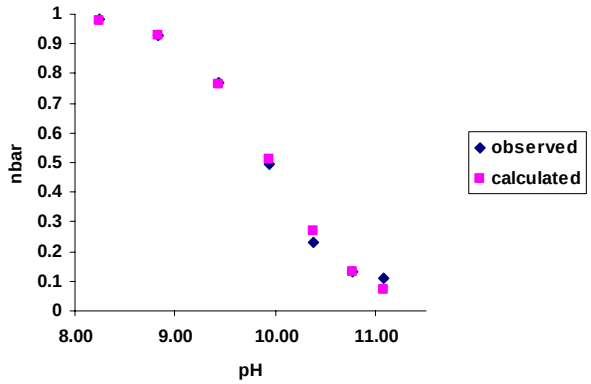

b.)

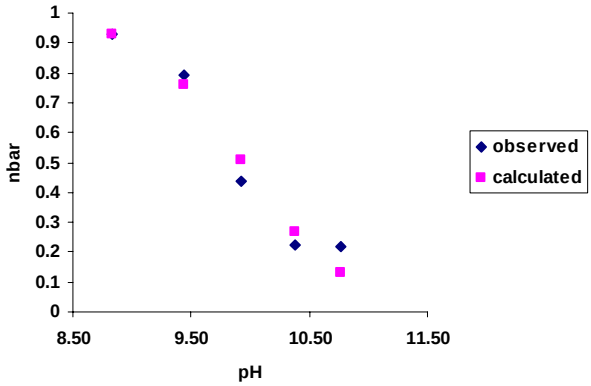

c.)

Figure 66: Comparison of $\bar{n}$ observed versus $\bar{n}$ calculated with respect to pH at wavelengths of a.) 228 nm, b.) 237 nm, and c.) 260 nm for the titration of PDALC ($2x10^{-5}$ *M*) with Zr(IV) ($1x10^{-5}$ *M*) for determining the $ML(OH)_4$ value. The theoretical curves were calculated from an apparent pK_a of 9.94.

Zr(IV) with PDALC using Equations (1-9). When compared to the log K_1 of 1,10 phenanthroline, which is 6.6, PDALC showed a slight decrease in complex stability.[21] A Δ log K_1 of about 1.29 shows a quantitative difference in stability between the PDALC complex and the 1,10 phenanthroline complex of Zr(IV). There was no log K_1 reported for EDDE with Zr(IV) to compare to PDALC with and because of the acidic nature of the Zr(IV) and its low solubility, the log K_1 of EDDE could not be measured with the techniques available.

Potentiometric titrations involving EDDE

The titration experiments were performed utilizing a glass electrode as an analytical tool to detect metal complex formation involving EDDE. Potential readings were recorded as additions of nitric acid were made. Before the titration could be performed on EDDE, the electrode was calibrated with the 0.01 *M* HNO_3 and 0.09 *M* $NaNO_3$ solution titrated into 0.01 *M* NaOH and 0.09 *M* $NaNO_3$. The potential readings, in mV, were plotted against the calculated pH, based on the concentration of acid in the solution, to yield a straight line. The slope and the y-intercept are calculated by EXCEL and were used to calculate the pH of following titrated solutions. The slope ranged from 56.1 to 56.5 and the y-intercept ranged from 399 to 405.

In order to determine the protonation constants for the ligand, EDDE, a titration experiment was performed at 25.0 ± 0.1 °C in 0.10 *M* $NaClO_4$ for ionic strength. Figure 67 shows potential, in mV, versus the volume of acid added. The two peaks in the graph represent the two protonation events of EDDE. Figure 68 shows the plot of $\bar{n}$ versus pH, which was calculated from the potential reading, and used to calculate the protonation constants of EDDE. The protonation constants, the pK_{a1} and pK_{a2}, values were calculated to be 9.36 and 6.37, respectively. These values agree with the literature values of pK_{a1} and pK_{a2} of 9.24 and 6.26.[21]

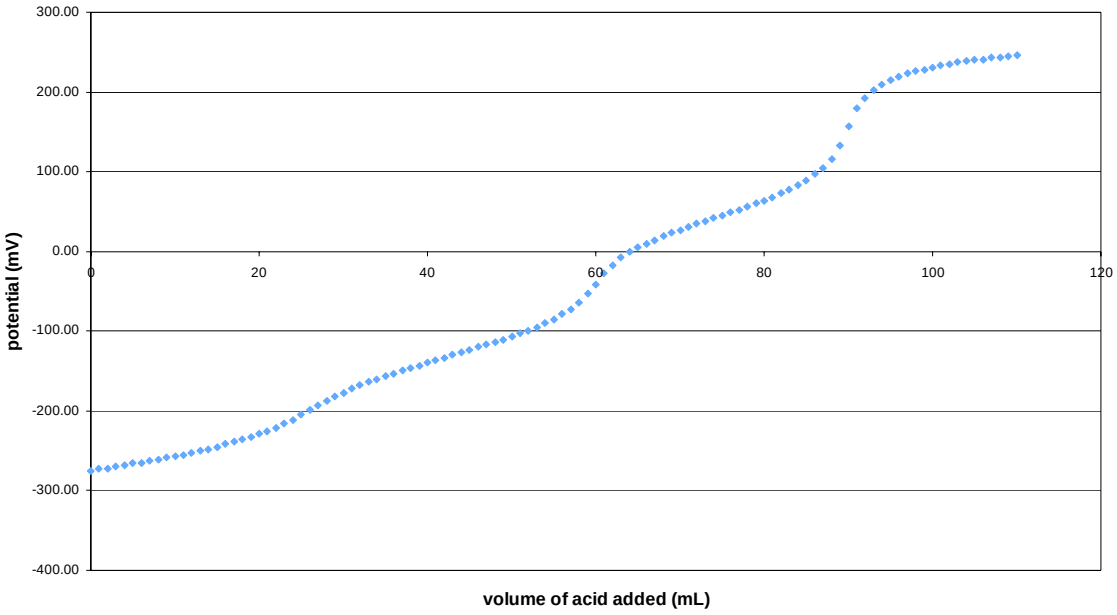

Figure 67: Plot of potential (mV) versus the volume of acid added (mL) for the titration of EDDE (0.01 *M*) with HNO_3 (0.01 *M*) in 0.1 M $NaNO_3$ at 25 ± 0.1 ºC.

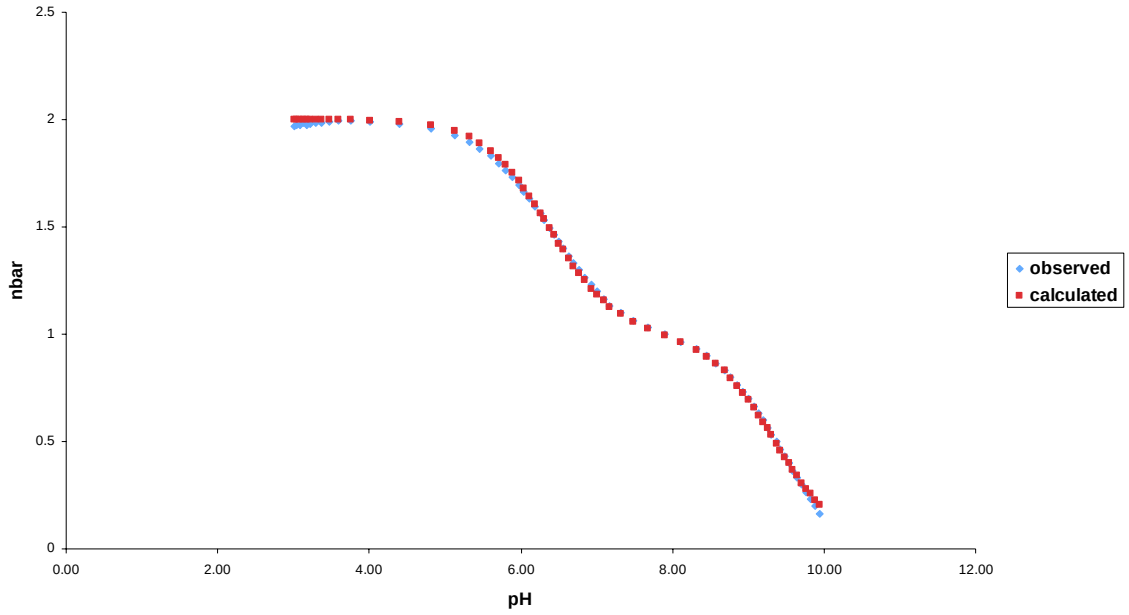

Figure 68: Comparison of $\bar{n}$ observed versus $\bar{n}$ calculated with respect to pH for the titration of EDDE (0.01 *M*) in 0.1 M $NaNO_3$ at 25 ± 0.1 ºC used to calculate the value of pK_1 and pK_2.

Potentiometric titrations involving metals with EDDE

EDDE-Calcium(II) results

Calcium(II) has an ionic radius of 1.00 Å, which lies in the middle of the range of metals tested. The observed and calculated $\bar{n}$ versus plots are shown in Figure 69. Using this data, a log K_1 of 1.08 was calculated using Equations (1-9).

EDDE-Lanthanum(III) results

Lanthanum(III) has an ionic radius of 1.03 Å, which lies in the middle of the range of metals tested. The observed and calculated $\bar{n}$ versus plots are shown in Figure 70. Using this data, a log K_1 of 4.30 was calculated using Equations (1-9).

EDDE-Magnesium(II) results

Magnesium(II) has an ionic radius of 0.74 Å, which is one of the smaller metals tested. The observed and calculated $\bar{n}$ versus plots are shown in Figure 71. Using this data, a log K_1 of 1.24 was calculated using Equations (1-9).

Crystal Structure Results

No crystal structures have been reported for PDALC. Crystals have been grown with Bi(III), Ca(II), Cd(II), Cu(II), Gd(III), Mg(II), Ni(II), Pb(II), and Zn(II) and confirmed through IR analysis. Crystal structures for Bi(III), Ca(II), Cd(II), Gd(III), and Pb(II) have been sent out for analysis. Structures for Bi(III), Ca(II), and Pb(II) have been completed.

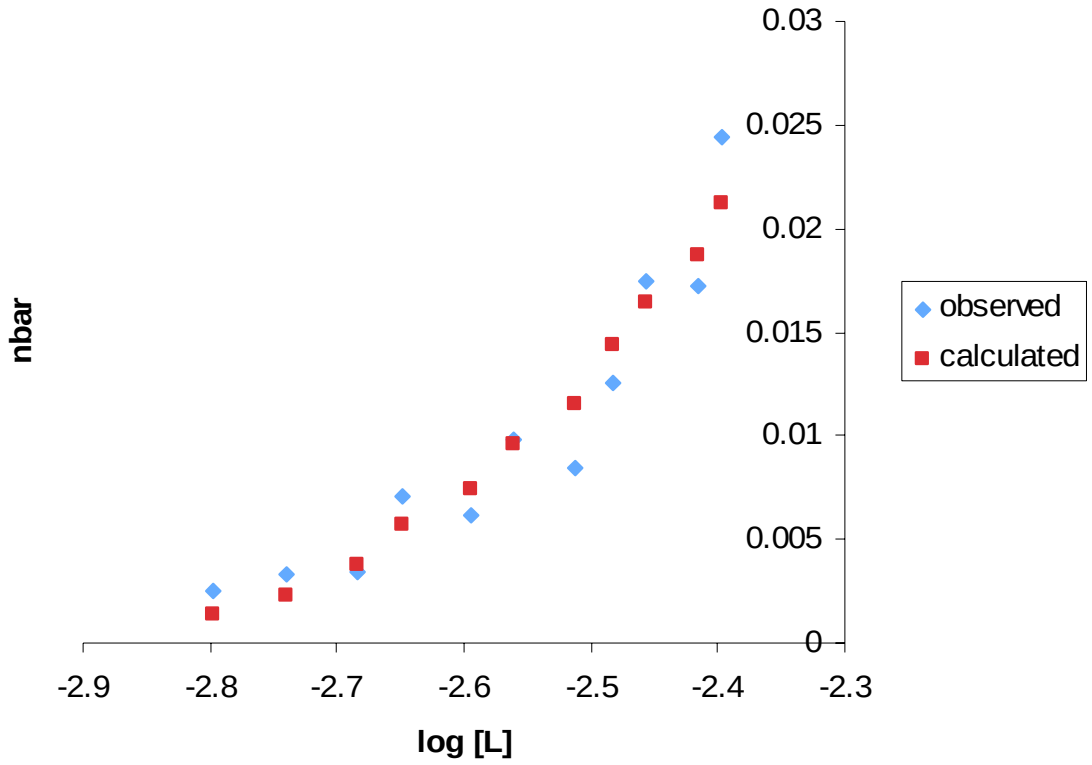

Figure 69: Comparison of $\bar{n}$ observed versus $\bar{n}$ calculated with respect to pH for the titration of EDDE (0.01 *M*) with Ca(II) (0.0333 *M*) at 25 ± 0.1 ºC used to calculate the value of log K_1. The theoretical curve was calculated with a log K_1 of 1.08 for the Ca(II)-EDDE complex.

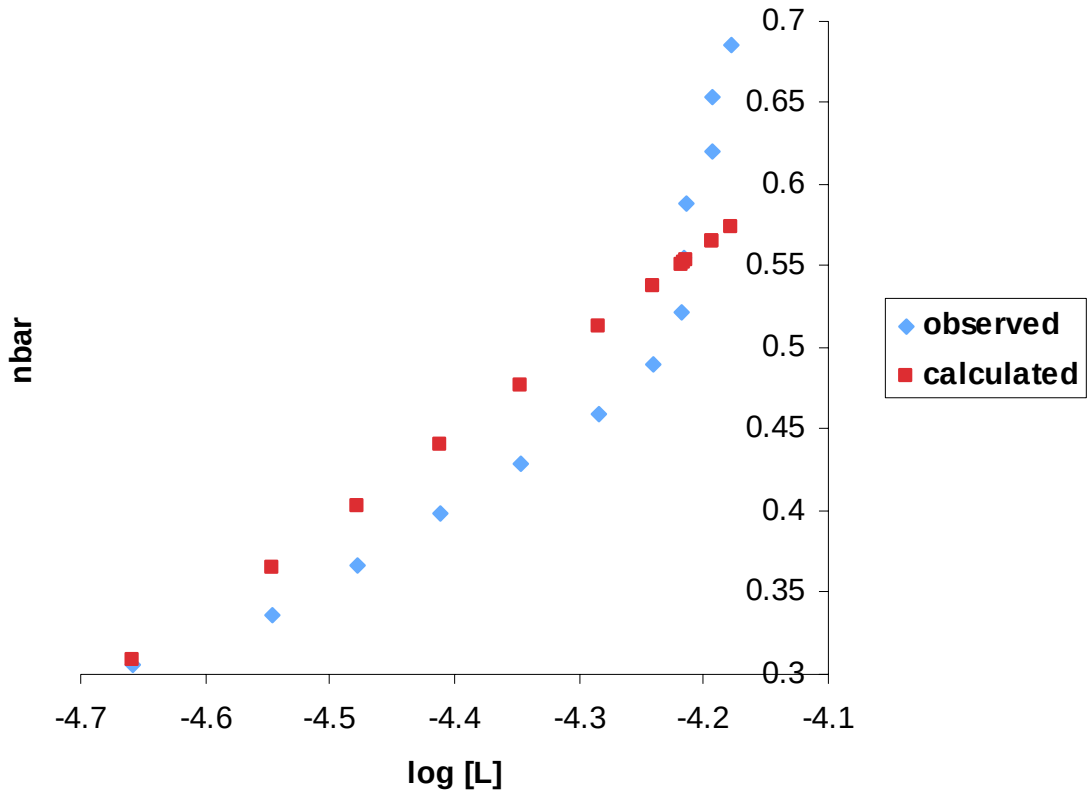

Figure 70: Comparison of $\bar{n}$ observed versus $\bar{n}$ calculated with respect to pH for the titration of EDDE (0.01 *M*) with La(III) (0.01 *M*) in 0.1 M $NaNO_3$ at 25 ± 0.1 ºC used to calculate the value of log K_1. The theoretical curve was calculated with a log K_1 of 4.30 for the La(III)-EDDE complex.

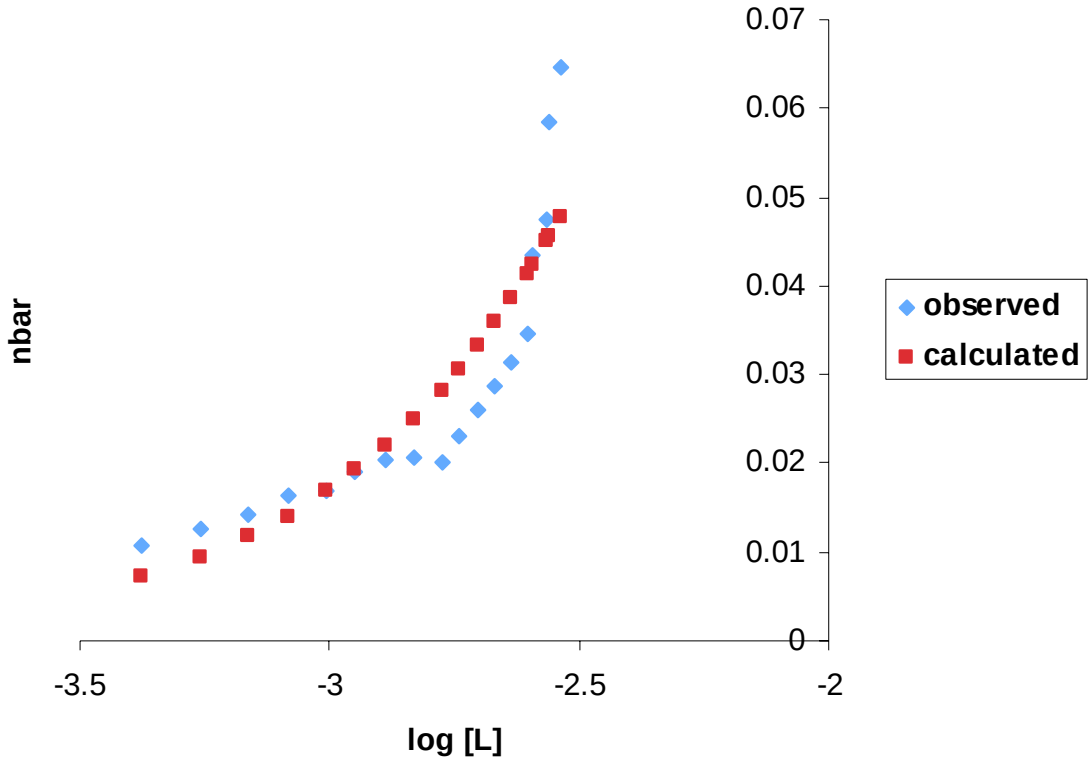

Figure 71: Comparison of $\bar{n}$ observed versus $\bar{n}$ calculated with respect to pH for the titration of EDDE (0.01 *M*) with Mg(II) (0.01 *M*) in 0.1 M $NaNO_3$ at 25 ± 0.1 ºC used to calculate the value of log K_1. The theoretical curve was calculated with a log K_1 of 1.24 for the Mg(II)-EDDE complex.

The $[Bi(PDALC)(H_2O)_2]\cdot(ClO_4)_3\cdot H_2O$ crystal structure

The synthesis of $[Bi(PDALC)(H_2O)_2]\cdot(ClO_4)_3\cdot H_2O$ crystals produced crystals that were thick brown needles on the interface of the *n*-butanol/H_2O layers. The IR analysis, shown in Figure 72, indicates that the ligand is present, but the peaks are shifted, suggesting complex formation. The crystal structure of $[Bi(PDALC)(H_2O)_2]\cdot(ClO_4)_3\cdot H_2O$ consists of a Bi(III) metal ion coordinated with one PDALC molecule through all four donor atoms along with two H_2O molecules as in Figure 73. The Bi(III) was coordinated to both neutral nitrogen donor atoms and both neutral oxygen donor atoms of PDALC, giving Bi(III) a coordination number of six including the coordinated H_2O molecules. Since Bi(III) is such an acidic metal ion, it was predicted that the alcohol groups in PDALC would be deprotonated upon complexation. This was not seen in the structure, and is likely due to the acidic nature of the H_2O layer which was necessary to keep the Bi(III) dissolved. The complex also showed two H_2O molecules coordinated to Bi(III) which makes the metal six coordinate. The crystal data and structural refinement parameters for the $[Bi(PDALC)(H_2O)_2]^{3+}$ complex are listed in Table 2. In addition, the spatial coordinates of the atoms for the $[Bi(PDALC)(H_2O)_2]^{3+}$ complex are given in Tables 3 and 4.

The bond distances and angles for the $[Bi(PDALC)(H_2O)_2]^{3+}$ complex are shown in Table 5 and 6 respectively. Each unit cell of the crystal contained a Bi(III) ion positioned among the four donor atoms of PDALC. The bond distance between the Bi(III) and nitrogens of PDALC were 2.354 and 2.350 Å, which were shorter bonds than that for the alcoholic groups of the PDALC. The Bi(III) and alcoholic oxygen bond distances from PDALC were 2.469 and 2.450 Å. Two H_2O molecules were also coordinated to the Bi(III) metal ion, which had Bi(III) and

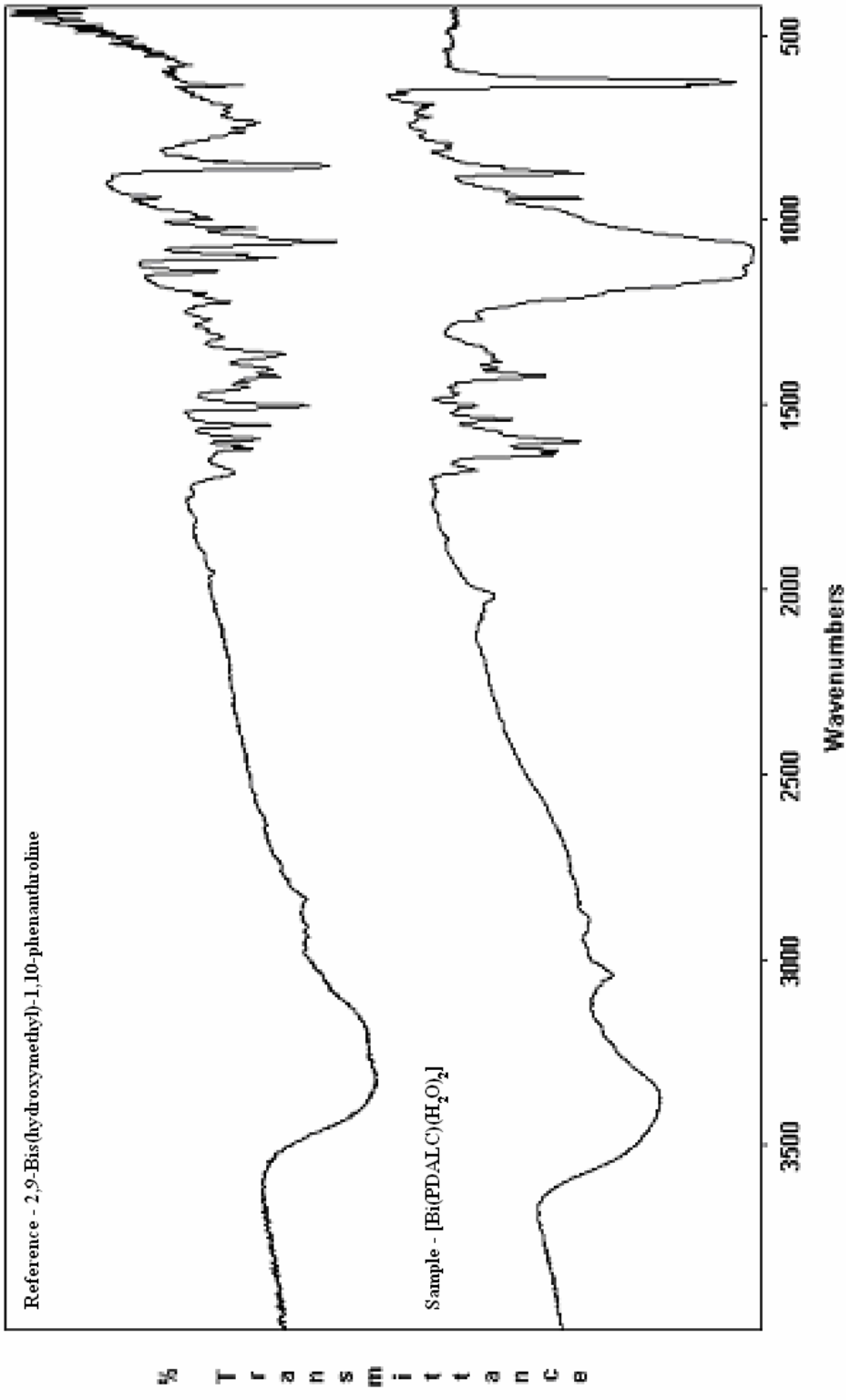

Figure 72: IR spectrum of $[Bi(PDALC)(H_20)_2]\cdot(ClO_4)_3\cdot H_2O$ crystals with the IR spectrum of PDALC as a reference.

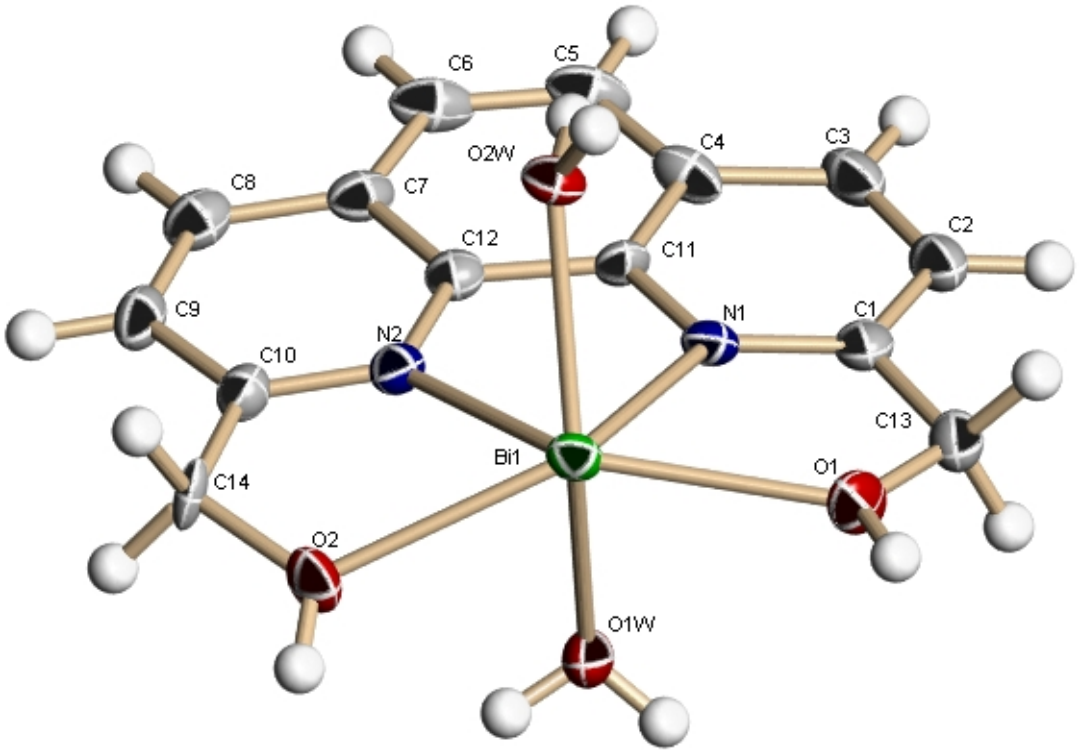

Figure 73: Crystal structure and atom assignments for the [Bi(PDALC)($H_20)_2$] complex. Note the apparent gap in the coordination geometry around Bi(III) in the O(1)-Bi-O(2) angle, suggesting the presence of a stereochemically active lone pair.[31]

Table 2: Crystal data and structure refinement for the [Bi(PDALC)(H_2O)$_2$] complex.

Identification code	rh65a
Empirical formula	C14 H18 Bi Cl3 N2 O17
Formula weight	801.63
Temperature	110(2) K
Wavelength	0.71073 Å
Crystal system	Monoclinic
Space group	P2(1)/c
Unit cell dimensions	a = 12.8140(17) Å □= 90°.
	b = 19.242(3) Å □= 91.763(2)°.
	c = 9.2917(12) Å □ = 90°.
Volume	2289.9(5) Å^3
Z	4
Density (calculated)	2.325 Mg/m^3
Absorption coefficient	8.140 mm^{-1}
F(000)	1544
Crystal size	0.30 x 0.20 x 0.20 mm^3
Theta range for data collection	4.20 to 25.00°.
Index ranges	-15<=h<=15, -22<=k<=22, -11<=l<=11
Reflections collected	16624
Independent reflections	3904 [R(int) = 0.0871]
Completeness to theta = 25.00°	96.9 %
Absorption correction	Semi-empirical from equivalents
Max. and min. transmission	0.2929 and 0.1939
Refinement method	Full-matrix least-squares on F^2
Data / restraints / parameters	3904 / 18 / 334
Goodness-of-fit on F^2	1.025
Final R indices [I>2sigma(I)]	R1 = 0.0428, wR2 = 0.1020
R indices (all data)	R1 = 0.0497, wR2 = 0.1099
Largest diff. peak and hole	5.935 and -1.313 e.Å^{-3}

Table 3: Atomic coordinates (x 10^4) and equivalent isotropic displacement parameters ($Å^2$x 10^3) for [Bi(PDALC)(H_2O)$_2$]. U(eq) is defined as one third of the trace of the orthogonalized U^{ij} tensor.

	x	y	z	U(eq)
Bi(1)	8316(1)	9584(1)	8219(1)	19(1)
N(2)	7500(4)	10490(2)	6916(6)	19(1)
O(1)	7968(4)	8339(2)	8476(5)	28(1)
O(2)	8333(3)	10726(2)	9432(5)	26(1)
O(1W)	6744(4)	9641(2)	9352(6)	32(1)
O(2W)	9249(3)	9645(2)	6007(5)	21(1)
O(3W)	8918(4)	7333(2)	9875(5)	35(1)
N(1)	7140(4)	9125(3)	6470(5)	19(1)
C(1)	6909(5)	8456(3)	6366(7)	24(1)
C(2)	6277(5)	8207(4)	5219(7)	27(1)
C(3)	5890(5)	8652(4)	4172(7)	28(2)
C(4)	6129(5)	9374(4)	4275(7)	25(1)
C(5)	5753(5)	9880(4)	3279(7)	30(2)
C(6)	5956(5)	10558(4)	3499(8)	30(2)
C(7)	6561(5)	10794(3)	4716(7)	23(1)
C(8)	6727(5)	11506(4)	5040(7)	27(2)
C(9)	7256(5)	11685(3)	6284(7)	25(1)
C(10)	7629(5)	11162(3)	7217(7)	21(1)
C(11)	6745(5)	9582(3)	5474(7)	18(1)
C(12)	6944(5)	10312(3)	5698(7)	20(1)
C(13)	7305(5)	7976(3)	7518(7)	26(1)
C(14)	8209(5)	11317(3)	8527(7)	19(1)

Table 4: Hydrogen coordinates (x 10^4) and isotropic displacement parameters ($Å^2$x 10^3) for [Bi(PDALC)(H_2O)$_2$].

	x	y	z	U(eq)
H(1A)	8262	8119	9172	34
H(2A)	8408	10763	10341	32
H(1W1)	6506	9308	9847	38
H(2W1)	6779	9992	9906	38
H(1W2)	8905	9618	5212	25
H(2W2)	9794	9418	5803	25
H(1W3)	9056	7152	9069	52
H(2W3)	9233	7375	10690	52
H(2)	6114	7726	5163	33
H(3)	5468	8480	3392	33
H(5)	5356	9739	2450	36
H(6)	5689	10889	2824	36
H(8)	6473	11855	4398	32
H(9)	7370	12161	6515	30
H(13A)	6710	7780	8041	31
H(13B)	7688	7586	7082	31
H(14A)	8906	11496	8286	23
H(14B)	7842	11686	9054	23

Table 5: Bond lengths (Å) for [Bi(PDALC)(H_2O)$_2$].

Bond	Bond Length (Å)
Bi(1)-O(1W)	2.303(5)
Bi(1)-N(2)	2.350(5)
Bi(1)-N(1)	2.354(5)
Bi(1)-O(2W)	2.412(5)
Bi(1)-O(1)	2.450(4)
Bi(1)-O(2)	2.469(4)
N(2)-C(10)	1.332(8)
N(2)-C(12)	1.363(9)
O(1)-C(13)	1.399(8)
O(2)-C(14)	1.420(7)
N(1)-C(1)	1.323(8)
N(1)-C(11)	1.363(8)
C(1)-C(2)	1.404(9)
C(1)-C(13)	1.491(10)
C(2)-C(3)	1.377(10)
C(3)-C(4)	1.425(10)
C(4)-C(11)	1.404(9)
C(4)-C(5)	1.418(10)
C(5)-C(6)	1.345(10)
C(6)-C(7)	1.425(10)
C(7)-C(12)	1.381(9)
C(7)-C(8)	1.417(10)
C(8)-C(9)	1.366(10)
C(9)-C(10)	1.403(9)
C(10)-C(14)	1.436(9)
C(11)-C(12)	1.441(8)

Table 6: Bond angles (º) for [Bi(PDALC)(H_2O)$_2$].

Bond	Bond Angle (º)	Bond	Bond Angle (º)
O(1W)-Bi(1)-N(2)	79.58(18)	C(2)-C(1)-C(13)	120.6(6)
O(1W)-Bi(1)-N(1)	77.50(18)	C(3)-C(2)-C(1)	120.8(6)
N(2)-Bi(1)-N(1)	70.00(18)	C(2)-C(3)-C(4)	119.1(6)
O(1W)-Bi(1)-O(2W)	148.26(18)	C(11)-C(4)-C(5)	119.6(6)
N(2)-Bi(1)-O(2W)	75.49(16)	C(11)-C(4)-C(3)	116.5(6)
N(1)-Bi(1)-O(2W)	75.73(16)	C(5)-C(4)-C(3)	123.9(6)
O(1W)-Bi(1)-O(1)	80.68(16)	C(6)-C(5)-C(4)	120.4(7)
N(2)-Bi(1)-O(1)	134.17(17)	C(5)-C(6)-C(7)	121.9(6)
N(1)-Bi(1)-O(1)	65.52(16)	C(12)-C(7)-C(8)	117.5(6)
O(2W)-Bi(1)-O(1)	103.09(15)	C(12)-C(7)-C(6)	118.8(6)
O(1W)-Bi(1)-O(2)	75.23(15)	C(8)-C(7)-C(6)	123.5(6)
N(2)-Bi(1)-O(2)	64.70(16)	C(9)-C(8)-C(7)	119.5(6)
N(1)-Bi(1)-O(2)	130.25(16)	C(8)-C(9)-C(10)	119.5(6)
O(2W)-Bi(1)-O(2)	110.37(14)	N(2)-C(10)-C(9)	121.9(6)
O(1)-Bi(1)-O(2)	145.58(15)	N(2)-C(10)-C(14)	115.9(5)
C(10)-N(2)-C(12)	118.6(5)	C(9)-C(10)-C(14)	122.2(6)
C(10)-N(2)-Bi(1)	124.1(4)	N(1)-C(11)-C(4)	122.8(6)
C(12)-N(2)-Bi(1)	117.0(4)	N(1)-C(11)-C(12)	118.1(6)
C(13)-O(1)-Bi(1)	122.4(4)	C(4)-C(11)-C(12)	119.0(6)
C(14)-O(2)-Bi(1)	116.3(4)	N(2)-C(12)-C(7)	123.0(6)
C(1)-N(1)-C(11)	120.1(5)	N(2)-C(12)-C(11)	116.8(6)
C(1)-N(1)-Bi(1)	123.5(4)	C(7)-C(12)-C(11)	120.2(6)
C(11)-N(1)-Bi(1)	116.2(4)	O(1)-C(13)-C(1)	109.5(5)
N(1)-C(1)-C(2)	120.6(6)	O(2)-C(14)-C(10)	112.4(5)
N(1)-C(1)-C(13)	118.7(6)		

Symmetry transformations used to generate equivalent atoms

1: -x, -y+½, z+½ **2:** -x, -y+½, z-½ **3:** -x, -y+1, z

oxygen bond distances of 2.412 and 2.303 Å. Table 7 gives a list of the anisotropic displacement parameters for $[Bi(PDALC)(H_2O)_2]^{3+}$.

One important quality of this crystal structure is the open site opposite of PDALC. This is an indication of a lone pair of electrons on bismuth[31] which gives this atom an egg-shaped coordination. The bond length between bismuth and the first H_2O molecule is the shortest bond to bismuth. The bonds between bismuth and the two nitrogen atoms have the next shortest bonds to bismuth. The two alcohol groups have larger bond lengths to bismuth, with the second H_2O molecule having the largest bond length to bismuth.

The $[Ca(PDALC)_2]\cdot H_2O$ crystal structure

The synthesis of $[Ca(PDALC)_2]\cdot H_2O$ crystals produced crystals that were tan needle clusters on the interface of the *n*-butanol/H_2O layers. The IR analysis, shown in Figure 74, indicates that the ligand is present, but the peaks are shifted, suggesting complex formation. The crystal structure of $[Ca(PDALC)_2]\cdot H_2O$ consists of a Ca(II) metal ion coordinated with two PDALC molecules through all four donor atoms of two separate PDALC ligands as shown in Figure 75. The two PDALC ligands are bound to the same Ca(II) metal ion and are perpendicular to each other. The Ca(II) was coordinated to both neutral nitrogen donor atoms and both neutral oxygen donor atoms of two separate PDALC ligands. The complex also showed no H_2O molecules coordinated to the eight coordinate Ca(II) metal ion. The crystal data and structural refinement parameters for the $[Ca(PDALC)_2]^{2+}$ complex are listed in Table 8. In addition, the spatial coordinates of the atoms for the $[Ca(PDALC)_2]^{2+}$ complex are given in Tables 9 and 10.

Table 7: Anisotropic displacement parameters ($Å^2 x\ 10^3$) for [Bi(PDALC)(H_2O)$_2$]. The anisotropic displacement factor exponent takes the form: $-2\pi^2[\ h^2\ a^{*2}U^{11} + ...\ + 2\ h\ k\ a^*\ b^*\ U^{12}]$.

	U^{11}	U^{22}	U^{33}	U^{23}	U^{13}	U^{12}
Bi(1)	24(1)	20(1)	13(1)	0(1)	-1(1)	3(1)
N(2)	19(2)	20(2)	19(3)	2(2)	3(2)	1(2)
O(1)	41(3)	20(2)	22(2)	6(2)	-4(2)	7(2)
O(2)	36(2)	21(2)	22(2)	-6(2)	-7(2)	-1(2)
O(1W)	49(3)	17(2)	31(3)	-1(2)	16(2)	-1(2)
O(2W)	19(2)	27(2)	17(2)	-2(2)	2(2)	5(2)
O(3W)	42(3)	33(3)	28(3)	7(2)	-1(2)	9(2)
N(1)	22(3)	22(3)	13(2)	-1(2)	2(2)	1(2)
C(1)	26(3)	24(3)	22(3)	-1(3)	9(3)	-3(3)
C(2)	31(4)	26(3)	26(4)	-7(3)	7(3)	-8(3)
C(3)	30(3)	30(4)	24(3)	-11(3)	4(3)	-7(3)
C(4)	21(3)	33(4)	20(3)	-9(3)	-2(2)	2(3)
C(5)	27(3)	48(5)	16(3)	-4(3)	-6(3)	11(3)
C(6)	26(3)	47(4)	17(4)	4(3)	0(3)	15(3)
C(7)	21(3)	28(3)	20(3)	5(3)	5(2)	7(3)
C(8)	23(3)	30(4)	28(4)	8(3)	3(3)	3(3)
C(9)	27(3)	16(3)	34(4)	5(3)	7(3)	4(3)
C(10)	22(2)	19(2)	24(3)	3(2)	3(2)	-1(2)
C(11)	23(3)	20(3)	11(3)	3(2)	-1(2)	0(2)
C(12)	17(3)	23(3)	20(3)	1(3)	3(2)	0(2)
C(13)	30(3)	19(3)	30(4)	-2(3)	6(3)	-1(3)
C(14)	19(2)	8(2)	29(2)	7(2)	-10(2)	-5(2)
Cl(1)	33(1)	27(1)	19(1)	-4(1)	-4(1)	3(1)
O(5)	33(3)	39(3)	18(3)	-3(2)	3(2)	8(2)
O(6)	80(5)	52(4)	27(3)	19(2)	27(3)	31(3)
O(7)	50(3)	33(3)	33(3)	9(2)	5(2)	11(2)
O(8)	59(4)	71(5)	112(7)	-51(5)	-43(4)	4(4)
Cl(2)	26(1)	22(1)	20(1)	1(1)	0(1)	-3(1)
O(9)	62(4)	32(3)	43(3)	10(2)	-6(3)	-21(3)
O(10)	29(2)	29(3)	35(3)	-7(2)	0(2)	5(2)
O(11)	56(3)	37(3)	23(3)	9(2)	-8(2)	-3(3)
O(12)	36(3)	52(3)	30(3)	-8(2)	7(2)	5(2)
Cl(3)	26(1)	23(1)	21(1)	-2(1)	-2(1)	3(1)
O(13)	30(3)	39(3)	32(3)	0(2)	-5(2)	12(2)
O(14)	24(2)	22(2)	25(2)	-5(2)	1(2)	5(2)
O(15)	28(2)	37(3)	17(2)	3(2)	-4(2)	8(2)
O(16)	47(3)	24(2)	37(3)	-6(2)	-3(2)	1(2)

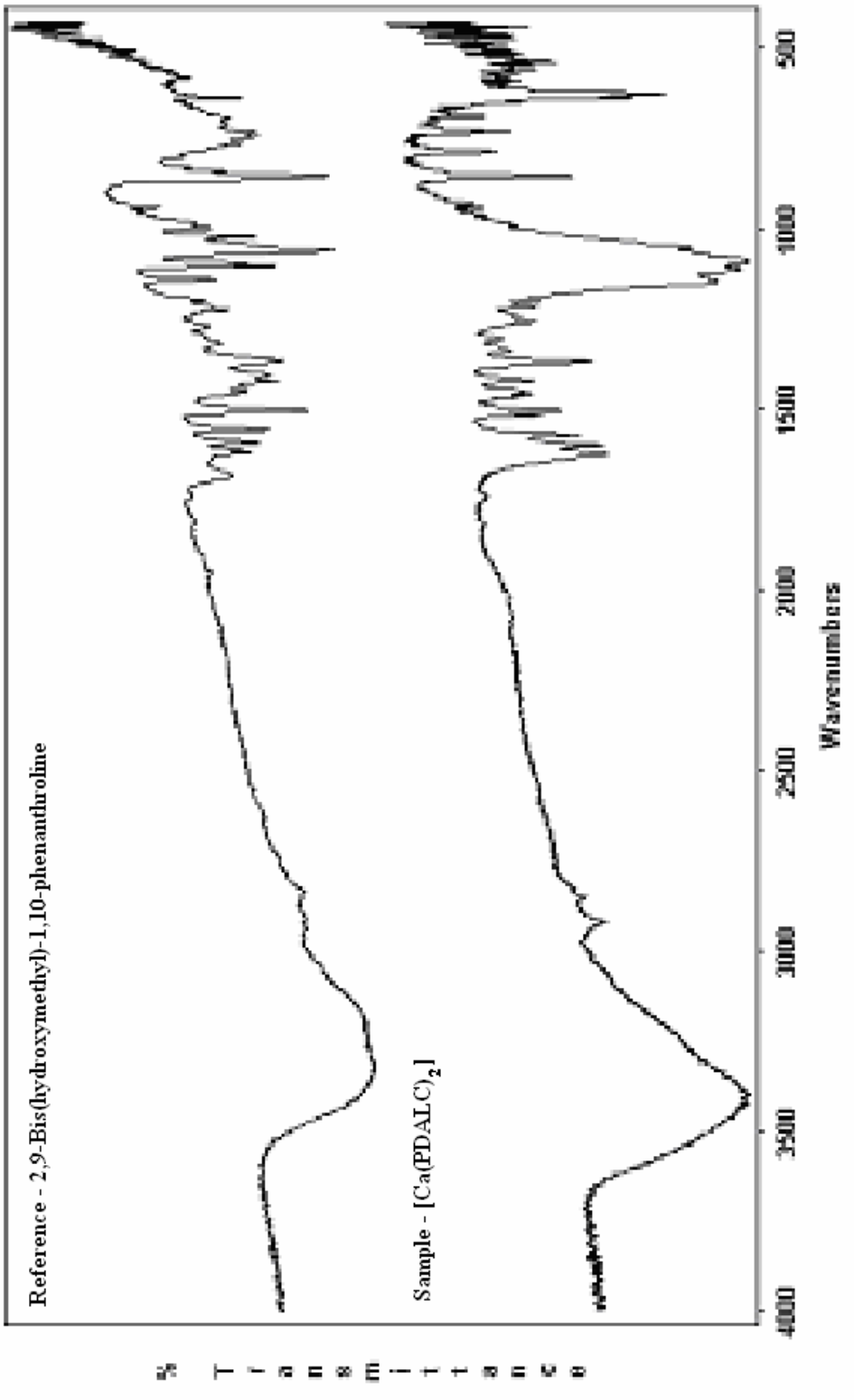

Figure 74: IR spectrum of $[Ca(PDALC)_2]\cdot H_2O$ crystals with the IR spectrum of PDALC as a reference.

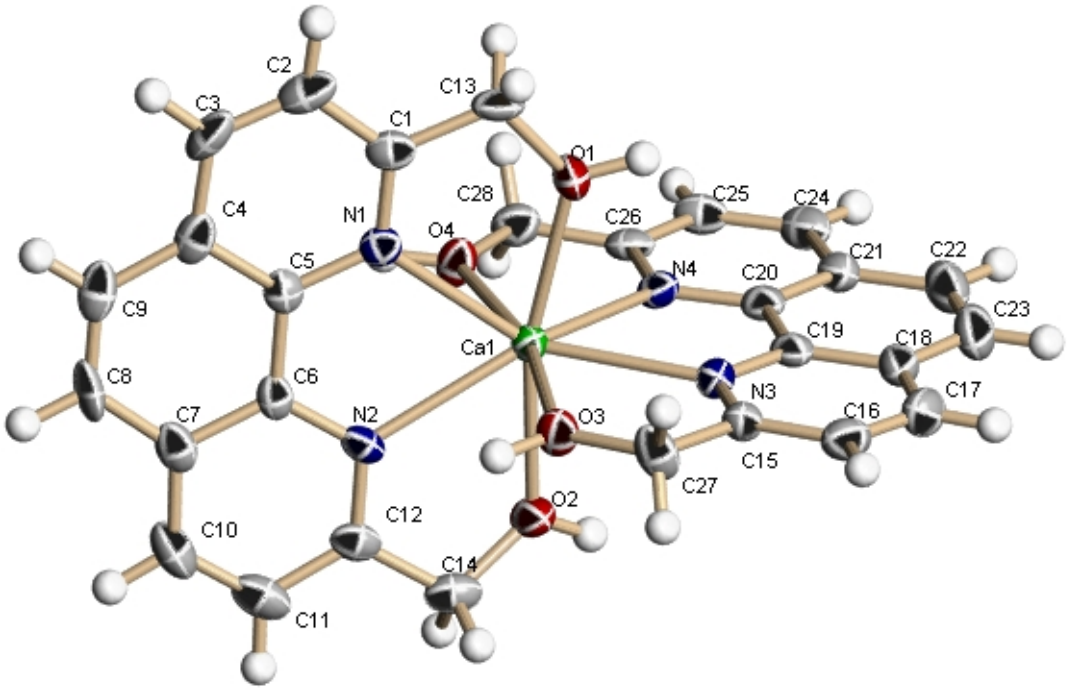

Figure 75: Crystal structure and atom assignments for the [Ca(PDALC)$_2$] complex.

Table 8: Crystal data and structure refinement for the [Ca(PDALC)$_2$] complex.

Identification code	rh63	
Empirical formula	C28 H24 Ca Cl2 N4 O12	
Formula weight	719.49	
Temperature	110(2) K	
Wavelength	0.71073 Å	
Crystal system	Triclinic	
Space group	P-1	
Unit cell dimensions	a = 7.646(3) Å	□= 72.976(6)°.
	b = 13.927(4) Å	□= 89.731(6)°.
	c = 14.859(5) Å	□ = 78.895(6)°.
Volume	1482.5(8) Å^3	
Z	2	
Density (calculated)	1.612 Mg/m^3	
Absorption coefficient	0.466 mm^{-1}	
F(000)	740	
Crystal size	0.10 x 0.10 x 0.05 mm^3	
Theta range for data collection	1.44 to 24.99°.	
Index ranges	-9<=h<=9, -16<=k<=16, -17<=l<=17	
Reflections collected	24173	
Independent reflections	4907 [R(int) = 0.0974]	
Completeness to theta = 24.99°	94.1 %	
Absorption correction	Semi-empirical from equivalents	
Max. and min. transmission	0.9771 and 0.9549	
Refinement method	Full-matrix least-squares on F^2	
Data / restraints / parameters	4907 / 0 / 424	
Goodness-of-fit on F^2	1.068	
Final R indices [I>2sigma(I)]	R1 = 0.0818, wR2 = 0.1822	
R indices (all data)	R1 = 0.1068, wR2 = 0.1955	
Largest diff. peak and hole	0.788 and -0.492 e.Å^{-3}	

Table 9: Atomic coordinates (x 10^4) and equivalent isotropic displacement parameters ($Å^2$x 10^3) for [Ca(PDALC)$_2$]. U(eq) is defined as one third of the trace of the orthogonalized U^{ij} tensor.

	x	y	z	U(eq)
Ca(1)	5452(2)	2058(1)	2192(1)	20(1)
Cl(1)	1876(2)	5968(1)	1098(1)	27(1)
Cl(2)	4071(2)	8260(1)	4129(1)	28(1)
O(1)	3409(6)	3324(3)	1016(3)	36(1)
O(2)	7146(6)	979(3)	3646(3)	33(1)
O(3)	3246(5)	998(3)	2678(3)	31(1)
O(4)	7971(5)	2787(3)	1532(3)	31(1)
O(5)	999(7)	5228(4)	907(4)	59(2)
O(6)	3732(6)	5591(4)	1163(4)	65(2)
O(7)	1393(7)	6910(3)	352(3)	42(1)
O(8)	1277(9)	6127(4)	1962(4)	74(2)
O(9)	2889(7)	7618(4)	4565(3)	55(1)
O(10)	5699(7)	7649(5)	3969(4)	71(2)
O(11)	3299(7)	8930(3)	3235(3)	45(1)
O(12)	4457(8)	8863(4)	4707(3)	57(2)
N(1)	5397(6)	1783(4)	608(3)	23(1)
N(2)	7275(6)	382(3)	2128(3)	23(1)
N(3)	3208(6)	2612(4)	3260(3)	24(1)
N(4)	5949(6)	3570(4)	2671(3)	23(1)
C(1)	4461(8)	2469(5)	-123(4)	27(1)
C(2)	4523(9)	2369(5)	-1030(4)	36(2)
C(3)	5567(9)	1529(5)	-1179(4)	36(2)
C(4)	6569(8)	763(5)	-422(4)	28(1)
C(5)	6456(7)	930(4)	471(4)	23(1)
C(6)	7420(7)	177(4)	1285(4)	23(1)
C(7)	8485(8)	-736(5)	1175(4)	29(1)
C(8)	8552(8)	-872(5)	263(5)	36(2)
C(9)	7673(8)	-160(5)	-494(5)	33(2)
C(10)	9373(9)	-1433(5)	1995(5)	40(2)
C(11)	9201(9)	-1235(5)	2827(5)	38(2)
C(12)	8146(8)	-308(4)	2879(4)	26(1)
C(13)	3278(8)	3378(5)	52(4)	33(2)
C(14)	7948(9)	-79(5)	3801(4)	34(2)
C(15)	1870(8)	2138(4)	3539(4)	26(1)
C(16)	565(9)	2450(5)	4115(4)	36(2)
C(17)	673(9)	3272(5)	4414(4)	37(2)
C(18)	2070(8)	3810(5)	4127(4)	30(1)
C(19)	3316(8)	3441(4)	3544(4)	24(1)
C(20)	4772(7)	3960(4)	3239(4)	24(1)
C(21)	4933(8)	4816(5)	3509(4)	28(1)
C(22)	3622(9)	5186(5)	4091(4)	39(2)
C(23)	2272(9)	4694(5)	4388(5)	41(2)
C(24)	6394(9)	5281(5)	3197(4)	33(1)
C(25)	7573(8)	4898(5)	2629(4)	30(1)
C(26)	7274(8)	4049(4)	2365(4)	26(1)
C(27)	1754(8)	1219(5)	3215(5)	35(2)
C(28)	8494(8)	3661(5)	1706(4)	31(1)

Table 10: Hydrogen coordinates (x 10^4) and isotropic displacement parameters ($Å^2$x 10^3) for $[Ca(PDALC)_2]$.

	x	y	z	U(eq)
H(1A)	2622	3831	1214	44
H(2A)	7279	1277	4134	39
H(3A)	3386	389	2497	37
H(4A)	8671	2473	1127	37
H(2)	3840	2884	-1540	43
H(3)	5621	1458	-1796	43
H(8)	9240	-1486	188	43
H(9)	7789	-273	-1094	40
H(10)	10108	-2055	1965	48
H(11)	9793	-1722	3382	46
H(13A)	3630	4014	-336	39
H(13B)	2026	3402	-135	39
H(14A)	7195	-517	4203	40
H(14B)	9135	-232	4133	40
H(16)	-383	2093	4294	43
H(17)	-189	3485	4816	44
H(22)	3708	5779	4266	46
H(23)	1433	4942	4782	50
H(24)	6563	5858	3380	39
H(25)	8572	5200	2418	35
H(27A)	1735	618	3770	42
H(27B)	634	1360	2826	42
H(28A)	8456	4211	1103	37
H(28B)	9734	3463	1982	37

The bond distances and angles for the $[Ca(PDALC)_2]^{2+}$ complex are shown in Table 11 and 12 respectively. Each unit cell of the crystal contained a Ca(II) ion positioned among the four donor atoms of PDALC. The bond distance between the Ca(II) and nitrogens of each PDALC ligand were 2.495 and 2.505 Å for the first PDALC and 2.498 and 2.505 Å for the second PDALC, which were longer bonds than that for the alcoholic groups of the PDALC. The Ca(II) and alcoholic oxygen bond distances from each PDALC were 2.401 and 2.445 Å for the first PDALC and 2.419 and 2.423 Å for the second PDALC. Table 13 gives a list of the anisotropic displacement parameters for $[Ca(PDALC)_2]^{2+}$.

The $[Pb(PDALC)(ClO_4)_2]\cdot H_2O$ crystal structure

The synthesis of $[Pb(PDALC)(ClO_4)_2]\cdot H_2O$ crystals produced crystals that were thick pale yellow needles on the interface of the *n*-butanol/H_2O layers. The IR analysis, shown in Figure 76, indicates that the ligand is present, but the peaks are shifted, suggesting complex formation. The crystal structure of $[Pb(PDALC)(ClO_4)_2]\cdot H_2O$ consists of a Pb(II) metal ion coordinated with one PDALC molecule through all four donor atoms of PDALC and two ClO_4^- ions as shown in Figure 77. The Pb(II) was coordinated to both neutral nitrogen donor atoms and both neutral oxygen donor atoms of two separate PDALC ligands. The complex also showed two ClO_4^- ions coordinated to Pb(II) and the metal is six coordinate. The crystal was also found to be twinned, shown in Figure 78. The $[Pb(PDALC)(ClO_4)_2]\cdot H_2O$ complexes are connected by a long interaction between a second oxygen of the ClO_4^- ion and the Pb(II) of a neighboring $[Pb(PDALC)(ClO_4)_2]\cdot H_2O$ complex. The crystal data and structural refinement parameters for the $[Pb(PDALC)(ClO_4)_2]$ complex are listed in Table 14. In addition, the spatial coordinates of the atoms for the $[Pb(PDALC)(ClO_4)_2]$ complex are given in Tables 15 and 16.

Table 11: Bond lengths (Å) for [Ca(PDALC)$_2$].

Bond	Bond Length (Å)	Bond	Bond Length (Å)
Ca(1)-O(1)	2.401(4)	C(1)-C(2)	1.395(8)
Ca(1)-O(4)	2.419(4)	C(1)-C(13)	1.496(9)
Ca(1)-O(3)	2.423(4)	C(2)-C(3)	1.359(9)
Ca(1)-O(2)	2.445(4)	C(3)-C(4)	1.406(9)
Ca(1)-N(1)	2.495(4)	C(4)-C(5)	1.413(8)
Ca(1)-N(3)	2.498(4)	C(4)-C(9)	1.427(9)
Ca(1)-N(4)	2.505(5)	C(5)-C(6)	1.441(8)
Ca(1)-N(2)	2.505(5)	C(6)-C(7)	1.424(8)
Cl(1)-O(6)	1.409(5)	C(7)-C(10)	1.396(9)
Cl(1)-O(8)	1.424(5)	C(7)-C(8)	1.421(9)
Cl(1)-O(5)	1.425(5)	C(8)-C(9)	1.341(9)
Cl(1)-O(7)	1.433(4)	C(10)-C(11)	1.344(10)
Cl(2)-O(9)	1.415(5)	C(11)-C(12)	1.407(9)
Cl(2)-O(10)	1.427(5)	C(12)-C(14)	1.496(9)
Cl(2)-O(11)	1.432(5)	C(15)-C(16)	1.400(8)
Cl(2)-O(12)	1.432(5)	C(15)-C(27)	1.511(8)
O(1)-C(13)	1.414(7)	C(16)-C(17)	1.361(9)
O(2)-C(14)	1.433(7)	C(17)-C(18)	1.414(9)
O(3)-C(27)	1.426(7)	C(18)-C(19)	1.410(8)
O(4)-C(28)	1.442(7)	C(18)-C(23)	1.429(9)
N(1)-C(1)	1.319(7)	C(19)-C(20)	1.442(8)
N(1)-C(5)	1.370(7)	C(20)-C(21)	1.390(8)
N(2)-C(12)	1.321(7)	C(21)-C(24)	1.407(9)
N(2)-C(6)	1.363(7)	C(21)-C(22)	1.440(8)
N(3)-C(15)	1.323(7)	C(22)-C(23)	1.350(10)
N(3)-C(19)	1.358(7)	C(24)-C(25)	1.372(9)
N(4)-C(26)	1.325(7)	C(25)-C(26)	1.408(8)
N(4)-C(20)	1.375(7)	C(26)-C(28)	1.493(8)

Table 12: Bond angles (º) for $[Ca(PDALC)_2]$.

Bond	Bond Angle (º)	Bond	Bond Angle (º)
O(1)-Ca(1)-O(4)	91.91(15)	C(1)-N(1)-Ca(1)	121.8(4)
O(1)-Ca(1)-O(3)	92.19(16)	C(5)-N(1)-Ca(1)	119.5(3)
O(4)-Ca(1)-O(3)	165.71(14)	C(12)-N(2)-C(6)	118.2(4)
O(1)-Ca(1)-O(2)	166.13(14)	C(12)-N(2)-Ca(1)	122.6(4)
O(4)-Ca(1)-O(2)	93.55(15)	C(6)-N(2)-Ca(1)	119.2(4)
O(3)-Ca(1)-O(2)	85.62(15)	C(15)-N(3)-C(19)	118.4(5)
O(1)-Ca(1)-N(1)	64.24(14)	C(15)-N(3)-Ca(1)	121.9(4)
O(4)-Ca(1)-N(1)	79.75(14)	C(19)-N(3)-Ca(1)	119.7(4)
O(3)-Ca(1)-N(1)	89.73(14)	C(26)-N(4)-C(20)	117.7(5)
O(2)-Ca(1)-N(1)	129.62(15)	C(26)-N(4)-Ca(1)	122.5(4)
O(1)-Ca(1)-N(3)	81.57(15)	C(20)-N(4)-Ca(1)	119.7(3)
O(4)-Ca(1)-N(3)	129.62(15)	N(1)-C(1)-C(2)	122.8(6)
O(3)-Ca(1)-N(3)	64.58(15)	N(1)-C(1)-C(13)	117.4(5)
O(2)-Ca(1)-N(3)	85.13(15)	C(2)-C(1)-C(13)	119.8(5)
N(1)-Ca(1)-N(3)	136.62(16)	C(3)-C(2)-C(1)	119.5(6)
O(1)-Ca(1)-N(4)	83.79(15)	C(2)-C(3)-C(4)	120.2(5)
O(4)-Ca(1)-N(4)	64.18(14)	C(3)-C(4)-C(5)	116.8(5)
O(3)-Ca(1)-N(4)	129.92(14)	C(3)-C(4)-C(9)	124.9(5)
O(2)-Ca(1)-N(4)	87.13(15)	C(5)-C(4)-C(9)	118.3(6)
N(1)-Ca(1)-N(4)	130.76(15)	N(1)-C(5)-C(4)	122.2(5)
N(3)-Ca(1)-N(4)	65.46(15)	N(1)-C(5)-C(6)	117.4(5)
O(1)-Ca(1)-N(2)	129.41(15)	C(4)-C(5)-C(6)	120.4(5)
O(4)-Ca(1)-N(2)	85.77(14)	N(2)-C(6)-C(7)	123.1(5)
O(3)-Ca(1)-N(2)	81.05(14)	N(2)-C(6)-C(5)	117.9(5)
O(2)-Ca(1)-N(2)	63.80(14)	C(7)-C(6)-C(5)	119.0(5)
N(1)-Ca(1)-N(2)	65.65(15)	C(10)-C(7)-C(8)	125.5(6)
N(3)-Ca(1)-N(2)	135.42(15)	C(10)-C(7)-C(6)	115.8(5)
N(4)-Ca(1)-N(2)	137.13(16)	C(8)-C(7)-C(6)	118.6(6)
C(13)-O(1)-Ca(1)	125.4(3)	C(9)-C(8)-C(7)	122.0(5)
C(14)-O(2)-Ca(1)	123.6(3)	C(8)-C(9)-C(4)	121.7(6)
C(27)-O(3)-Ca(1)	125.0(3)	C(11)-C(10)-C(7)	120.7(6)
C(28)-O(4)-Ca(1)	125.2(3)	C(10)-C(11)-C(12)	120.2(6)

Table 12 cont.

Bond	Bond Angle (º)	Bond	Bond Angle (º)
C(1)-N(1)-C(5)	118.6(5)	N(2)-C(12)-C(11)	121.9(6)
N(2)-C(12)-C(14)	117.5(5)	N(4)-C(20)-C(21)	122.8(5)
C(11)-C(12)-C(14)	120.6(5)	N(4)-C(20)-C(19)	116.6(5)
O(1)-C(13)-C(1)	110.5(5)	C(21)-C(20)-C(19)	120.5(5)
O(2)-C(14)-C(12)	109.9(5)	C(20)-C(21)-C(24)	117.8(5)
N(3)-C(15)-C(16)	123.1(5)	C(20)-C(21)-C(22)	119.3(6)
N(3)-C(15)-C(27)	118.0(5)	C(24)-C(21)-C(22)	122.8(6)
C(16)-C(15)-C(27)	118.9(5)	C(23)-C(22)-C(21)	120.3(6)
C(17)-C(16)-C(15)	119.0(6)	C(22)-C(23)-C(18)	121.8(6)
C(16)-C(17)-C(18)	119.9(6)	C(25)-C(24)-C(21)	119.7(6)
C(19)-C(18)-C(17)	116.9(6)	C(24)-C(25)-C(26)	118.7(5)
C(19)-C(18)-C(23)	119.1(6)	N(4)-C(26)-C(25)	123.2(5)
C(17)-C(18)-C(23)	124.0(6)	N(4)-C(26)-C(28)	117.7(5)
N(3)-C(19)-C(18)	122.6(5)	C(25)-C(26)-C(28)	119.1(5)
N(3)-C(19)-C(20)	118.5(5)	O(3)-C(27)-C(15)	110.1(5)
C(18)-C(19)-C(20)	118.9(5)	O(4)-C(28)-C(26)	110.4(5)

Symmetry transformations used to generate equivalent atoms

1: -x, -y+½, z+½ **2:** -x, -y+½, z-½ **3:** -x, -y+1, z

Table 13: Anisotropic displacement parameters ($Å^2 x\ 10^3$) for $[Ca(PDALC)_2]$. The anisotropic displacement factor exponent takes the form: $-2\pi^2[\ h^2\ a^{*2}U^{11} + ...\ + 2\ h\ k\ a^*\ b^*\ U^{12}]$.

	U^{11}	U^{22}	U^{33}	U^{23}	U^{13}	U^{12}
Ca(1)	25(1)	17(1)	19(1)	-6(1)	3(1)	-4(1)
Cl(1)	30(1)	19(1)	29(1)	-5(1)	1(1)	-3(1)
Cl(2)	35(1)	26(1)	23(1)	-4(1)	2(1)	-9(1)
O(1)	48(3)	27(2)	29(2)	-12(2)	4(2)	9(2)
O(2)	49(3)	27(2)	20(2)	-7(2)	-1(2)	-2(2)
O(3)	38(2)	23(2)	34(2)	-11(2)	12(2)	-10(2)
O(4)	40(2)	27(2)	31(2)	-14(2)	15(2)	-15(2)
O(5)	47(3)	45(3)	96(4)	-29(3)	4(3)	-20(3)
O(6)	29(3)	51(3)	99(5)	-3(3)	-5(3)	5(2)
O(7)	65(3)	23(2)	31(2)	-4(2)	6(2)	1(2)
O(8)	129(6)	45(3)	40(3)	-14(3)	17(3)	5(3)
O(9)	70(4)	57(3)	44(3)	-9(3)	19(3)	-39(3)
O(10)	45(3)	72(4)	84(4)	-20(3)	10(3)	8(3)
O(11)	73(3)	30(3)	29(2)	-3(2)	-4(2)	-12(2)
O(12)	88(4)	73(4)	28(2)	-24(3)	14(3)	-44(3)
N(1)	24(2)	23(3)	21(2)	-6(2)	1(2)	-6(2)
N(2)	21(2)	15(2)	29(3)	-2(2)	1(2)	-3(2)
N(3)	27(3)	23(3)	20(2)	-7(2)	3(2)	-4(2)
N(4)	30(3)	21(3)	17(2)	-5(2)	2(2)	-7(2)
C(1)	27(3)	25(3)	25(3)	-2(3)	-1(2)	-10(3)
C(2)	48(4)	41(4)	21(3)	-3(3)	-3(3)	-22(3)
C(3)	56(4)	43(4)	19(3)	-15(3)	12(3)	-25(3)
C(4)	35(3)	33(3)	29(3)	-19(3)	9(3)	-18(3)
C(5)	20(3)	22(3)	29(3)	-9(2)	6(2)	-9(2)
C(6)	20(3)	23(3)	29(3)	-11(2)	6(2)	-5(2)
C(7)	27(3)	22(3)	43(4)	-14(3)	9(3)	-8(3)
C(8)	36(4)	28(4)	55(4)	-32(3)	12(3)	-3(3)
C(9)	32(3)	42(4)	42(4)	-29(3)	15(3)	-19(3)
C(10)	33(4)	27(4)	61(5)	-18(3)	5(3)	2(3)
C(11)	36(4)	22(3)	51(4)	-1(3)	-4(3)	-7(3)
C(12)	25(3)	21(3)	29(3)	1(3)	0(2)	-9(3)
C(13)	31(3)	30(4)	23(3)	8(3)	-2(2)	2(3)
C(14)	36(4)	31(4)	29(3)	2(3)	-2(3)	-13(3)
C(15)	31(3)	20(3)	25(3)	-5(2)	6(2)	-5(3)
C(16)	33(4)	35(4)	31(3)	0(3)	7(3)	-3(3)
C(17)	34(4)	37(4)	35(3)	-9(3)	12(3)	-3(3)
C(18)	34(3)	27(3)	24(3)	-8(3)	1(3)	4(3)
C(19)	32(3)	20(3)	17(3)	-2(2)	-5(2)	0(3)
C(20)	29(3)	22(3)	17(3)	-2(2)	-4(2)	-3(2)
C(21)	37(4)	22(3)	23(3)	-6(2)	0(3)	-1(3)
C(22)	47(4)	31(4)	39(4)	-19(3)	-3(3)	1(3)
C(23)	38(4)	41(4)	43(4)	-19(3)	6(3)	7(3)
C(24)	47(4)	26(3)	26(3)	-9(3)	-8(3)	-9(3)
C(25)	31(3)	24(3)	32(3)	-1(3)	-3(3)	-12(3)
C(26)	33(3)	20(3)	19(3)	2(2)	-4(2)	-6(3)
C(27)	30(3)	24(3)	57(4)	-16(3)	14(3)	-10(3)
C(28)	36(4)	28(3)	28(3)	-4(3)	4(3)	-11(3)

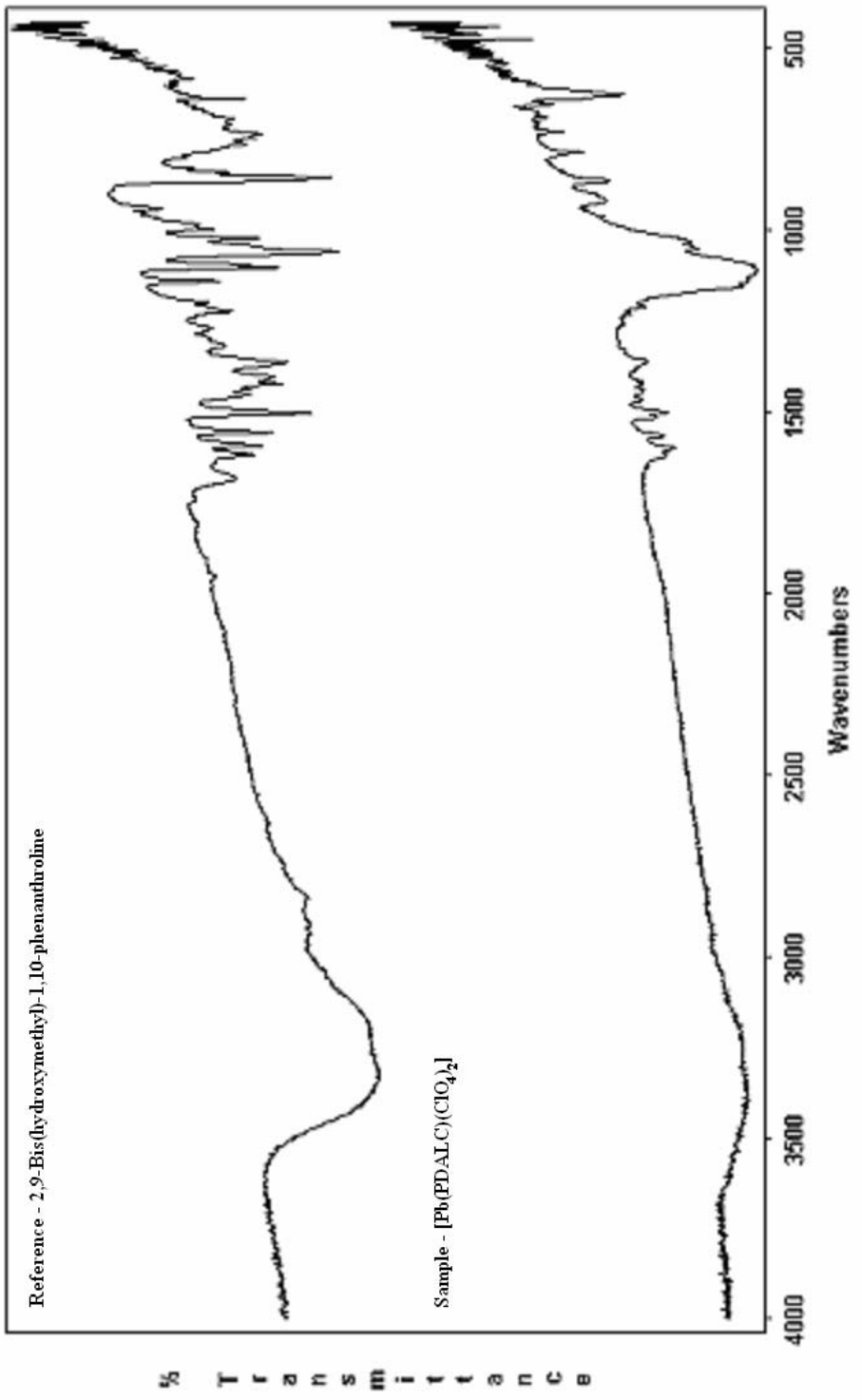

Figure 76: IR spectrum of $[Pb(PDALC)(ClO_4)_2]\cdot H_2O$ crystals with the IR spectrum of PDALC as a reference.

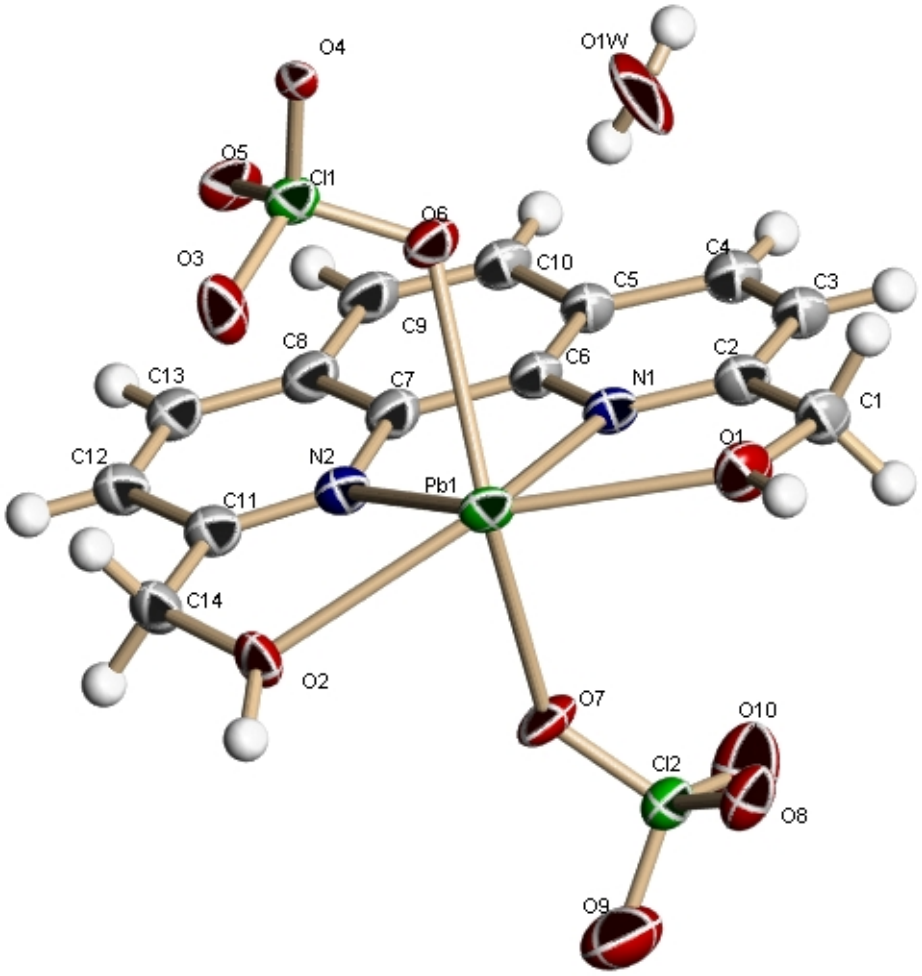

Figure 77: Crystal structure and atom assignments for the $[Pb(PDALC)(ClO_4)_2]\cdot H_2O$ complex.

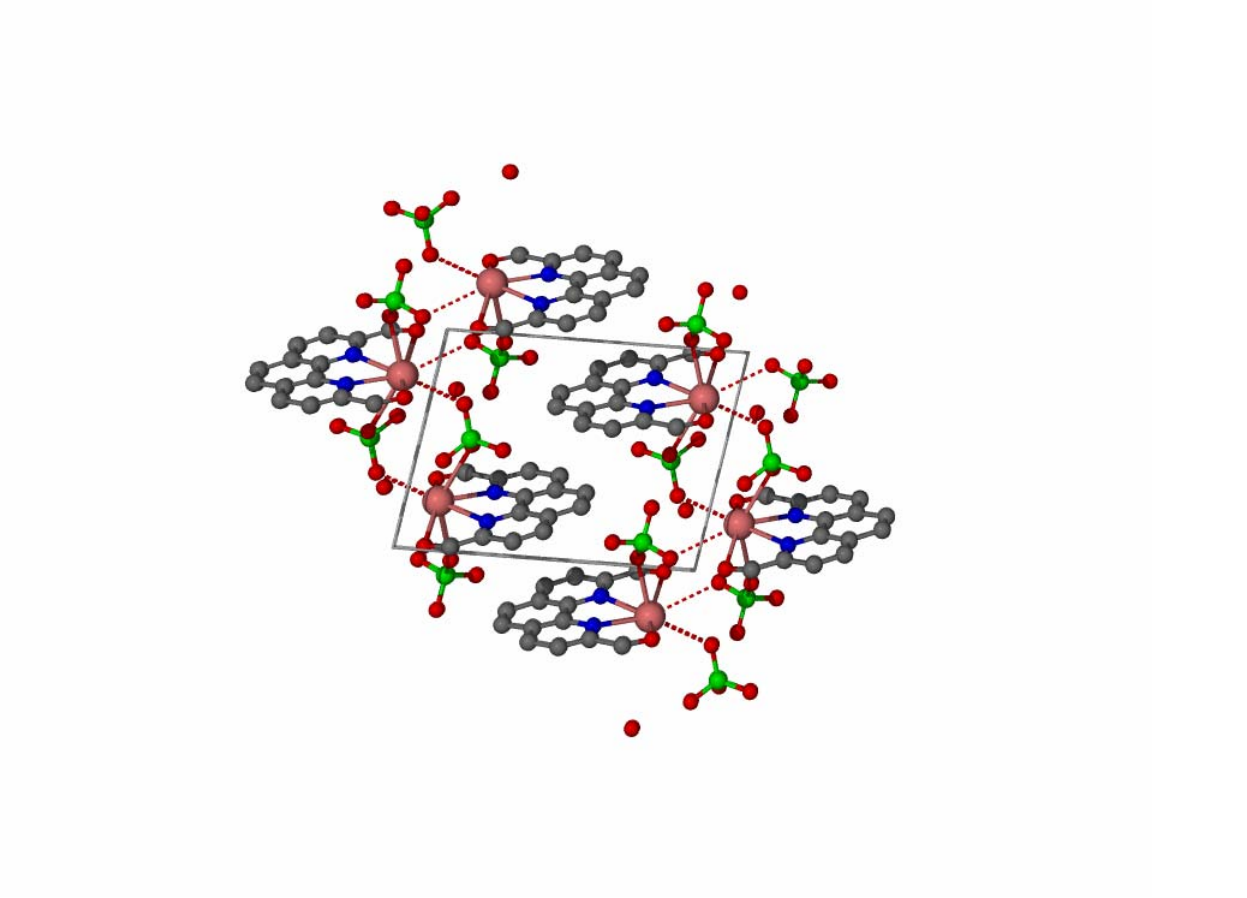

Figure 78: Crystal structure showing the twinned complexation of the $[Pb(PDALC)(ClO_4)_2]\cdot H_2O$ complex.

Table 14: Crystal data and structure refinement for the [Pb(PDALC)(ClO_4)$_2$] complex.

Identification code	rh61	
Empirical formula	C14 H12 Cl2 N2 O11 Pb	
Formula weight	662.35	
Temperature	110(2) K	
Wavelength	1.54184 Å	
Crystal system	Triclinic	
Space group	P-1	
Unit cell dimensions	a = 8.84380(10) Å	□= 74.427(3)°.
	b = 9.0751(15) Å	□= 78.403(13)°.
	c = 12.178(2) Å	□ = 80.053(11)°.
Volume	915.0(2) Å^3	
Z	2	
Density (calculated)	2.404 Mg/m^3	
Absorption coefficient	21.254 mm^{-1}	
F(000)	628	
Crystal size	0.03 x 0.02 x 0.02 mm^3	
Theta range for data collection	3.82 to 58.80°.	
Index ranges	-9<=h<=9, -9<=k<=10, 0<=l<=13	
Reflections collected	2648	
Independent reflections	2770 [R(int) = 0.0000]	
Completeness to theta = 58.80°	87.4 %	
Absorption correction	Semi-empirical from equivalents	
Max. and min. transmission	0.6759 and 0.5681	
Refinement method	Full-matrix least-squares on F^2	
Data / restraints / parameters	2770 / 174 / 272	
Goodness-of-fit on F^2	1.111	
Final R indices [I>2sigma(I)]	R1 = 0.0665, wR2 = 0.1729	
R indices (all data)	R1 = 0.0776, wR2 = 0.1944	
Largest diff. peak and hole	3.628 and -2.486 e.Å^{-3}	

Table 15: Atomic coordinates (x 10^4) and equivalent isotropic displacement parameters ($Å^2$x 10^3) for [Pb(PDALC)(ClO_4)$_2$]. U(eq) is defined as one third of the trace of the orthogonalized U^{ij} tensor.

	x	y	z	U(eq)
Pb(1)	2226(1)	2237(1)	1080(1)	24(1)
O(1)	3203(15)	4829(15)	830(12)	33(3)
O(2)	175(15)	417(14)	997(12)	27(3)
O(1W)	7315(18)	2419(18)	766(15)	57(5)
Cl(1)	4857(5)	1043(5)	-1654(4)	25(1)
O(3)	5913(17)	1203(15)	-939(13)	37(3)
O(4)	3298(12)	1310(12)	-1160(10)	13(2)
O(5)	5250(15)	2017(14)	-2792(11)	29(3)
O(6)	5128(14)	-538(14)	-1735(12)	27(2)
Cl(2)	-1114(5)	4982(5)	1910(4)	27(1)
O(7)	-405(14)	3415(14)	1953(12)	30(2)
O(8)	-490(16)	6044(14)	884(12)	32(3)
O(9)	-2697(19)	4990(19)	1895(17)	58(4)
O(10)	-1010(20)	5436(19)	2896(16)	58(4)
N(1)	2836(17)	2748(17)	2850(14)	26(2)
N(2)	1468(17)	243(18)	2850(14)	26(2)
C(1)	3590(20)	5240(20)	1741(17)	29(3)
C(2)	3410(20)	4010(20)	2853(18)	29(2)
C(3)	3880(20)	4150(20)	3805(18)	30(3)
C(4)	3760(20)	3070(20)	4824(19)	30(3)
C(5)	3150(20)	1670(20)	4818(18)	27(2)
C(6)	2690(20)	1600(20)	3862(17)	24(2)
C(7)	2010(20)	260(20)	3848(18)	25(2)
C(8)	1900(20)	-970(20)	4804(18)	28(2)
C(9)	2490(20)	-880(20)	5801(18)	31(3)
C(10)	3090(20)	390(20)	5827(18)	28(3)
C(11)	790(20)	-960(20)	2842(18)	29(2)
C(12)	700(20)	-2300(20)	3849(18)	29(3)
C(13)	1260(20)	-2240(20)	4765(18)	28(3)
C(14)	230(20)	-1040(20)	1857(18)	28(3)

Table 16: Hydrogen coordinates (x 10^4) and isotropic displacement parameters ($Å^2$x 10^3) for [Pb(PDALC)(ClO_4)$_2$].

	x	y	z	U(eq)
H(1C)	3303	5525	89	39
H(2A)	-524	703	455	33
H(1W1)	8028	2464	977	86
H(2W1)	6612	2203	1020	86
H(1A)	2913	6195	1860	35
H(1B)	4677	5469	1541	35
H(3A)	4318	5051	3759	36
H(4A)	4045	3210	5496	36
H(9A)	2462	-1730	6456	37
H(10A)	3453	433	6497	34
H(12A)	248	-3180	3840	34
H(13A)	1220	-3098	5417	34
H(14A)	-821	-1362	2094	34
H(14B)	919	-1840	1508	34

The bond distances and angles for the [Pb(PDALC)(ClO_4)$_2$] complex are shown in Table 17 and 18 respectively. Each unit cell of the crystal contained a Pb(II) ion positioned among the four donor atoms of PDALC. The bond distance between the Pb(II) and nitrogens of PDALC were 2.473 and 2.498 Å, which were shorter bonds than that for the alcoholic groups of the PDALC. The Pb(II) and alcoholic oxygen bond distances from each PDALC were 2.566 and 2.688 Å. Two ClO_4^- molecules were also coordinated to the Pb(II) metal ion, which had Pb(II) and oxygen bond lengths of 2.538 and 2.708 Å. Table 19 gives a list of the anisotropic displacement parameters for [Pb(PDALC)(ClO_4)$_2$].

Similar to the [Bi(PDALC)(H_2O)$_2$]$^{3+}$ crystal structure, [Pb(PDALC)(ClO_4)$_2$] also shows an open site due to a lone pair of electrons. The shortest bond lengths to lead are from the two nitrogen atoms. The second shortest bond length is from the first H_2O molecule. The next longer bond lengths are to the two alcohol groups, leaving the second H_2O molecule with the longest bond to lead. This shows a similar egg-shape for the bonding of the lead atom.

[Cd(PDALC)] crystal synthesis

The synthesis of [Cd(PDALC)] crystals produced crystals that were fine white needles on the interface of the *n*-butanol/H_2O layers. The IR analysis, shown in Figure 79, indicates that the ligand is present, but the peaks are shifted, suggesting complex formation. A few crystals were sent for analysis and the results are pending.

[Cu(PDALC)] crystal synthesis

The synthesis of [Cu(PDALC)] crystals produced crystals that were bright yellow needles on the interface of the *n*-butanol/H_2O layers. The IR analysis, shown in Figure 80, indicates that

Table 17: Bond lengths (Å) for [Pb(PDALC)(ClO_4)$_2$].

Bond	Bond Length (Å)	Bond	Bond Length (Å)
Pb(1)-N(2)	2.473(15)	C(1)-C(2)	1.51(3)
Pb(1)-N(1)	2.498(17)	C(1)-H(1A)	0.9900
Pb(1)-O(7)	2.538(12)	C(1)-H(1B)	0.9900
Pb(1)-O(1)	2.566(13)	C(2)-C(3)	1.35(3)
Pb(1)-O(2)	2.688(12)	C(3)-C(4)	1.36(3)
Pb(1)-O(6)#1	2.708(12)	C(3)-H(3A)	0.9500
O(1)-C(1)	1.38(2)	C(4)-C(5)	1.46(3)
O(1)-H(1C)	0.9500	C(4)-H(4A)	0.9500
O(2)-C(14)	1.45(2)	C(5)-C(6)	1.33(3)
O(2)-H(2A)	0.9500	C(5)-C(10)	1.45(3)
O(1W)-H(1W1)	0.7389	C(6)-C(7)	1.45(3)
O(1W)-H(2W1)	0.6727	C(7)-C(8)	1.38(3)
Cl(1)-O(4)	1.397(12)	C(8)-C(13)	1.39(3)
Cl(1)-O(6)	1.440(14)	C(8)-C(9)	1.44(3)
Cl(1)-O(5)	1.442(13)	C(9)-C(10)	1.35(3)
Cl(1)-O(3)	1.446(15)	C(9)-H(9A)	0.9500
O(6)-Pb(1)#1	2.708(12)	C(10)-H(10A)	0.9500
Cl(2)-O(10)	1.40(2)	C(11)-C(14)	1.41(3)
Cl(2)-O(9)	1.403(17)	C(11)-C(12)	1.48(3)
Cl(2)-O(8)	1.433(14)	C(12)-C(13)	1.33(3)
Cl(2)-O(7)	1.444(13)	C(12)-H(12A)	0.9500
N(1)-C(2)	1.33(3)	C(13)-H(13A)	0.9500
N(1)-C(6)	1.38(2)	C(14)-H(14A)	0.9900
N(2)-C(11)	1.33(3)	C(14)-H(14B)	0.9900
N(2)-C(7)	1.40(3)		

Table 18: Bond angles (º) for [Pb(PDALC)(ClO_4)$_2$].

Bond	Bond Angle (º)	Bond	Bond Angle (º)
N(2)-Pb(1)-N(1)	67.3(5)	C(2)-C(3)-C(4)	123.5(19)
N(2)-Pb(1)-O(7)	76.4(5)	C(2)-C(3)-H(3A)	118.2
N(1)-Pb(1)-O(7)	78.1(5)	C(4)-C(3)-H(3A)	118.2
N(2)-Pb(1)-O(1)	130.4(5)	C(3)-C(4)-C(5)	115(2)
N(1)-Pb(1)-O(1)	63.6(5)	C(3)-C(4)-H(4A)	122.3
O(7)-Pb(1)-O(1)	87.3(4)	C(5)-C(4)-H(4A)	122.3
N(2)-Pb(1)-O(2)	62.5(5)	C(6)-C(5)-C(10)	121.2(18)
N(1)-Pb(1)-O(2)	126.8(5)	C(6)-C(5)-C(4)	118.4(18)
O(7)-Pb(1)-O(2)	74.4(4)	C(10)-C(5)-C(4)	120.3(18)
O(1)-Pb(1)-O(2)	154.8(4)	C(5)-C(6)-N(1)	123.3(18)
N(2)-Pb(1)-O(6)#1	72.5(4)	C(5)-C(6)-C(7)	119.7(17)
N(1)-Pb(1)-O(6)#1	67.2(5)	N(1)-C(6)-C(7)	117.0(17)
O(7)-Pb(1)-O(6)#1	140.1(4)	C(8)-C(7)-N(2)	121.0(18)
O(1)-Pb(1)-O(6)#1	94.1(4)	C(8)-C(7)-C(6)	120.4(19)
O(2)-Pb(1)-O(6)#1	111.0(4)	N(2)-C(7)-C(6)	118.6(16)
C(1)-O(1)-Pb(1)	121.9(10)	C(7)-C(8)-C(13)	119(2)
C(1)-O(1)-H(1C)	119.1	C(7)-C(8)-C(9)	118.0(18)
Pb(1)-O(1)-H(1C)	119.1	C(13)-C(8)-C(9)	122.8(18)
C(14)-O(2)-Pb(1)	113.8(10)	C(10)-C(9)-C(8)	121.7(18)
C(14)-O(2)-H(2A)	123.1	C(10)-C(9)-H(9A)	119.1
Pb(1)-O(2)-H(2A)	123.1	C(8)-C(9)-H(9A)	119.1
H(1W1)-O(1W)-H(2W1)	134.6	C(9)-C(10)-C(5)	118.8(19)
Cl(1)-O(6)-Pb(1)#1	117.1(7)	C(9)-C(10)-H(10A)	120.6
Cl(2)-O(7)-Pb(1)	133.4(7)	C(5)-C(10)-H(10A)	120.6
C(2)-N(1)-C(6)	118.0(17)	N(2)-C(11)-C(14)	121.6(17)
C(2)-N(1)-Pb(1)	123.6(13)	N(2)-C(11)-C(12)	120.8(18)
C(6)-N(1)-Pb(1)	118.1(12)	C(14)-C(11)-C(12)	117.5(18)
C(11)-N(2)-C(7)	119.1(16)	C(13)-C(12)-C(11)	117.4(18)
C(11)-N(2)-Pb(1)	122.8(13)	C(13)-C(12)-H(12A)	121.3
C(7)-N(2)-Pb(1)	117.3(11)	C(12)-C(13)-C(8)	121.3
O(1)-C(1)-C(2)	113.1(16)	C(12)-C(13)-C(8)	122.3(18)
O(1)-C(1)-H(1A)	109.0	C(12)-C(13)-H(13A)	118.8
C(2)-C(1)-H(1A)	109.0	C(8)-C(13)-H(13A)	118.8
O(1)-C(1)-H(1B)	109.0	C(11)-C(14)-O(2)	112.4(16)
C(2)-C(1)-H(1B)	109.0	C(11)-C(14)-H(14A)	109.1
H(1A)-C(1)-H(1B)	107.8	O(2)-C(14)-H(14A)	109.1
N(1)-C(2)-C(3)	121.1(18)	C(11)-C(14)-H(14B)	109.1
N(1)-C(2)-C(1)	117.7(18)	O(2)-C(14)-H(14B)	109.1
C(3)-C(2)-C(1)	121.2(18)	H(14A)-C(14)-H(14B)	107.9

Symmetry transformations used to generate equivalent atoms

1: -x, -y+½, z+½ **2:** -x, -y+½, z-½ **3:** -x, -y+1, z

Table 19: Anisotropic displacement parameters ($Å^2 x\ 10^3$) for [Pb(PDALC)(ClO_4)$_2$]. The anisotropic displacement factor exponent takes the form: $-2\pi^2[\ h^2\ a^{*2}U^{11} + ...\ + 2\ h\ k\ a^*\ b^*\ U^{12}]$.

	U^{11}	U^{22}	U^{33}	U^{23}	U^{13}	U^{12}
Pb(1)	24(1)	21(1)	24(1)	2(1)	-13(1)	1(1)
O(1)	38(5)	24(5)	32(6)	4(5)	-13(5)	-4(5)
O(2)	32(5)	24(5)	32(6)	-4(5)	-18(5)	-9(4)
O(1W)	43(9)	58(10)	79(12)	-14(10)	-2(9)	-41(8)
Cl(1)	24(2)	21(2)	28(2)	3(2)	-11(2)	-1(2)
O(3)	49(7)	23(6)	39(7)	10(6)	-19(6)	-19(5)
O(4)	15(4)	16(4)	10(4)	-6(3)	-6(3)	0(3)
O(5)	31(6)	24(6)	24(6)	12(5)	-14(5)	0(5)
O(6)	23(4)	19(4)	32(5)	0(4)	-4(4)	1(4)
Cl(2)	27(2)	21(2)	33(2)	-5(2)	-7(2)	1(2)
O(7)	23(4)	19(4)	38(5)	-3(4)	2(4)	8(4)
O(8)	44(6)	20(6)	30(6)	-4(6)	-9(5)	3(5)
O(9)	40(7)	47(7)	77(8)	-8(7)	-10(7)	10(6)
O(10)	88(8)	38(7)	45(7)	-7(7)	-6(7)	-11(7)
N(1)	25(4)	21(4)	30(5)	-1(4)	-15(4)	1(4)
N(2)	24(4)	23(4)	30(4)	-3(4)	-10(4)	0(4)
C(1)	33(5)	23(5)	32(5)	3(5)	-16(4)	-4(4)
C(2)	29(4)	23(4)	34(4)	0(4)	-16(4)	-1(4)
C(3)	29(5)	26(5)	37(5)	-4(5)	-15(4)	0(4)
C(4)	28(5)	27(5)	36(5)	-7(5)	-12(4)	0(4)
C(5)	26(4)	23(4)	32(4)	-5(4)	-13(4)	0(4)
C(6)	24(4)	21(4)	28(4)	-4(4)	-11(4)	2(3)
C(7)	26(4)	22(4)	27(4)	-4(4)	-8(4)	2(4)
C(8)	27(4)	23(4)	30(4)	-2(4)	-8(4)	2(4)
C(9)	29(5)	25(5)	33(5)	2(5)	-10(4)	4(4)
C(10)	28(5)	24(5)	31(5)	-2(5)	-12(4)	2(4)
C(11)	27(4)	26(4)	34(4)	-2(4)	-12(4)	-2(4)
C(12)	26(5)	26(5)	33(5)	-3(5)	-11(4)	-3(4)
C(13)	27(5)	24(5)	32(5)	-3(5)	-8(4)	0(4)
C(14)	30(5)	25(5)	32(5)	-3(5)	-16(4)	-6(4)

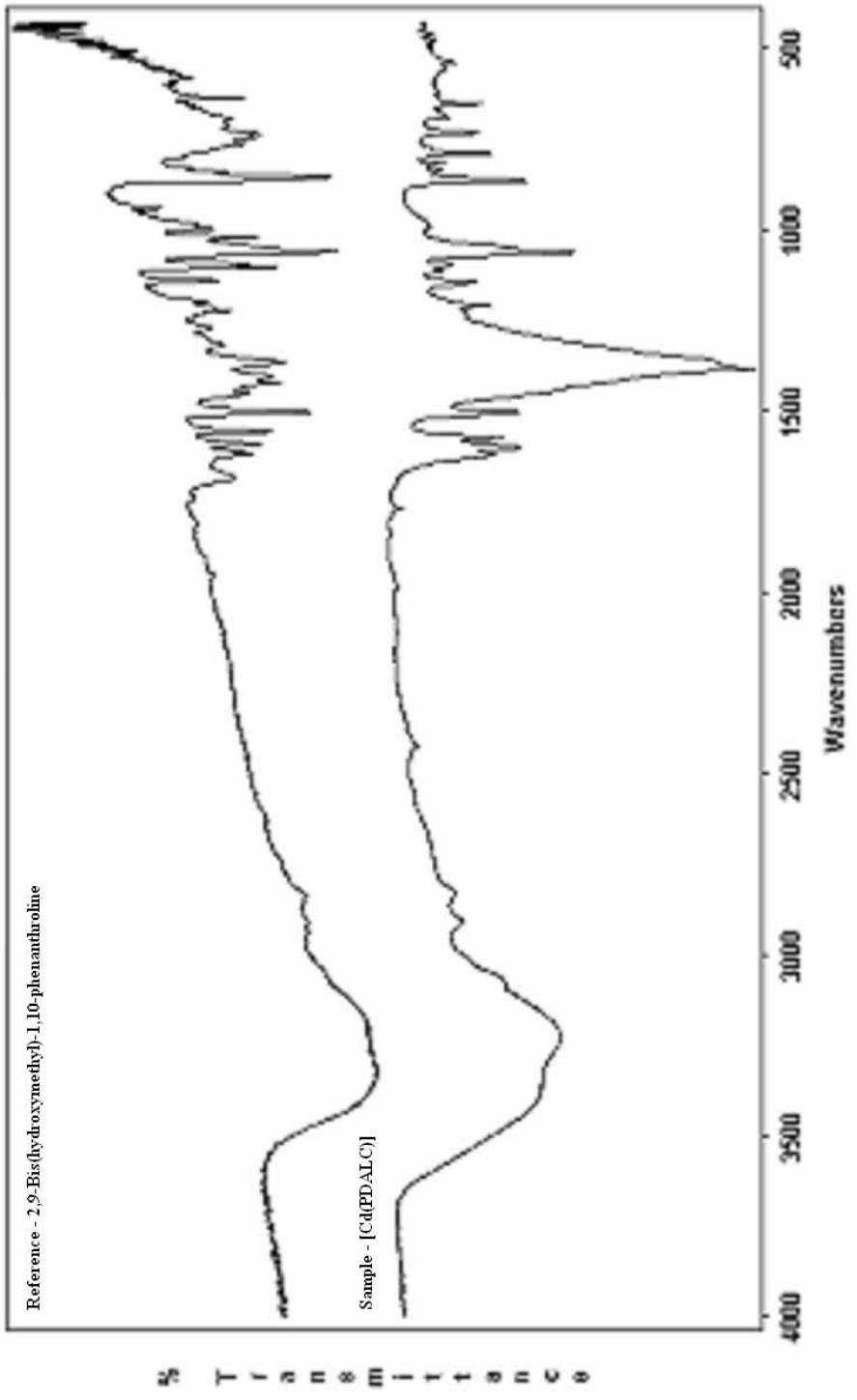

Figure 79: IR spectrum of [Cd(PDALC)] crystals with the IR spectrum of PDALC as a reference.

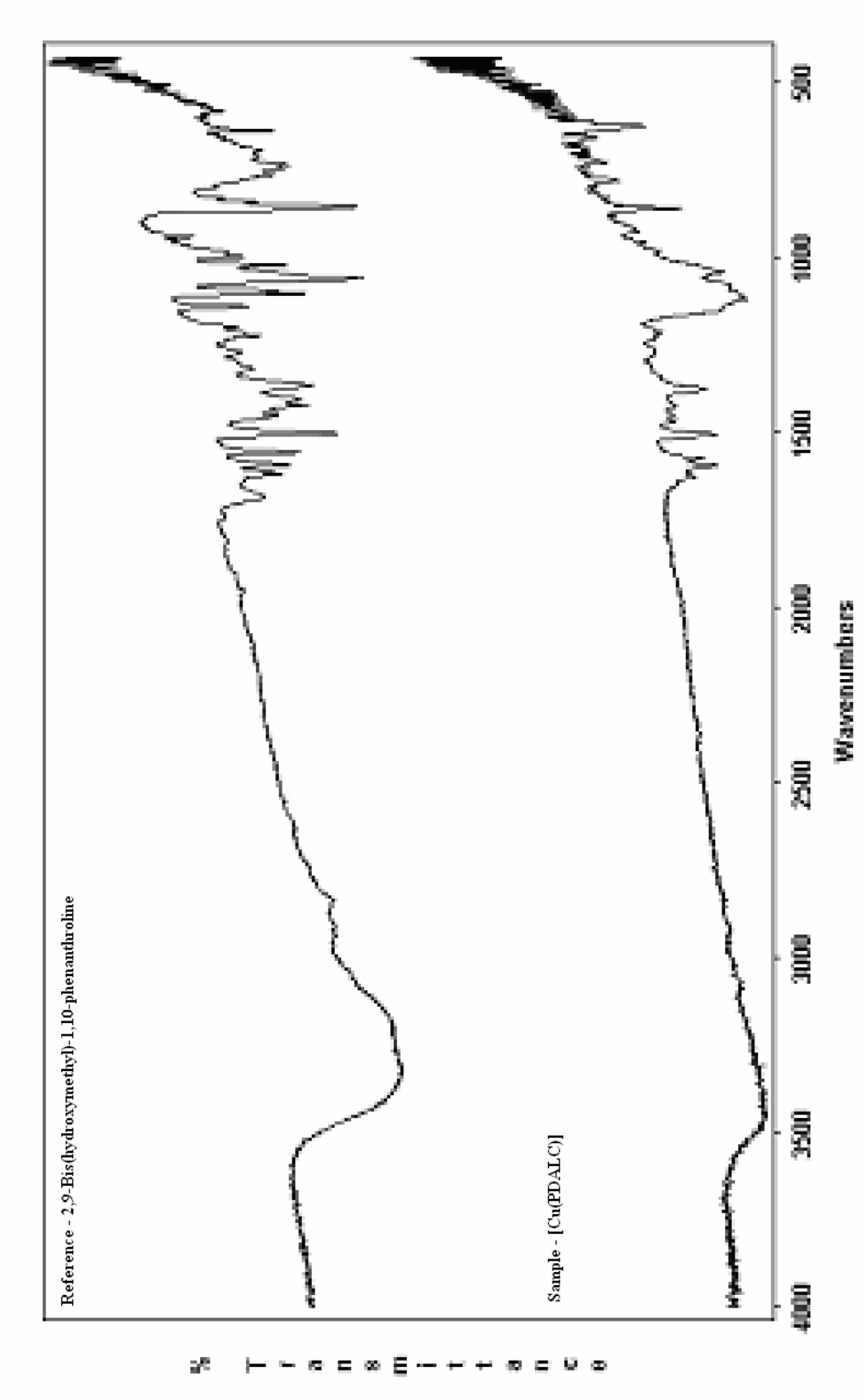

Figure 80: IR spectrum of [Cu(PDALC)] crystals with the IR spectrum of PDALC as a reference.

the ligand is present, but the peaks are shifted, suggesting complex formation. A few crystals were separated and have been sent for analysis.

[Gd(PDALC)] crystal synthesis

The synthesis of [Gd(PDALC)] crystals produced crystals that were very fine white needles on the interface of the *n*-butanol/H_2O layers. The IR analysis, shown in Figure 81, indicates that the ligand is present, but the peaks are shifted, suggesting complex formation. A few crystals were sent for analysis and the results are pending.

[Mg(PDALC)] crystal synthesis

The synthesis of [Mg(PDALC)] crystals produced crystals that were fine white needles on the interface of the *n*-butanol/H_2O layers. The IR analysis, shown in Figure 82, indicates that the ligand is present, but the peaks are shifted, suggesting complex formation. A few crystals were separated and have been sent for analysis.

[Ni(PDALC)] crystal synthesis

The synthesis of [Ni(PDALC)] crystals produced crystals that were fine green needles on the interface of the *n*-butanol/H_2O layers. The IR analysis, shown in Figure 83, indicates that the ligand is present, but the peaks are shifted, suggesting complex formation. A few crystals were separated and have been sent for analysis.

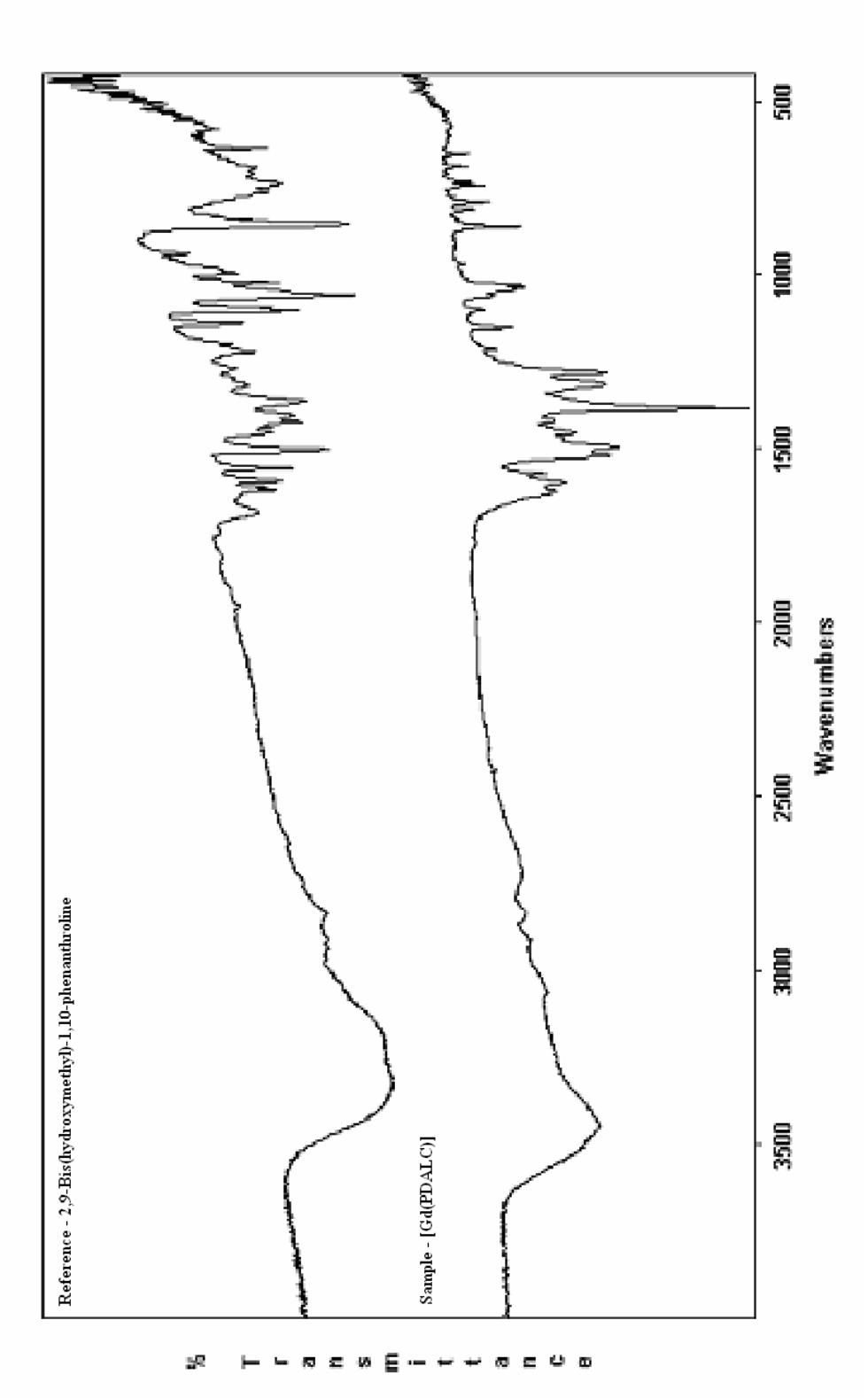

Figure 81: IR spectrum of [Gd(PDALC)] crystals with the IR spectrum of PDALC as a reference.

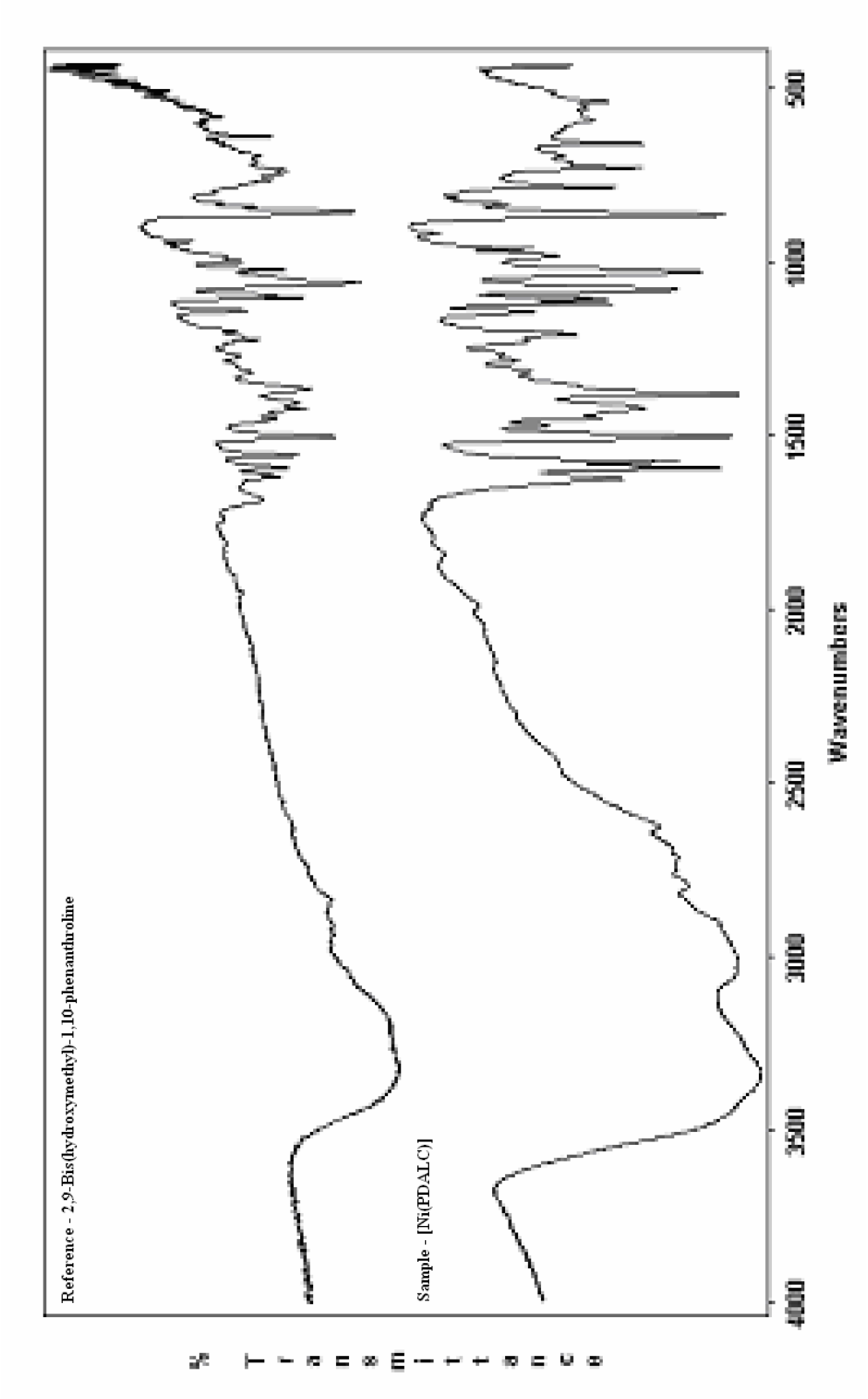

Figure 82: IR spectrum of [Ni(PDALC)] crystals with the IR spectrum of PDALC as a reference.

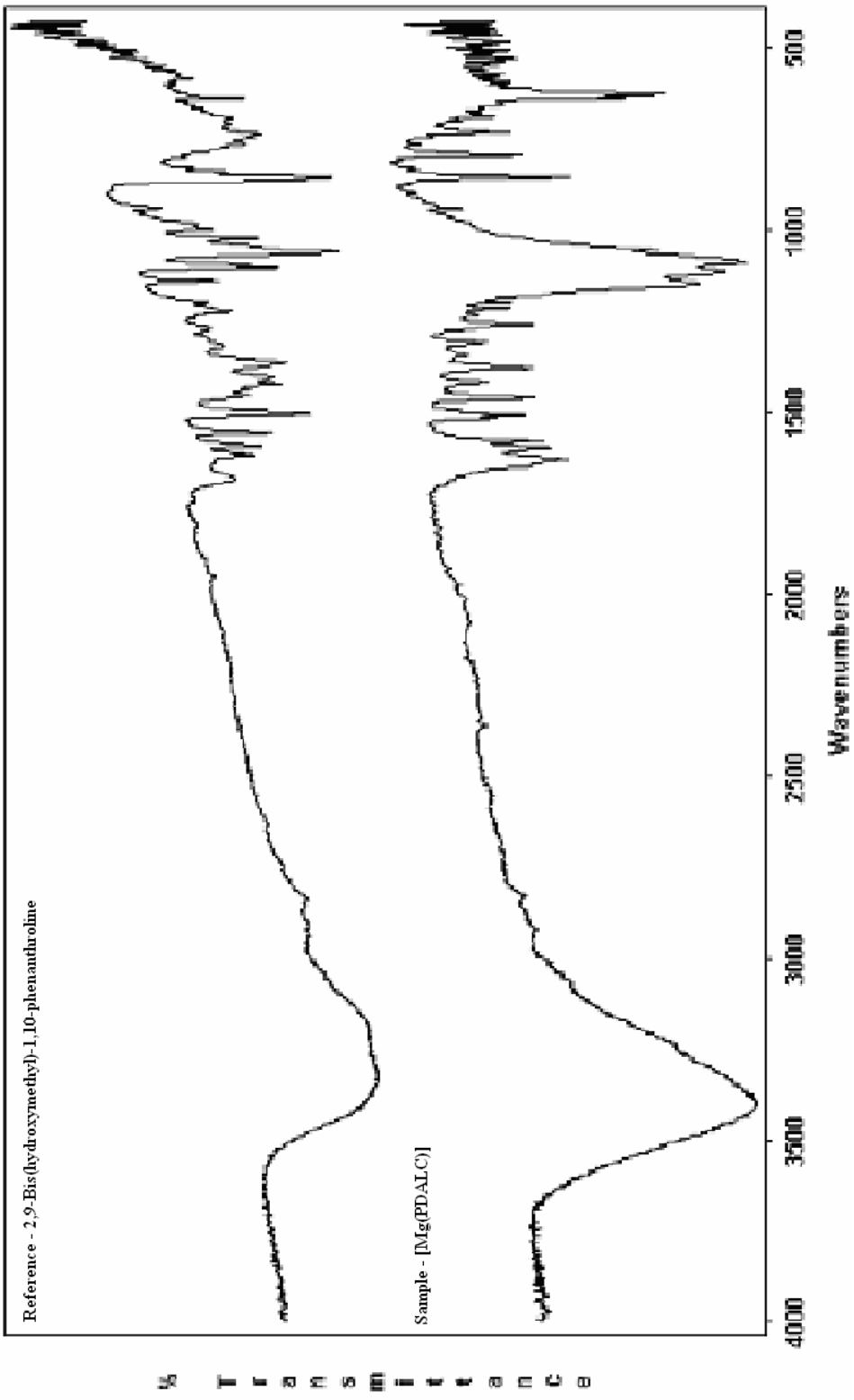

Figure 83: IR spectrum of [Mg(PDALC)] crystals with the IR spectrum of PDALC as a reference.

[Zn(PDALC)] crystal synthesis

The synthesis of [Zn(PDALC)] crystals produced crystals that were thick tan needles on the interface of the *n*-butanol/H_2O layers. The IR analysis, shown in Figure 84, indicates that the ligand is present, but the peaks are shifted, suggesting complex formation. A few crystals were separated and have been sent for analysis.

CONCLUSION

Preorganization has been proven to show an increase in metal-ligand stability as in the case of macrocycles and cryptands. These rigid molecules form very stable complexes with metal ions that match the size selectivity of the ligand. These preorganized ligands show an increase in metal ion selectivity over their unpreorganized counterparts. This study shows that 2,9-bis(hydroxymethyl)-1,10-phenanthroline (PDALC), a rigid, preorganized ligand, was able to increase the stability of complexes with metal ions around the size of 1.0 Å. This selectivity for larger metal ions is the product of two major factors. First, the chelate rings formed by the complex are all five-membered rings, which favor larger metal ions over smaller metal ions. Second, neutral oxygen donor atoms from the hydroxymethyl groups favor chelation with larger metal ions over smaller metal ions.

The synthesis of PDALC followed the process described in Chandler, et al.[27] with general agreement in results. The first step of the synthesis, with 1,10-phenanthroline-2,9-dicarbaldehyde (PDALD) as the product, was found to have impurities that were difficult to separate from the desired product. The impurities were removed when reducing PDALD to PDALC which was obtained as pure product after recrystallization from deionized (DI) H_2O.

Using UV-Vis spectrophotometry to determine the protonation constant of PDALC and the formation constants of PDALC with various metal ions has proven to be a valid method.

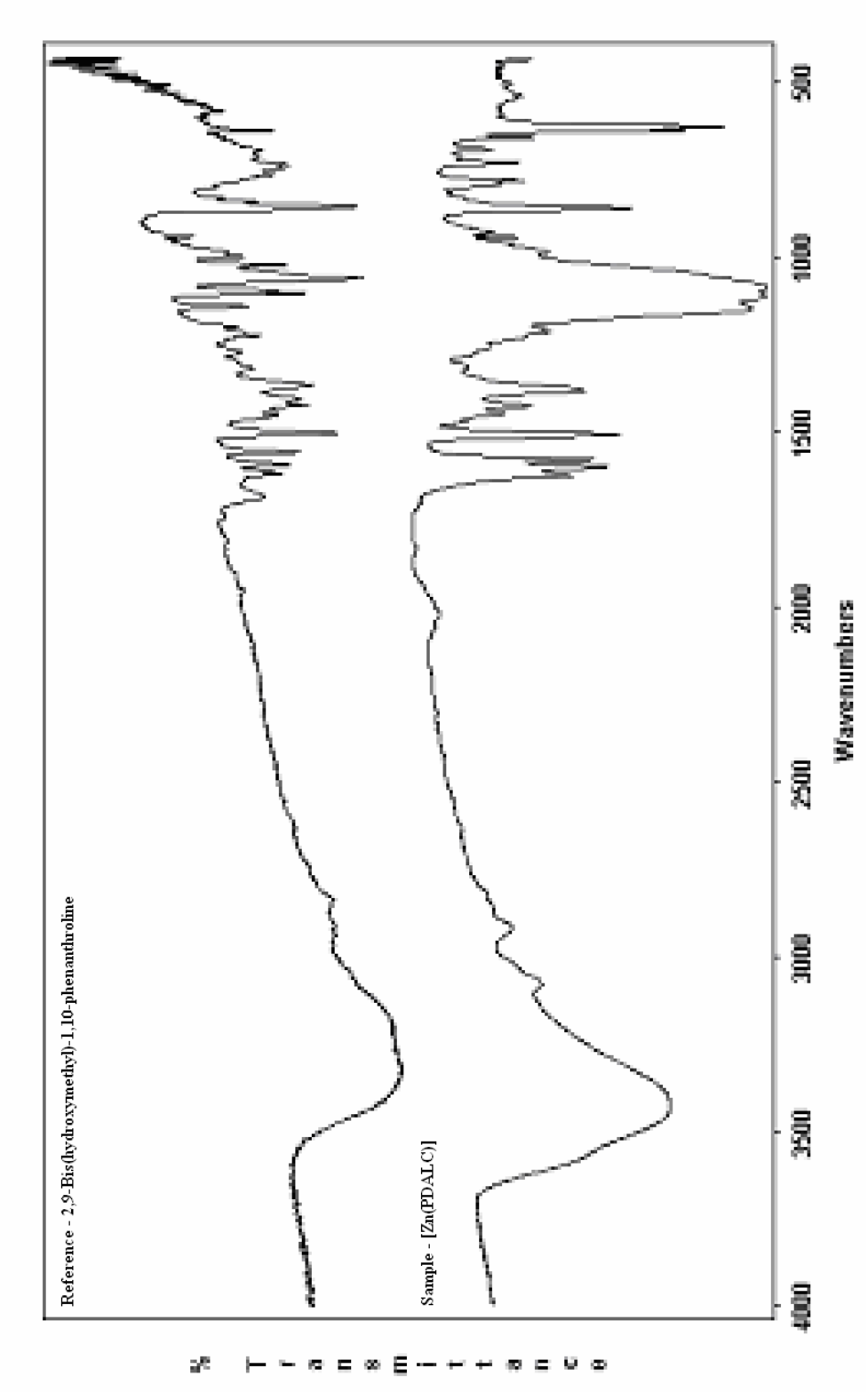

Figure 84: IR spectrum of [Zn(PDALC)] crystals with the IR spectrum of PDALC as a reference.

This method showed the distinction between PDALC complexed with a metal ion and PDALC as a free ligand. The formation constants for PDALC compared with N,N'-bis(2-hydroxymethyl)-ethylenediamine (EDDE) as expected by increasing the formation constants with larger metal ions more than with the smaller metal ions. In addition, Cu(II), a small metal ion, actually saw a decrease in the formation constant with PDALC when compared with EDDE. When compared with 1,10-phenanthroline, PDALC saw the greatest increase in the formation constant for metal ions that are close to 1.0 Å. For some small metal ions, a decrease in the formation constant was actually observed.

Using the glass electrode to determine the protonation constants of EDDE and the formation constants of EDDE with various metal ions has proven to be a valid method. The protonation constants of EDDE that were calculated from the glass electrode method were close to the reported values. The formation constants that were calculated for some metal ions that had no reported value were determined with a low standard difference, even for weak complexes such as with Ca(II).

Nine crystals were obtained for PDALC and various metal ions. The crystals that were analyzed were complexes of large metal ions which did not require any conformational change from PDALC. As illustrated by the structures, the metal ions were able to coordinate with all of the donor atoms of PDALC. In the case of Ca(II), complexation occurred by coordinating with eight donor atoms, all four donor atoms of two different PDALC ligands.

PDALC is expected to form stronger complexes with larger metal ions versus smaller metal ions because of its neutral oxygen donor atoms and the chelate ring size rule. According to Pearson's HSAB classification system, the hydroxymethyl groups of PDALC would be hard bases and the nitrogens of the pyridine ring would be borderline bases. Therefore, PDALC

would be expected to form stronger complexes with metal ions that are between intermediate and hard acids. Small metal ions that were observed to form strong complexes with PDALC included Ni(II), Cu(II), Zn(II), Zr(IV), and Co(II). Of these metal ions, only Zr(IV) was hard, with all others being intermediate. For these metal ions that are intermediates, when the complexes with PDALC were compared to the complexes formed with 1,10-phenanthroline, either no change or a decrease in complex stability was observed. Therefore, the hard bases from the hydroxymethyl groups proved to be a hindrance for complex formation. The proper size for the preorganized PDALC ligand is around 1.0 Å. This is the size of Ca(II) and Cd(II) which showed the greatest increase in formation constants of PDALC when compared to its unpreorganized precursor, EDDE.

Literature Cited

1. Guo, Zijian and Peter J. Sadler, *Agnew. Chem. Int. Ed.*, **1999**. 38. 1512-1531.

2. Pearson, R. G. and J. Songstad, *J. Amer. Chem. Soc.*, **1967**. 89:8. 1827-1836.

3. Pearson, R. G., *J. Amer. Chem. Soc.*, **1963**. 85:22. 3533-3539.

4. Cukrowski, I., E. Cukrowska, R. D. Hancock, and I. G. Anderegg, *Anal. Chem. Acta.*, **1995**. 312. 307-321.

5. Cukrowski, I., F. Marsicano, R. D. Hancock, P. T. Tshetlho and W. A. L. Van Otterlo, *Polyhedron*, **1995**. 14:12. 1661-1674.

6. Hancock, R. D., R. Bhavan, P. W. Wade, J. C. A. Boeyens, and S. M. Dobson, *Inorganic Chemica*, **1989**. 28. 187-194.

7. Evers, A., R. D. Hancock, A. E. Martell, and R. J. Motekaitis, *Inorganic Chemica*, **1989**. 28. 2189-2195.

8. Hay, B. P. and R. D. Hancock, *Coordination Chemistry Reviews*, **2001**. 212. 61-78.

9. Cram, D. J., "The design of molecular hosts, guests, and their complexes." Nobel Lecture, **1987**.

10. Mukherjee, Rabindranath, *Coord. Chem. Reviews*, **2000**. 203. 151-218.

11. Edwards, J.O., Pearson, R.G. *J. Am. Chem. Soc.*, **1962**. 84. 16.

12. Martell, A. E., and R. D. Hancock, *Metal Complexes in Aqueous Solutions*, Plenum, New York, 1996.

13. Pinto, Gabriel, *J. Chem. Educ*. **1998**. 75. 725-726.

14. Raymond, K. N., G. Meuller, B. F. Matzanke, *Top. Curr. Chem.* **1984**. 123. 49.

15. Raymond, K. N., G. E. Freeman, M. J. Kappel, *Inorganic Chim Acta.* **1984**. 94. 193.

16. Harris, W. R., A. E. Martell, *Inorg. Chem.* **1976.** 15. 713.

17. Yoshida, I., I. Murase, R. J. Motekaitis, A. E. Martell, *Can. J. Chem.* **1983**. 61. 2740.

18. Sun, Y., A. E. Martell, R. J. Motekaitis, *Inorg. Chem.* **1985**.24. 4343.

19. Mathias, C. J., Y. Sun, M. J. Welch, M. A. Green, J. A. Thomas, K. R. Wade, A. E. Martell, *Nucl. Med. Biol.* **1988**. 15. 69.

20. Lauffer, R. C., *Chem. Rev.* **1987**. 87. 901.

21. Martell, A.E., R. M. Smith, *Critical Stability Constant Database, 46.* National Institute of science and Technology (NIST): Gaithersburg, MD, USA, **2003**.

22. Comba, P., A. Fath, A. Kuhner, B. Nuber, *J. Chem. Soc.* **1997**. 11. 1889-1898.

23. Huskens, J., H. Van Bekkum, J. A. Peters, *Computers and Chemistry.* **1995**. 19. 409-416.

24. Brouwers, A., et al., *Cancer and Biotherapy and Radiopharmaceuticals*, **2004**. 19. 155-163.

25. Verel, I., et al., *Journal of Nuclear Medicine*, **2003**. 44. 1271-1281.

26. Verel, I., et al. *Cancer and Biotherapy and Radiopharmaceuticals*, **2003**. 18. 655-661.

27. Downey, J. Z., and H. L. Sharma, *International Journal of radiation applications and instrumentation*, *Part A, radiation and isotopes*, **1991**. 42:2. 199-201.

28. Chandler, C.J., L. W. Deady, and J. A. Reiss. *J. Heterocyclic Chem.*, **1981**. *18*. 599-601.

29. Melton, Darren. (2005) Metal Ion Complexing Properties of the 2-dimensional, Highly Preorganized Ligand 1,10-phenanthroline-2,9-dicarboxylic acid. Department of Chemistry. Wilmington, University of North Carolina Wilmington.

30. R. Luckay, I. Cukrowski, J. Mashishi, J. H. Reibenspies, A. H. Bond, R. D. Rogers, and R. D. Hancock, *J. Chem. Soc., Dalton Trans.*, **1997**. 901-908.

31. Comba, Peter, *Coord. Chem. Reviews.* **1999**. 185-186. 81-98.

APPENDIX

PDALC 2,9-bis(hydroxymethyl)-1,10-phenanthroline

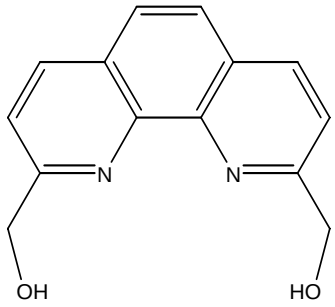

PDALD 1,10-phenanthroline-2,9-dicarboxaldehyde

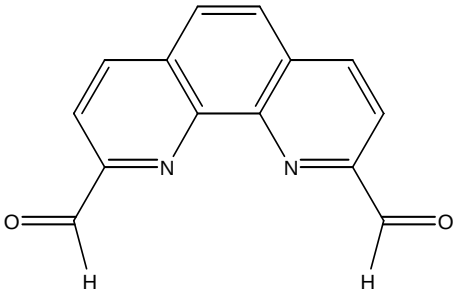

EDDE N,N’-Bis(2-hydroxyethyl)-ethylenediamine

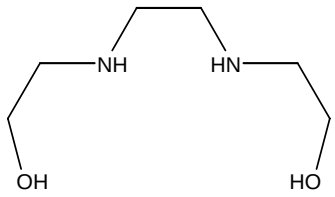

EGTA ethylenebis(oxyethylenenitrilo) tetra-ethylene glycol bis(2-aminoethyl ether)-N,N,N'N'-tetraacetic acid

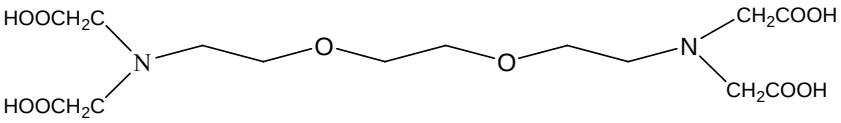

HSAB Hard and Soft Acids and Bases

PET Positron Emission Tomography

DI deionized